CHAPTER 2

Update on Global Ozone: Past, Present, and Future

Lead Authors:
S. Pawson
W. Steinbrecht

Coauthors:
A.J. Charlton-Perez
M. Fujiwara
A.Yu. Karpechko
I. Petropavlovskikh
J. Urban
M. Weber

Contributors:
V. Aquila
W. Chehade
I. Cionni
M. Coldewey-Egbers
A. Delcloo
S.S. Dhomse
V. Eyring
E. Fleming
S.M. Frith
L. Froidevaux
N.P. Gillett
B. Hassler
M.I. Hegglin
D.E. Kinnison
D. Loyola
C.A. McLinden
L.D. Oman
D.A. Plummer
L.E. Revell
T. Sakazaki
W. Seviour
S. Tegtmeier
R.J. van der A
J. Wild

Chapter Editors:
V.E. Fioletov
U. Langematz

[Formatted for double-sided printing.]

From:
WMO (World Meteorological Organization), *Scientific Assessment of Ozone Depletion: 2014*, Global Ozone Research and Monitoring Project – Report No. 55, 416 pp., Geneva, Switzerland, 2014.

This chapter should be cited as:
Pawson, S., and W. Steinbrecht (Lead Authors), A.J. Charlton-Perez, M. Fujiwara, A.Yu. Karpechko, I. Petropavlovskikh, J. Urban, and M. Weber, Update on global ozone: Past, present, and future, Chapter 2 in *Scientific Assessment of Ozone Depletion: 2014*, Global Ozone Research and Monitoring Project – Report No. 55, World Meteorological Organization, Geneva, Switzerland, 2014.

CHAPTER 2

UPDATE ON GLOBAL OZONE: PAST, PRESENT, AND FUTURE

Contents

SCIENTIFIC SUMMARY

Past Changes in Total Column Ozone

This chapter deals with the evolution of global ozone outside of the polar regions. The increase of ozone-depleting substance (ODS) concentrations caused the large ozone decline observed from 1980 to the mid-1990s. Since the late 1990s, concentrations of ODSs have been declining due to the successful implementation of the Montreal Protocol. As reported in the last Assessment, global ozone levels have remained stable since 2000. Ozone columns observed in the last four years have largely remained in the range observed since 2000.

Over the next decades we expect increasing global-mean stratospheric ozone columns, as ODSs decline further. Climate change and emissions of greenhouse gases, especially carbon dioxide (CO_2), methane (CH_4), and nitrous oxide (N_2O), also affect the evolution of global stratospheric ozone, particularly in the second half of the 21st century, when ODS concentrations are expected to be low.

- Compared to 1964–1980 total column ozone, ground-based and space-based observations show that present-day (circa 2008–2013) ozone columns are:
    - lower by about 2% for the near-global average (60°S–60°N), compared to 2.5% reported in the last Assessment;
    - lower by about 3.5% in the Northern Hemisphere (35°N–60°N), as reported in the last Assessment;
    - lower by about 6% in the Southern Hemisphere (35°S–60°S), as reported in the last Assessment. The larger depletion in the Southern Hemisphere is linked to the Antarctic ozone hole; and
    - almost unchanged in the tropics (20°S–20°N), as in the last Assessment.

- **Ground- and space-based observations indicate that near-global (60°S–60°N) column ozone has increased by around 1% ± 1.7% (2 sigma) between 2000 and 2013.** However, there is substantial disagreement among the data sets about the magnitude and statistical significance of this increase. Two out of three independent data sets show increases at the upper end; one recently updated data set shows an increase at the lower end. The CCMVal-2 multi-model mean predicts a 1% increase between 2000 and 2013 for the near-global (60°S–60°N) column ozone.

- **Total column ozone (dominated by lower stratospheric ozone) displays large, dynamically forced year-to-year variability in the middle and high latitudes, exemplified by unusually high ozone in 2010 and low ozone in 2011 in the Northern Hemisphere, and low ozone in 2006 in the Southern Hemisphere.** The recent decline (15% since 1997) in concentrations of ODSs, as described by Equivalent Effective Stratospheric Chlorine (EESC), is expected to have had only a small impact on total ozone recovery (approximately 3 Dobson units (DU), or 1%, since 2000). Separation of the small recent ODS-related ozone increase from the large natural variability (up to 15 DU or 5% change from one year to the next) can currently not be made with a high level of confidence.

Past Changes in Ozone Profiles

Additional and improved data sets have strengthened our ability to assess ozone profile changes over the last 10 to 15 years. Data from the upper stratosphere now confirm the significance of ozone increases that were already suggested in the last Assessment. Large ozone variability in the lower stratosphere complicates the identification of long-term ozone changes in this region. Chemistry-climate model (CCM) simulations that include realistic time variations of greenhouse gas (GHG) and ODS concentrations

capture changes in the ozone profile that agree quite well with those observed. These CCM simulations provide a means of attributing changes in ozone to different processes.

- **Measurements show a statistically significant increase in upper stratospheric ozone (35–45 km altitude) in middle latitudes and the tropics since around 2000.** Following a large observed decline of 5–8% per decade through the 1980s and middle 1990s, ozone has increased by 2.5–5% per decade over the 2000 to 2013 period.
- **About half of the upper stratospheric ozone increase after 2000 can be attributed to the decline of ODS since the late 1990s.** Increasing CO_2 concentrations have led to a cooling of the upper stratosphere. CCM simulations reveal that, between the 1980s and the present this has contributed to an increase in ozone concentrations. Before the middle 1990s, this ozone increase was substantially smaller than the ozone decrease caused by ODS increases. From 2000 to 2013, the ozone increase arising from the decline in ODS concentrations is of comparable magnitude to that caused by upper stratospheric cooling.
- **As reported in the last Assessment (WMO, 2011), CCMs consistently show a long-term decline of ozone in the lowermost tropical stratosphere by up to 20% between 1960 and 2060.** This modeled ozone decline is caused by an increase in the strength of upwelling in the tropical lower stratosphere. This increased upwelling is associated with a strengthening Brewer-Dobson circulation caused by GHG-induced climate change.
- **In-situ and space-based observations reveal that ozone concentrations in the lowermost tropical stratosphere have declined by as much as 10% between 1984 and 2005.** There are several additional data sets available since 2002. Continued ozone decreases are not detected in the presence of large natural variability during 2002–2013. This observed behavior is consistent with that computed in CCMs, which also show periods of strong interannual and decadal variability.

Future Ozone Changes

The chemistry-climate model simulations used in the last Assessment are still the main source for projection of future ozone levels and the dates of return of ozone to 1980 levels. Declining ODS concentrations, upper stratospheric cooling because of increased CO_2, and the possible strengthening of the Brewer-Dobson circulation from climate change are all likely to affect recovery of global column ozone, with different relative contributions in various latitude regions.

- Estimates of the likely return dates of total column ozone concentrations to their 1980 values have not changed since the last Assessment. The best estimates are:
    - by midcentury for global mean annually averaged ozone;
    - between 2015 and 2030 for annually averaged Northern Hemisphere midlatitude ozone;
    - between 2030 and 2040 for annually averaged Southern Hemisphere midlatitude ozone; and
    - for annual average tropical column ozone, slowly increasing until the middle of the 21st century, before leveling off at values about 0–3% below 1980s columns.
- **The updated lifetimes estimated for ODSs in the SPARC lifetimes report have no significant impact on model projections of future ozone evolution.**
- **Projections of future ozone levels depend substantially on the assumed scenario of greenhouse gas (GHG) emissions, especially in the later half of the 21st century.** Six chemistry-climate model simulations show that projected total ozone columns in 2100 differ by up to 20 DU or 7% in the global average, by up to 40 DU or 12% in midlatitudes, and by up to 10 DU or 4% in the tropics between minimum and maximum radiative forcing Representative Concentration Pathway scenarios for future CO_2, N_2O, and CH_4 emissions. These new estimates of scenario uncertainty are broadly consistent with previous estimates from different models and scenarios reported in the last

Assessment. Our confidence in the magnitude of this scenario uncertainty remains low because of the small number of models and scenarios assessed.

- **Part of the scenario uncertainty in future column ozone is due to differences in emissions of N_2O and CH_4 between different scenarios.** Increases of stratospheric N_2O and CH_4 impact the chemical cycles relevant for ozone. Higher N_2O emissions tend to reduce column ozone, whereas higher CH_4 tends to increase column ozone, each by a few percent from 2020 to 2100. The magnitude of these effects on ozone is comparable to what is expected from stratospheric cooling by CO_2 increases. The influence of each individual trace gas on ozone also depends on emissions of the others, meaning that their impacts on ozone are strongly scenario dependent.

- **Given that ODS levels remain high, a large enhancement of stratospheric sulfate aerosol in the next decade, e.g., due to a volcanic eruption of the same size as Mt. Pinatubo, could result in chemical losses of at least 2% in total ozone columns over much of the globe.** Confidence in this conclusion is strengthened because the long-standing puzzle about the midlatitude hemispheric asymmetry in the midlatitude ozone response to Mt. Pinatubo aerosols is now much better understood. Studies have shown that enhanced ozone transport in the Brewer-Dobson circulation more than compensated the enhanced chemical loss in the Southern Hemisphere.

2.1 INTRODUCTION

2.1.1 Main Findings of WMO-UNEP 2010

The 2010 Assessment (WMO, 2011) provided strong evidence that the limitations imposed by the Montreal Protocol on ozone-depleting substance (ODS) emissions were leading to a slowdown in chemical ozone destruction after 1997. Observations showed a leveling off of ozone values at almost all latitudes and altitudes, with a distinct change in the trend: A strong negative ozone trend between the 1970s and the late 1990s was superseded by a period of almost no significant change in ozone until the end of the record in 2009. A broad range of numerical modeling studies, using chemical transport models (CTMs) and chemistry-climate models (CCMs), demonstrated that we have a robust scientific understanding of the mechanisms of ozone depletion. Further, the CCMs demonstrated at least three important connections between climate change and ozone depletion. First, observations and models demonstrated that the ozone hole impacts atmospheric heating rates, leading to a dynamical response of the springtime polar vortex that couples to the summertime dynamics of the Antarctic troposphere. Second, model simulations indicated that increasing greenhouse gases (GHGs) would further cool the stratosphere, thus slowing gas-phase reactions that destroy ozone in the upper stratosphere, and generally increase ozone and accelerate ozone increases. Third, the model simulations consistently predicted an increase in the strength of the Brewer-Dobson circulation (BDC), leading to lower ozone concentrations in the tropical lower stratosphere and higher values in the extratropics than might be otherwise expected. In WMO (2011) the observational evidence for this latter change was weak.

These changes in stratospheric temperatures and tropical upwelling contribute substantially to projections of ozone change through the 21st century. CCM projections showed that, in the extratropics, ozone would recover to 1980 levels as ODSs were flushed from the atmosphere, with "return dates" occurring in the 2030s to 2060s. As GHG-induced climate change continued to increase the tropical upwelling, many CCMs indicated that ozone concentrations in the tropical lower stratosphere would continue to decrease through the 21st century. In the tropics, this dynamically induced decline in ozone would offset the impacts of chemical recovery. Likewise, CCMs predicted that, in the upper stratosphere, the lower temperature resulting from increasing GHGs and declining ODSs would lead to ozone increases through the 21st century.

2.1.2 Major New Developments Since 2010

With the decline in emissions of ODSs and the consequent decrease in stratospheric chlorine- and bromine-containing compounds, a major component of the present Assessment concerns the detectability of any positive ozone trends over the past decade. The four additional years of observations available for analysis facilitate a new look at the potential recovery of ozone concentrations, with evidence that the positive trend associated with ODS reductions is becoming significant in some regions. Global ozone has been observed by spaceborne sensors for about 35 years. A continuous ozone profile data set based on one type of observations with global coverage is, however, not available. Since WMO (2011) the records of several instruments have been extended. These contribute substantially to the database of ozone profiles that supplements the sparse ground-based data sets. Long-term ozone profile data sets have been constructed by merging data from different instruments. New observations available since WMO (2011) have facilitated the investigation of the diurnal cycle of stratospheric ozone. This positions the research community to improve estimates of data set biases induced by diurnal effects (e.g., due to orbits that drift in local time), which can be particularly important in the upper stratosphere. The 2006 and 2010 Ozone Assessments drew heavily on model comparisons conducted by the SPARC (Stratosphere-troposphere Processes and their Role in Climate) Chemistry-Climate Model Validation (CCMVal) activity (Eyring et

al., 2010), with a consequent focus on differences among model predictions of ozone and some emphasis on the robustness of model simulations. Because the models used in CCMVal have not been substantially updated, no new multi-model comparison has been performed. New CCM simulations focus on different aspects of ozone change resulting from ODSs and GHGs, with a particular focus on the possible ozone distributions in the late 21st century, when chemical ozone destruction by halogens will have almost disappeared, and the main changes in ozone are driven by the assumed scenarios in greenhouse gas growth rates.

A main focus of this Assessment thus relies on better detection of ozone change, its attribution, and the robustness of recent changes detected in observations. The second main focus is on how ozone is expected to evolve in the presence of ODS reductions and how assumptions about greenhouse gas pathways impact future ozone change.

2.2 PAST OZONE IN OBSERVATIONS AND MODEL SIMULATIONS

2.2.1 Data Sources

As in the previous Assessments, carefully assessed, long-term ozone data sets have been used for trend analysis. Several new data sets have now become sufficiently long to examine ozone changes since 2000, particularly from instruments on the Odin, Envisat, and Aura satellite platforms, available since 2001, 2002, and 2004, respectively. Information about the ozone data sets used for this Assessment is summarized in Tables 2-1 (total ozone column) and 2-2 (ozone profiles). Detailed information about spatial and temporal coverage, vertical resolution, and systematic uncertainties is available from previous Assessments (WMO, 2007, 2011), and from recent SPARC initiatives on the evaluation of trace gas and aerosol climatologies (SPARC Data Initiative; Tegtmeier et al., 2013), and on past changes in the vertical distribution of ozone (SPARC/IO3C/IGACO-O3/NDACC = SI2N; Hassler et al., 2014).

Because trend detection requires time series of observations that are longer than the lifetime of most satellite instruments, several new merged ozone time series are used in this Assessment. Challenges for such long-term records come from inter-instrument biases, drifts, differing local measurement times, different coordinate systems (e.g., ozone mixing ratio in a pressure-based coordinate system, or number density in an altitude-based system), different vertical and temporal resolution, and different sampling patterns. Box 2-1, for example, discusses differences in ozone profile trends that can arise from the coordinate system used. Section 2.3.1 discusses possible effects of diurnal variations, which are, however, presently not corrected for in any merged data set. This Assessment draws heavily on recent activities to combine and homogenize ozone data sets for trend studies. The following data sets are used here:

- The most recent update of the monthly-mean zonal mean data set combining Brewer spectrometer, Dobson spectrometer, filter, and SAOZ (Système d'Analyse par Observation Zénithale) total ozone data from the ground covering the period from 1964 to present (Fioletov et al., 2002; WMO, 2011).
- Merged total ozone data sets from the Global Ozone Monitoring Experiments (GOME, GOME-2) and the Scanning Imaging Absorption Spectrometer for Atmospheric Chartography (SCIAMACHY): The Global Total Ozone data set (GTO: Chiou et al., 2014; Lerot et al., 2014) is based on the GODFIT (GOME Direct-FITting) retrieval (Loyola et al., 2009). An alternative data set is the weighting function differential optical absorption (WFDOAS) GOME/SCIAMACHY/ GOME-2 data set (GSG: Kiesewetter et al., 2010; Weber et al., 2011, 2013).
- The Multi Sensor Reanalysis (MSR), an assimilated total ozone data set using various satellite data (SBUVs, GOME, SCIAMACHY, GOME-2) and variants of retrieval algorithms as input (van der A et al., 2010). All satellite data sets have been bias corrected with respect to colocated ground Brewer and Dobson data.

Table 2-1. Merged total ozone column data sets used in this report (zonal monthly-mean data).

Data Set	Instruments	Record Length	Reference	URL
Ground-Based	Dobson, Brewer, SAOZ	01/1964 to 12/2013	Fioletov et al., 2002, 2008; Hendrick et al., 2011	http://www.woudc.org ftp://ftp.tor.ec.gc.ca/pub/woudc/Projects-Campaigns/ZonalMeans
SBUV MOD V8	BUV Nimbus-4, SBUV/TOMS Nimbus-7, SBUV/2 NOAA 9 to 19, OMI, TOMS EP	11/1978 to 12/2012	Stolarski and Frith, 2006	http://acd-ext.gsfc.nasa.gov/Data_ services/merged/
SBUV V8.6 NASA (MOD V8.6)	BUV Nimbus-4, SBUV Nimbus-7, SBUV/2 NOAA 9 to 19	BUV: 01/1970 to 05/1976 SBUV: 11/1978 to 12/2013	Chiou et al., 2014; Labow et al., 2013; McPeters et al., 2013	http://acd-ext.gsfc.nasa.gov/Data_ services/merged/
SBUV V8.6 NOAA	SBUV Nimbus-7, SBUV/2 NOAA 9 to 19	11/1978 to 12/2013		ftp://ftp.cpc.ncep.noaa.gov/SBUV_CDR/
GSG - Bremen	GOME, SCIAMACHY, GOME2	07/1995 to 12/2013	Weber et al., 2013	http://www.iup.uni-bremen.de/gome/wfdoas/
GTO - ESA/DLR	GOME, SCIAMACHY, GOME2	07/1995 to 12/2013	Chiou et al., 2014; Lerot et al., 2014	http://www.esa-ozone-cci.org
Multiple Satellite Reanalysis	assimilated TOMS, SBUV, GOME, SCIAMACHY, OMI	11/1978 to 12/2013	van der A et al., 2010	http://www.temis.nl/protocols/O3global.html

- Merged total ozone and ozone profile data sets from the V8.6 retrievals of the Solar Backscatter Ultraviolet (SBUV) instruments from NASA (MOD V8.6: DeLand et al., 2012; McPeters et al., 2013; Chiou et al., 2014), which supersede the SBUV/Total Ozone Mapping Spectrometer (TOMS)/Ozone Monitoring Instrument (OMI) MOD V8 data set (Stolarski and Frith, 2006; WMO, 2011). Another merged SBUV V8.6 data set from NOAA (MA-NOAA) uses inter-satellite adjustments similar to the previous SBUV/TOMS/OMI MOD V8 data set. It provides ozone time series very similar to MOD V8. Within the uncertainty margins discussed by Stolarski and Frith (2006), the new NASA and MA-NOAA SBUV V8.6 merged data sets agree over most of their 40-year time series (i.e., total ozone columns are usually within 1% or better; profile ozone data are within 5% or better). Trend results from both data sets are similar. The NOAA SBUV V8.6 merged data set is not used in this Assessment, because currently no validation has been published for this recently merged data set.
- Stratospheric Aerosol and Gas Experiment II (SAGE II) data, updated from Version 6.2 to 7.0 (Damadeo et al., 2013). For ozone, the new data version has not resulted in significant changes of SAGE II derived trends or long-term variability (Remsberg, 2014).
- The NASA "Making Earth System Data Records for Use in Research Environments" (MEaSUREs) Global OZone Chemistry And Related trace gas Data records for the Stratosphere (GOZCARDS) project (R. Wang et al., 2013), combining satellite ozone records primarily from Stratospheric Aerosol and Gas Experiments I and II (SAGE I, II, V6.20), Halogen Occultation Experiment (HALOE), Microwave Limb Sounders (Upper Atmosphere Research Satellite MLS, Aura MLS), and Atmospheric Chemistry Experiment (ACE-Fourier Transform Spectrometer). The quality of these data sets contributing to GOZCARDS was recently assessed in the SPARC Data Initiative

(Tegtmeier et al., 2013), which also considered results from the limb sounding instruments presented in the next bullet.

- The HARMonized data set of OZone profiles (HARMOZ: Sofieva et al., 2013) produced by the European Space Agency Ozone Climate Change Initiative (ESA O3-CCI). HARMOZ consists of quality-screened European individual limb sounder data sets that are provided in common ozone units and altitude grid. HARMOZ consists of ozone data from the Optical Spectrograph and Infrared Imaging System (OSIRIS), the Sub-Millimetre Radiometer (SMR), both on the Odin satellite since 2001, and from the Global Ozone Monitoring by Occultation of Stars (GOMOS), the Michelson Interferometer for Passive Atmospheric Sounding (MIPAS), and the Scanning Imaging Absorption Spectrometer for Atmospheric Chartography (SCIAMACHY), all on the Envisat platform from 2002 to 2012. Tegtmeier et al. (2013) and Sofieva et al. (2013) discuss these individual data sets and their differences. In the Assessment, only ozone anomalies averaged over all available HARMOZ instruments are used. This removes the average bias of individual instruments, and reduces effects from spurious anomalies and drifts of individual instruments (see also Steinbrecht et al., 2006; Jones et al., 2009; Nair et al., 2012). Results for individual instruments from the HARMOZ data set have been reported by Kyrölä et al. (2013), Eckert et al. (2014), and Gebhardt et al. (2014).

Table 2-2. Main ozone profile data sets used in this report.

Data Set	Instruments Most Relevant for Trend	Record Length	References	URL
SBUV V8.6 NASA (MOD V8.6)	BUV Nimbus-4, SBUV Nimbus-7, SBUV/2 NOAA 9 to 19	BUV: 01/1970 to 05/1976 SBUV: 11/1978 to 07/2013	Kramarova et al., 2013a; McPeters et al., 2013	http://acd-ext.gsfc.nasa.gov/ Data_ services/merged/
SBUV V8.6 NOAA	SBUV Nimbus-7, SBUV/2 NOAA 9 to 19	11/1978 to 12/2012		ftp://ftp.cpc.ncep.noaa.gov/ SBUV_CDR/
GOZCARDS	SAGE I, SAGE II, HALOE, MLS-Aura	02/1979 to 12/2013 Gap: 11/1981 to 10/1984	R. Wang et al., 2013	https://gozcards.jpl.nasa.gov/
SAGE II, V7.0	SAGE II	10/1984 to 08/2005	Damadeo et al., 2013	https://eosweb.larc.nasa.gov/project/ sage2/sage2_table
HARMOZ	ODIN: OSIRIS, SMR ACE-FTS; Envisat: GOMOS, MIPAS, SCIAMACHY	10/2001 to 12/2012 08/2002 to 12/2011	Sofieva et al., 2013	http://www.esa-ozone-cci.org
NDACC ground-based	lidars, microwave radiometers, FTIRs about 5 stations	late 1980s/early 1990s to 2012/2013, depending on station	Steinbrecht et al., 2009; Vigoroux et al., 2008	http://www.ndacc.org see also Table 2-3
Umkehr	about 5 stations	1956 (Arosa) 1984 (Lauder) to 2012	Petropavlovskikh et al., 2005 ; Tourpali et al., 2007	http://www.esrl.noaa.gov/gmd/ozwv/ umkehr/
Ozonesondes	about 50 stations	Late 1960s / mid-1990s to 2012/2013 depending on station	Smit et al., 2007; Deshler et al., 2008; Thompson et al., 2012	http://www.woudc.org http://www.ndacc.org http://nadir.nilu.no http://croc.gsfc.nasa.gov/shadoz/

Box 2-1. Ozone Trends in Different Coordinates

Different instruments retrieve ozone in different fundamental units. SAGE and lidars, for example, provide ozone number density as a function of altitude. MLS provides ozone mixing ratio as a function of pressure. SBUV retrieves partial column ozone between two pressure levels, equivalent to mixing ratio versus pressure. All these quantities are linked through the background stratosphere (pressure and temperature), which is changing due to ozone and climate changes. Changing temperature and pressure profiles affect the different ozone coordinate systems. Since most ozone data sets come without corresponding temperature measurements, background atmospheres from operational meteorological analyses, or reanalyses (all with uncertainties; see Chapter 4), have to be used for unit conversion. This adds uncertainty to the comparison of ozone trends in different units.

McLinden and Fioletov (2011) assessed these differences using observed decadal temperature trends (see Chapter 4) to determine changes in the standard atmosphere. Stratospheric cooling leads to a contraction of the stratosphere, so pressure and ozone mixing ratio are shifted to lower geometric altitudes. As a result, above the mixing ratio peak (5 hPa, 35 km), lower ozone from higher altitudes replaces higher values at constant height surfaces. This makes ozone trends in mixing ratio versus altitude more negative than in mixing ratio versus pressure. The effect is enhanced for number density versus altitude trends by smaller pressures at the same altitude. Below the ozone maximum, atmospheric "shrinking" due to cooling is less pronounced and the contraction brings down higher ozone mixing ratios from above. Lower temperatures enhance number densities. As a consequence, below ~10 hPa or 30 km, number density versus altitude trends are slightly more positive than mixing ratio versus pressure trends.

The figure panel shows the result of McLinden and Fioletov (2011) applied to trends in mixing ratio versus pressure, *VMR(p)*, and in number density vs. altitude, *nd(z)*. Trends are shown for the two periods: 1979–1997, when both stratospheric ozone and temperature declined; and 2000–2013, when ozone increased and the temperature decreased. The biggest effects of cooling and the largest differences in ozone trends occur above 35 km. The clear 1–2% per decade effect near 2 hPa before 1997 is consistent with differences between upper stratospheric trends from SAGE (*nd(z)*) and SBUV (*VMR(p)*). After 2000, the trend differences are smaller (1% per decade or less), because the temperature decline was 60% less than that before 1997 (see Chapter 4). The substantial uncertainty of ozone trends derived from any given instrument means that the smaller coordinate-related differences after 2000 are hard to resolve.

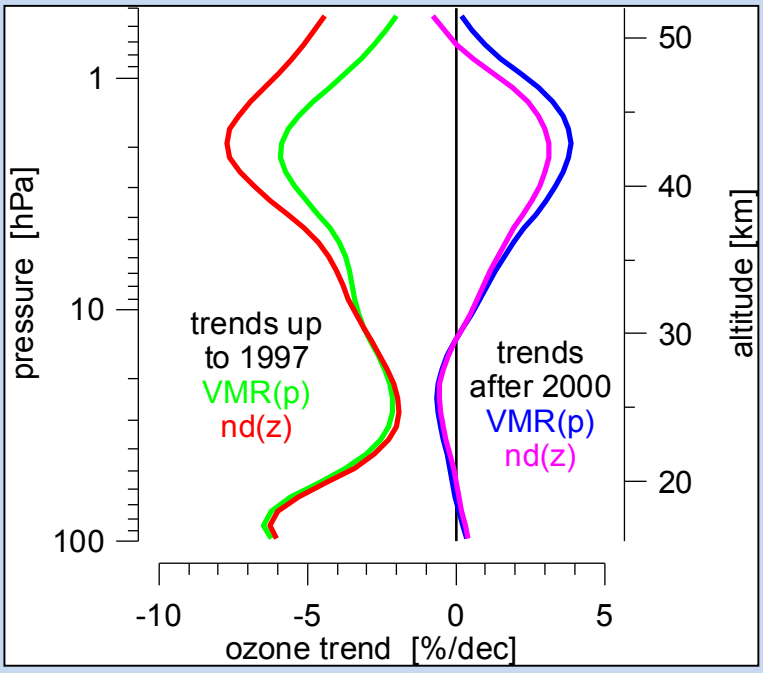

2.2.2 Data Quality

Since the WMO (2011) Assessment there have been small improvements, but no major changes in data quality and uncertainty estimates for ground- and space-based ozone observing systems. Uncertainties for total ozone columns, monthly or annual means, are typically below 1%. Biases of individual systems are typically also 1% or less. Recent studies confirm this: UV total ozone data sets created from GOME, SCIAMACHY, and GOME-2 ozone records (Table 2-1), for example, show very good agreement with ground data and other satellites, within 1% in monthly zonal means, and with drifts generally well below 1%/decade (Weber et al., 2005; Koukouli et al., 2012; Chiou et al., 2014; Lerot et al., 2014). Comparisons of column ozone from SBUV V8.6 with Dobson- and Brewer-spectrometer data also show agreement, 1% or better, over a thirty-year time span (Labow et al., 2013; McPeters et al., 2013).

For ozone profiles, uncertainties are generally larger, of the order of 2 to 5% for the best instruments. Since the last Assessment (WMO, 2011), the SPARC Data Initiative (Tegtmeier et al., 2013), and the SI2N initiative on Past changes in the Vertical Distribution of Ozone (Hassler et al., 2014) have provided platforms to assess accuracy, precision, and stability of existing ozone profile records. Final results from SI2N are not yet available, but nearly all recent studies confirm the general picture that ozone profile uncertainties are smallest between 20 and 40 km altitude (pressures between 50 and 2 hPa), and are usually better than 10% for most instruments, and better than 2 to 5% for some instruments, including SAGE II, MLS, OSIRIS, and GOMOS (Tegtmeier et al., 2013; Adams et al., 2013, 2014; Eckert et al., 2014; Damadeo et al., 2013; Kramarova et al., 2013a; Remsberg, 2014). Above this region, ozone decreases rapidly and uncertainties increase, for many instruments to 20% and more. Diurnal variations also play an increasing role above 30 to 40 km (10 to 2 hPa pressure), see Section 2.3.1. Below 20 km (pressure higher than 50 hPa), transport-driven ozone variability increases considerably. Sharp vertical ozone gradients occur and, especially near the tropopause, ozone concentrations are very low. In this region uncertainties increase substantially, to values larger than 20 to 30%, also due to limitations in sampling and altitude resolution. Limb sounding instruments, for example, have typical altitude resolutions of only 2–3 km in this region (Tegtmeier et al., 2013; Sofieva et al., 2013; Hassler et al., 2014). SBUV ozone retrievals cannot separate contributions from lower stratospheric and tropospheric ozone (McPeters et al., 2013; Kramarova et al., 2013b).

Time series of monthly-mean inter-instrument differences evaluated, e.g., in the SPARC Data Initiative (Tegtmeier et al., 2013; see Figure 2-1) confirm that monthly, zonal-mean ozone values from several limb-sounding satellites usually differ by less than 10–15% near 16 km (100 hPa), and less than 2 –5% near 33 km (7 hPa). Some instruments, however, show substantial drifts and larger biases. A striking example is given in the left panel of Figure 2-1. At this particular pressure and latitude band, one data set (GOMOS) exhibits a clear drift and should probably not be used. Near 7 hPa (see Figure 2-1) SCIAMACHY shows a large time-varying bias against the other instruments, about ±5% in phase with the QBO. For SBUV, a QBO related bias is attributed to SBUV's very coarse altitude resolution (Kramarova et al., 2013b). Good long-term stability and drifts of less than 2% per decade over the altitude range from 20 to 40 km are reported for SAGE, HALOE, UARS MLS, and Aura MLS ozone records against ground-based lidars (Nair et al., 2011, 2012; Kirgis et al., 2013). More details on the various systems can be found in Appendix 2A. Overall, drift uncertainties in the best individual ozone profile records are usually smaller than 2 to 5% per decade, but larger in the lowermost stratosphere. Only multiple independent records allow identification of bad records (like GOMOS in Figure 2-1). Averaging over several records removes noise and improves the precision. In this Assessment, averaging is done (on the basis of anomalies where the average annual cycle and bias of each instrument has been removed) for the HARMOZ record, which combines six European satellite limb sounders. The ozone profile time series in Section 2.2.4 indicate that for the best data sets drifts, and trend uncertainties, better than 1 to 2% can be achieved over the last 10 to 15 years, where many ozone profile records exist. Before 1990, however, only few records exist and profile trend uncertainties are larger.

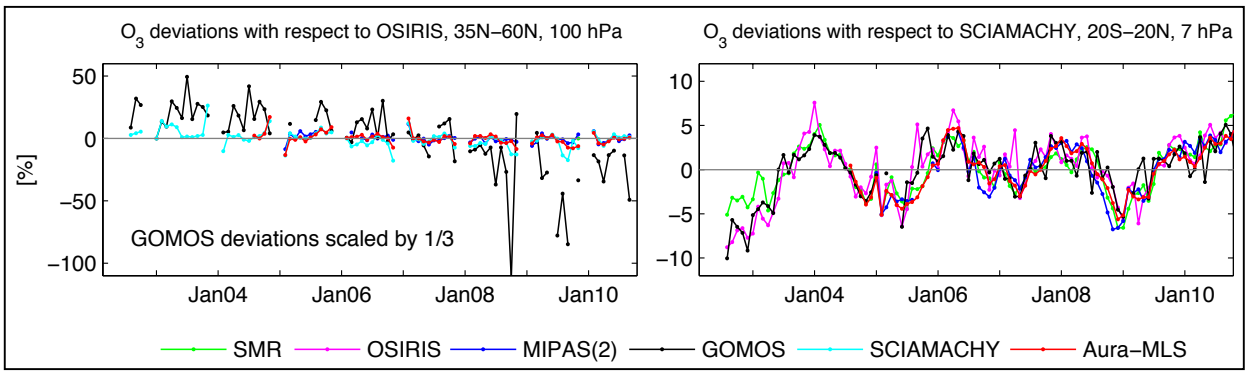

Figure 2-1. Time series showing zonal-, monthly-mean ozone differences between different instruments for 2002–2010. Differences are expressed as a percentage from the reference. The left-hand panel shows differences at northern middle latitudes near 100 hPa, using OSIRIS V5.0 data as the reference data set. Differences are shown for SMR (green), MIPAS (blue), SCIAMACHY (cyan), and Aura-MLS (red). Differences for GOMOS (V5.0) data are also shown (black) but these are scaled by 0.33 as they are much larger than those for the other data sets. Similarly, the right-hand panel shows differences relative to SCIAMACHY (V2.5) near 7 hPa in the tropics. Colors are the same as in the previous panel and the OSIRIS curve is shown in pink. Adapted from Tegtmeier et al. (2013).

2.2.3 Changes in Total Column Ozone

2.2.3.1 Time Series

For the total ozone data sets in Table 2-1, Figure 2-2 shows time-series of annual-mean total ozone anomalies since 1964 for four regions: global (60°S–60°N), midlatitudes in both hemispheres (35°–60°), and tropics (20°S–20°N). Anomalies were computed from monthly zonal mean total ozone data by subtracting the annual cycle over the period 1998–2008, individually for all data sets. This reference period was chosen because: (1) levels of ozone and ODSs were fairly constant from 1998 to 2008; (2) nearly all total column and profile ozone data sets provide data for a large part of this period; (3) it is long enough to cover one solar cycle and provide a stable baseline; and (4) it is not influenced by major volcanic eruptions.

In addition to the observations, the gray range in Figure 2-2 shows the range of simulated total ozone anomalies from the Chemistry-Climate Model Validation 2 activity (CCMVal-2, see Box 2-2: Eyring et al., 2010; SPARC, 2010). This ensemble of simulations from 17 CCMs was used in the WMO (2011) Assessment. Four of the same models have recently simulated ozone time series on the basis of recently updated ODS lifetimes, as described in Chapter 1 and SPARC (2013), but the long-term changes in ozone are virtually the same as those in CCMVal-2 (see Section 2.4.1). Thus the CCMVal-2 ozone results used in WMO (2011) remain viable for use in this Assessment.

The gray range of CCMVal-2 simulations in Figure 2-2 gives the multi-model mean anomaly (from the 1998 to 2008 baseline) and 2 standard deviations of individual annual mean anomalies. The multi-model mean (and standard deviation) comes from 15 CCMs. Two models (MRI and CNRM-CMM) with known deficiencies were omitted (see Oman et al., 2010b; Michou, 2011). This approach to presenting the CCMVal-2 results differs from the last Assessment, where the complex Time Series Adaptive Method (Scinocca et al., 2010; WMO, 2011) was used to define the range of simulated ozone values. Because the TSAM method cannot readily be applied to observed time series, the simpler approach of computing means and standard deviation over sliding five-year windows and multiple models defines the range of simulated interannual, and, to a lesser degree, intermodel variability. The use of a

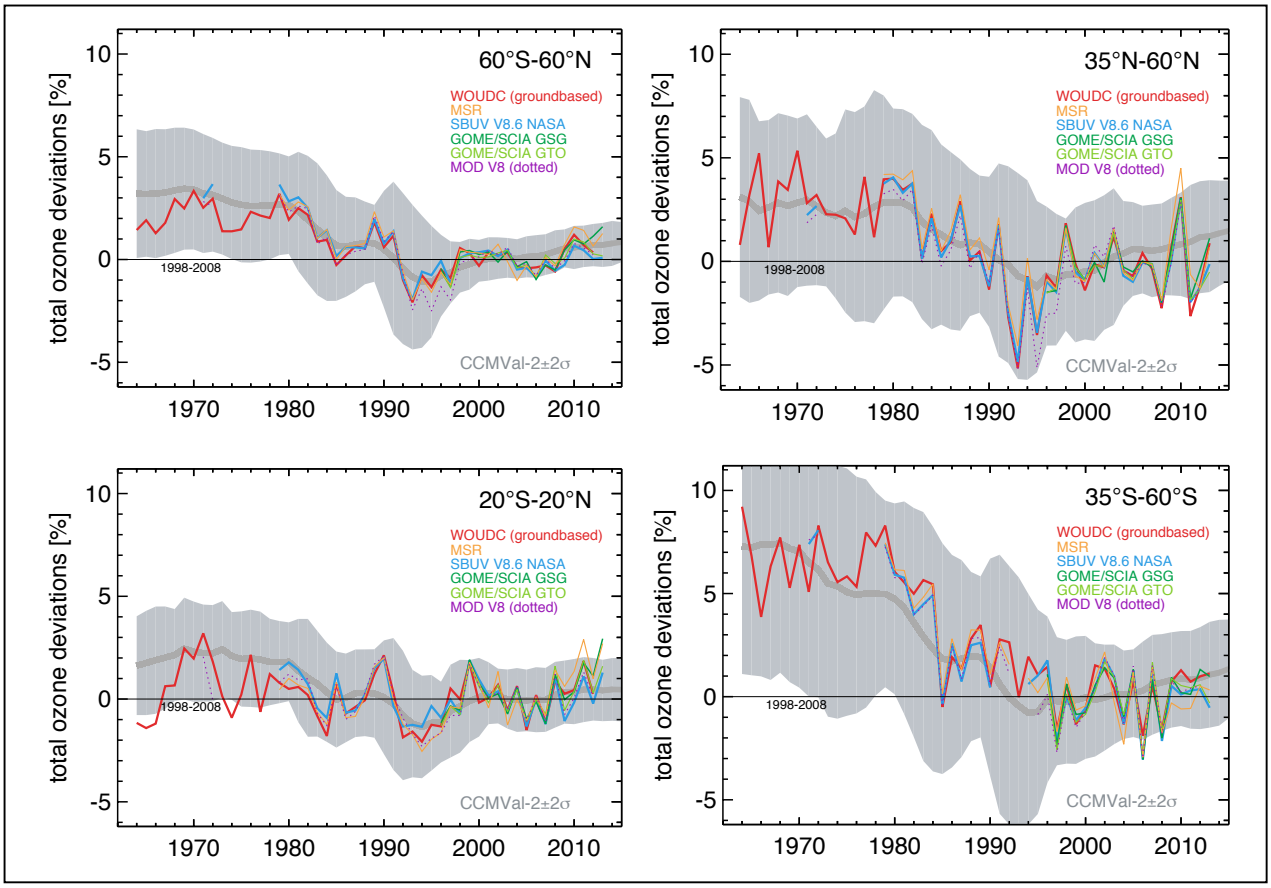

Figure 2-2. Total column ozone annual mean anomalies for different data sets. Anomalies are with respect to the 1998 to 2008 mean of each individual data set. Top left: 60°S–60°N (global), top right: 35°N–60°N (Northern Hemisphere), bottom left: 20°S–20°N (tropics), bottom right: 35°S–60°S (Southern Hemisphere). Colored lines give observed results for the data sets from Table 2-1. Gray line and gray range give multi-model mean and ±2 standard deviation range of annual mean anomalies simulated by CCMVal-2 models (Eyring et al., 2010; WMO, 2011). The model simulations account for changing ODSs, GHGs, and a QBO. Up to about 2000, all simulations also account for the 11-year solar cycle, volcanic aerosol, observed sea surface temperatures, and sea ice coverage. After about 2000, sea surface temperature and sea ice are prescribed from other model simulations, and no solar cycle is included for most models. See text for details.

1998–2008 baseline spreads systematic differences to the beginning and end of the time series. The nearly identical treatment of simulations and observations in Figure 2-2 (and later Figures 2-5 to 2-8) allows direct comparison of observed ozone variations with the range of simulated interannual variations. Note that reducing the number of models used (e.g., from 15 to 9 or 7) barely changes the width of the gray range in Figure 2-2 and later figures (see also Eyring et al., 2010; WMO, 2011). While recent studies discuss reducing the uncertainty range of multi-model simulations (Charlton-Perez et al., 2010; Strahan et al., 2011; Douglass et al., 2012; Karpechko et al., 2013), by selecting only a few (say, better-performing) models, this has not been done for the present Assessment. One motivation is that scenario uncertainty is not covered by the current CCMVal-2 simulations (all use the same scenario, see next paragraph), but will increase the range of simulated ozone, especially in the second half of the 21st century (Eyring et al., 2013; see also Section 2.4.3).

Box 2-2. Model Simulations

This Assessment uses simulations from a range of atmospheric models that have been used in previous Ozone Assessments and in recent international multi-model intercomparisons. These models can be divided into several general types:

- Chemical Transport Models (CTMs): CTMs are used for detailed calculations of chemical processes, using wind and temperature fields specified from meteorological analyses or from another model. There is no coupling between chemical species and radiation and transport in CTMs. They are often used for investigations of chemical processes.
- Chemistry-Climate Models (CCMs): These models explicitly couple chemical processes to radiation and transport in the model, but generally do not couple to ocean models. The chemistry mechanism can be appropriate for the stratosphere only, the troposphere only, or coupled troposphere-stratosphere investigations.
- Atmosphere-ocean general circulation models (AOGCMs): These models include a dynamic ocean and coupled atmosphere-land-ocean-sea ice interactions and are primarily developed to understand surface and tropospheric climate variability and change. They generally do not include interactive chemistry processes, and rely on prescribed data sets for ozone and other radiatively important species. Until recently, these models typically had coarse resolution in the stratosphere and lower model upper boundaries than CCMs.

While CCMs and AOGCMs have traditionally been used for different purposes, some AOGCMs now include some interactive chemistry and higher upper boundaries. Similarly, some CCMs now include a dynamical ocean and sea ice. CCMs and AOGCMs have been used in three recent multi-model intercomparisons that are drawn on in this Assessment:

- The second *Chemistry-Climate Model Validation (CCMVal-2)* activity (SPARC CCMVal, 2010) is a comparison of CCMs with stratospheric chemistry and a resolved stratosphere. This activity focused on understanding and projecting the evolution of stratospheric ozone and ozone-climate interactions. In these experiments, ozone-depleting substances (ODSs) followed the adjusted halogen scenario of WMO (2007). Greenhouse gases followed the Special Report on Emissions Scenarios (SRES) A1B scenario from the Intergovernmental Panel on Climate Change (IPCC) (2007). See Table 1 (below) for scenarios used. Many results from CCMVal-2 were discussed in the last Ozone Assessment (WMO, 2011).
- The *Coupled Model Intercomparison Project, Phase 5 (CMIP5)* (Taylor et al., 2012) is a comparison of AOGCMs that contributed significantly to the IPCC Assessment Report 5 (IPCC, 2013). Most (80%) of these models do not include interactive chemistry, and only one-third of them resolve the full stratosphere (model tops above 1 hPa). Both historical (1850–2005) and future scenario experiments (2006–2100) are included. See Table 1 for scenarios used.
- The *Atmospheric Chemistry and Climate Model Intercomparison Project (ACCMIP)* (Lamarque et al., 2013) is a comparison of CCMs with troposphere or troposphere-stratosphere chemistry. ACCMIP supplemented the CMIP5 simulations, focusing on tropospheric chemistry-climate interactions.

Box 2-2, Table 1: Summary of chemistry-climate model experiments used for this report.

Activity	Scenario	Model Type	Years	Stratospheric Ozone Forcing (ODS and precursor changes)	Other Forcings	Strato-spheric Chemistry	Interactive Ocean
CCMVal-2 [1]	REF-B1	CCM	1960–~2004	Observed	Observed GHGs, solar variability, volcanic aerosols, SST [x]	Yes	1 of 17 models
CCMVal-2 [1]	REF-B2	CCM	1960–2100	A1 scenario WMO (2007)	SRES A1B GHGs (IPCC, 2007), model SST, fixed solar [x, y]	Yes	1 of 17 models
CMIP5 [2]	Historical	AOGCM	1850–2005	Observed	Observed GHGs, volcanic and anthropogenic aerosols, solar variability [x]	18 out of 45 models	Yes
CMIP5 [2]	RCP 2.6, 4.5, 6.0, 8.5	AOGCM	2006–2100	A1 scenario WMO (2003)	Four RCP scenarios, aerosols, land-use, tropospheric ozone, repeating solar cycle [x]	18 out of 45 models	Yes
CMIP3 [3]	SRES A1B	AOGCM	2000–2099	A1 scenario WMO (2003)	Mid-range GHG emissions, aerosols, tropospheric ozone, fixed solar	No	Yes

[1] WMO (2011); Eyring et al. (2010). [2] Taylor et al. (2012); Eyring et al. (2013). [3] Meehl et al. (2007).
[x] Most CCMVal-2 simulations include a nudged or model-generated quasi-biennial oscillation (QBO), whereas most CMIP5 model simulations do not include a QBO. [y] Several CCMVal-2 models include variable solar cycle forcing in their REF-B2 simulations.

For Figure 2-2, (and Figures 2-5 to 2-8) up to 2004 (1999 for some models), the simulations account for changing ODSs (adjusted A1 scenario, WMO, 2007), changing GHGs (SRES A1B scenario, IPCC, 2007), solar cycle and volcanic forcings, observed sea surface temperatures and sea ice coverage, and the quasi-biennial oscillation (QBO) (REF-B1 scenario, see Table 1 in Box 2-2). After 2004 (or 1999 for some models), the simulations include changing ODSs and GHGs (same scenarios as above), modeled sea surface temperatures and sea ice, and an internally generated QBO (for models that have one), but no volcanic forcing and usually no solar cycle forcing (REF-B2 scenario). Three of the CCMs apply solar cycle forcing. The common 1998 to 2008 baseline and the sliding five-year window allow these REF-B1 and REF-B2 simulations to be combined, but the absence of volcanic and solar forcing substantially reduced the variability range after 2000 in Figure 2-2.

Figure 2-2 extends results from previous Assessments. At midlatitudes, and in the 60°S to 60°N near-global mean, total ozone columns show a clear decline from the late 1970s to the mid-1990s. This decline has stopped. Since about 2000, observed ozone columns have been fluctuating around a more or less constant level (compare with the 1998 to 2008 baseline in Figure 2-2). This long-term behavior is in good agreement with previous Assessments. Agreement between different data sets is also good, typically better than 1% (see also Section 2.2.2).

CCMVal-2 model simulations attribute most of the long-term ozone decrease before the mid-1990s to increasing ODSs and the subsequent leveling off to the small decline of ODSs, by about 15% since 2000 (WMO, 2003, 2007, 2011). The pronounced minimum in the Northern Hemispheric ozone in the 1990s arose from additional loss associated with the Mt. Pinatubo eruption in 1991 and several cold Arctic stratospheric winters (WMO, 2003, 2007, 2011). A clear minimum related to the Mt. Pinatubo eruption was not observed in the Southern Hemisphere (see also Section 2.3.4).

In the tropics, observed total ozone has remained nearly unchanged, with substantial interannual variability due to the QBO, tropical El Niño and La Niña events (El Niño-Southern Oscillation (ENSO)), and the 11-year solar cycle (see previous Assessments and Sections 2.3.2 and 2.3.3). Tropical ozone columns in recent years show a slight increase, as expected, at least in part, from the maximum of solar cycle 24 in 2012 to 2014. In contrast to the observations, which show little long-term column-ozone change from the 1960s/1970s to the 1990s, the CCMVal-2 simulations show a decline (Figure 2-2, lower left). However, this difference is less obvious in Figure 2-2 than reported in WMO (2011). Note that the difference relies on ground-based observations in the early years only, and is roughly twice the 1% systematic uncertainty of total ozone columns from Dobson spectrometers (Fioletov et al., 2008; Labow et al., 2013; Appendix 2A).

Between 60°S and 60°N current ozone levels are on average 2% below the 1964–1980 mean. At northern midlatitudes, ozone levels are on average 3.5% below the pre-1980 values. In the Southern Hemisphere, current levels are on average 6% below pre-1980 values. These numbers are essentially the same as reported in WMO (2011). Figure 2-2 shows superimposed substantial year-to-year variations by several percent, also in the last decade, which clearly complicate the identification of small trends, like the small increase expected since about 2000 from the turnaround of ODS and from model simulations.

2.2.3.2 INTERANNUAL VARIATIONS

Figure 2-3 focuses on ozone variations since the year 2000, a period with little overall change in total ozone levels (see Figure 2-2 and previous Assessments for variations before 2000). Most obvious are the QBO-related variations in the tropics and (usually of opposite sign) in the extratropics (Baldwin et al., 2001). Sometimes the tropical anomalies seem to be exported to the extratropics, delayed by about a year (Tegtmeier et al., 2010). The largest interannual variations occur in winter and at high latitudes, for example the high total ozone at northern midlatitudes in 2002/2003, 2009/2010, and 2013, or in the Southern Hemisphere in late 2002 (polar vortex split) and 2012/2013. Examples for large ozone deficits in the Northern Hemisphere (NH) are 2008 and 2011 (large polar ozone loss: see Chapter 3; Manney et al., 2011), or 2006 in the Southern Hemisphere (SH, largest ozone hole on record: see Chapter 3).

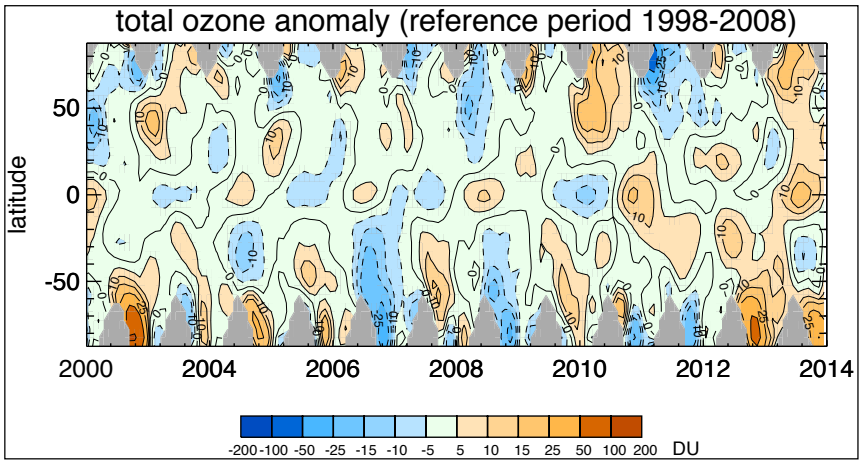

Figure 2-3. Observed monthly zonal mean total ozone anomalies as a function of time and latitude. Results are from the GOME/SCIAMACHY/GOME-2 (GSG) merged data set (see Table 2-1). Anomalies are with respect to the mean annual cycle obtained for the period 1998 to 2008. For clarity, data are smoothed over three months and three 5° latitude bands.

It is well known that these interannual variations are due to year-to-year variations in the strength of the polar winter vortices, (random) stratospheric warmings, and variation of the Brewer-Dobson circulation (BDC), which transports ozone from low latitudes to the winter pole (WMO, 1999, 2003, 2007, 2011). Recent studies have confirmed this and have quantified some of the very large variations observed since the last Assessment. The unusually high total ozone columns in the NH in 2010, for example, are related to the negative phase of the AO (Arctic Oscillation) or NAO (North Atlantic Oscillation) (Rieder et al., 2010a, 2010b; Ossó et al., 2011; Steinbrecht et al., 2011; Weber et al., 2011). Both oscillations are related to the BDC, and both describe nearly the same atmospheric anomalies. In the SH, the Antarctic Oscillation (AAO) plays a role for the high ozone columns in 2012 (Kramarova et al., 2014). Progress has been made on influences from ENSO (Brönnimann et al., 2013; Oman et al., 2013; Rieder et al., 2013; see also Section 2.3.3). Long-term variations in these large meteorological influences, which easily exceed 5% or 15 DU (see Figure 2-3; or Frossard et al., 2013), and uncertainty on the 11-year solar cycle variation (around 2% or 5 DU peak-to-peak, Brönniman et al., 2013; see also Section 2.3.2), complicate detection of the expected small total ozone increase due to declining ODSs, which is only about 1% or 3 DU since 2000; see the CCMVal-2 mean in Figure 2-2.

2.2.3.3 TOTAL OZONE TRENDS

As in previous Assessments (WMO, 1995, 2003, 2007, 2011), multiple linear regression (MLR) is used to estimate ozone trends and to account for the just-mentioned ozone variations due to natural factors (QBO, ENSO, volcanic aerosol, solar cycle). Here we use MLR on the basis of annual means for total ozone and monthly means for profile data (Section 2.2.4). ODS values reached their maximum around 1997 (Chapter 1) and there are different approaches to express ODS changes in the regression:

(a) Two simple linear trends that are not necessarily joined at the ODS inflection time.
(b) Piecewise linear trends (PWLT), with two linear trends connected at the ODS inflection time, or, alternatively, a continuous linear trend plus a trend-change term. Mathematically, both yield the same regressed time series (Newchurch et al., 2003; Reinsel et al., 2005; Jones et al., 2009; Nair et al., 2013; Chehade et al., 2014).
(c) Fitting Equivalent Effective Stratospheric Chlorine (EESC; Newman et al., 2007), as in Yang et al. (2006), Mäder et al. (2010), Steinbrecht et al. (2011), Nair et al. (2013), Frossard et al. (2013), and Chehade et al. (2014).

A disadvantage of fitting EESC is that the ratio of ozone "trend before" to "trend after" (the ODS inflection time) is prescribed by the shape of the EESC curve. While the goodness of EESC fits does indicate overall agreement of ozone and ODS changes, the prescribed shape of the EESC curve precludes the independent estimation of an ozone increase after the ODS maximum. This is possible with PWLT,

and most studies use 1997 as the inflection time (Harris et al., 2008; WMO, 2011), although the exact year is not very critical (Mäder et al., 2010). Low ozone values around the inflection time (e.g., due to Mt. Pinatubo aerosol after 1991) can result in a larger decline before 1997, and a larger increase after 1997 (see Figure 2-2). Therefore, in this Assessment a three-step process corresponding to regression approach (a) is used, similar to Newchurch et al. (2003). (1) A full MLR including PWLT (or EESC) contribution is applied to the time series, mainly to estimate QBO, ENSO, solar-cycle, and aerosol related ozone variations. (2) Ozone "residuals" are obtained by subtracting the QBO, ENSO, solar-cycle, and aerosol variations from step (1). These ozone "residuals" will then be rid of all contributions but still contain the long-term trends. (3) Two simple linear trends, from the beginning of each record up to 1997 and from 2000 to the end of each record, are fitted separately to the ozone "residuals." The year 2000 was selected as starting point for the second trend because: (1) it is after the peak of stratospheric chlorine loading; (2) the period between 2000 and the end of most data records (2011 to 2013) covers one full solar cycle, so this should minimize uncertainties in accounting for the solar cycle; and (3) 2000 is close to the beginning of the Odin- and Envisat-based HARMOZ ozone profile data sets starting in 2001/2002, allowing better comparison with results from this ozone profile data set.

Uncertainties for the derived trends are estimated from the standard deviation of the fit residual, as in Newchurch et al. (2003), Kyrolä et al. (2013), or Gebhardt et al. (2014), and are corrected for first-order autocorrelation in the fit residuals (Weatherhead et al., 2000). Note that this is not enough to account for longer-range correlations, so uncertainty bars may still be underestimated by a factor up to 1.5 (Vyushin et al., 2007, 2010). For the CCMVal-2 simulations, trends are estimated by linear regression, similar to the trend estimation for the observations. Trends are estimated individually for each model from the REF-B2 runs, which do not include forcing by solar cycle and volcanic aerosol. Individual model trends are then averaged over all models. Mean and standard deviation are used as CCMVal-2 multi-model trend and uncertainty (see also Figure 2-25 of WMO, 2011).

Figure 2-4 shows the resulting total ozone trends from 1979 to 1997, and from 2000 to 2013, as a function of latitude. Observed trends, derived by the three-step method, are given by the colored bars, which also give their uncertainty range. Dashed lines show the range of ozone trends obtained from fitting EESC to the observations (Approach c). The gray background gives the range of trends obtained from the CCMVal-2 simulations (see also Figure 2-2). Before 1997, the observed linear trends are negative everywhere, except for the inner tropics, and in good agreement with EESC trends, within uncertainty. Except for the tropics, observed trends before 1997 are also in good agreement with the simulations. These have a larger uncertainty range (Figure 2-2) due to differing sensitivity of models to ODS and other influences (Charlton-Perez et al., 2010; Strahan et al., 2011; Douglass et al., 2012). The negative ozone trends before 1997 are consistent with previous Assessments. Outside of the tropics they are largely due to increasing ODS (WMO, 1999, 2003, 2007, 2011).

After 2000, the computed linear trends are positive, around 1 to 2% per decade, at most latitudes. As expected due to the shorter period, uncertainty bars, ±1 to 2% per decade (2σ), are larger than for 1979 to 1997. Poleward of 40°N, the post-2000 trends are not significant for most of the data sets. SBUV V8.6 trends are not significantly different from zero in the entire NH. Poleward of 30° latitude in both hemispheres, the observed linear trends agree between data sets. There, they also agree with the range of trends obtained by fitting EESC (over the entire 40-year period) and with the range of CCMVal-2 simulated trends. Especially in the NH, transport variations play a significant role (e.g., Kiesewetter et al., 2010; Steinbrecht et al., 2011; Weber et al., 2011; Frossard et al., 2013; Rieder et al., 2013), but are not accounted for in the present regression (as in WMO, 2007, 2011). This contributes to the uncertainties.

Between 30°S and 30°N, however, the large observed 2000 to 2013 trends from ground-based, GOME-SCIAMACHY-GOME-2, and Multi-Satellite-Reanalysis (MSR) data are often outside of the ranges expected from EESC (dashed lines) and simulations (gray range). Trends from SBUV V8.6 (and V8.0) are smaller, and are compatible with EESC and with simulations. The reason for the fairly large positive trends of some data sets in the tropics is currently not clear. Changing the initial year for the trend computation (e.g., from 2000 to 1997) does not change the trends significantly. Figure 2-2 (lower left

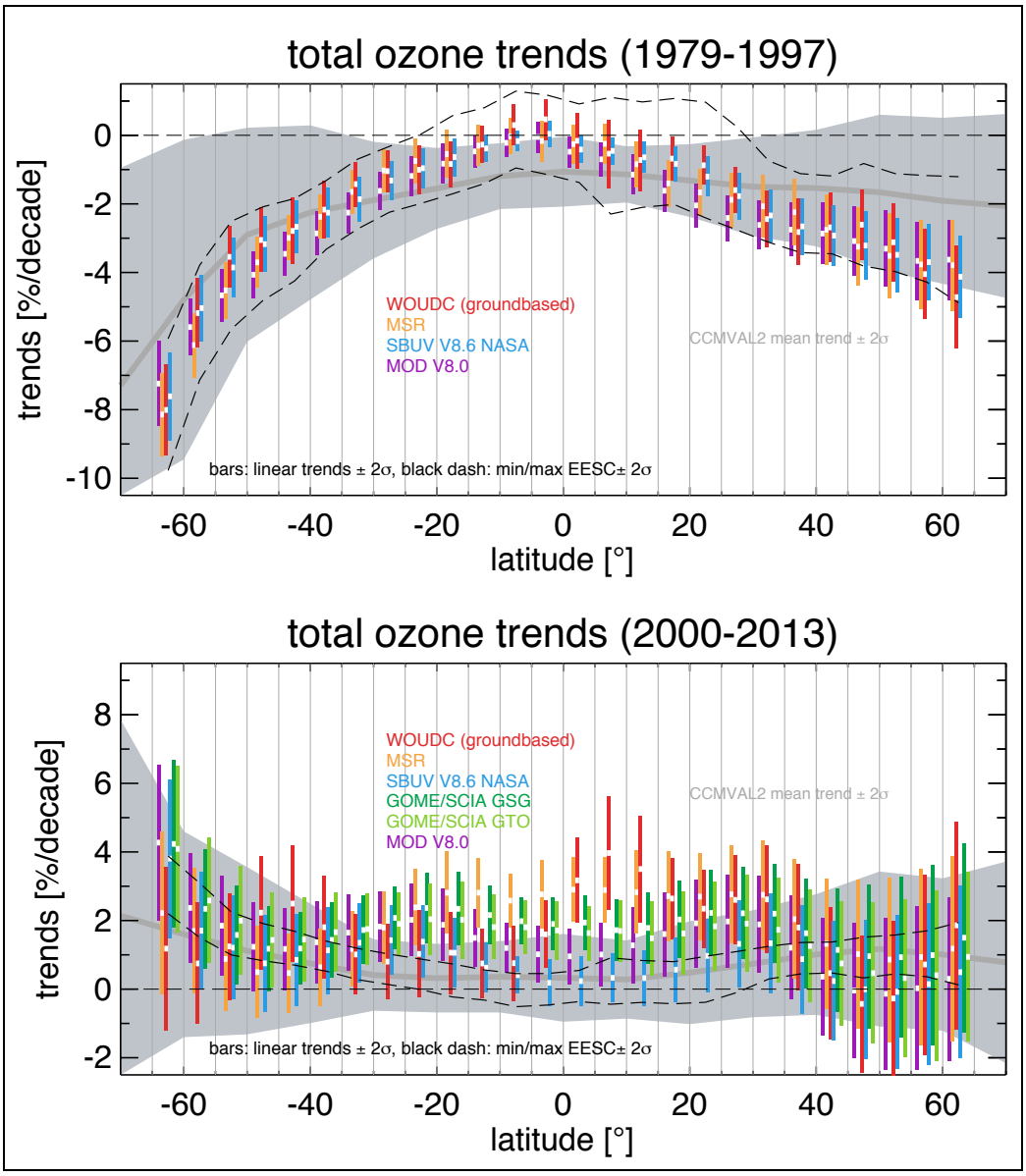

Figure 2-4. Ozone trends for different merged total ozone data sets, as a function of latitude. Top: Trends from 1979 to 1997. Bottom: Trends from 2000 to 2013. Observed trends are derived using multiple linear regression (MLR) to account for solar cycle, QBO, volcanic aerosols, and ENSO. See text for details. The white dots give the linear trend in % per decade, the colored vertical bars indicate the ±2σ uncertainty range from the regression. Gray areas give average trend and ±2 standard deviation range of individual model trends from CCMVal-2 simulations (Eyring et al., 2010; WMO, 2011). Model trends were derived from REF-B2 simulations accounting for ODS and GHG changes, and including an internal QBO, but using only modeled sea surface temperatures and sea ice. Different from Figure 2-2, forcings from volcanic aerosol and 11-year solar cycle were not included in these simulations (except for three models that did include the solar cycle). The black dashed lines give the range of linear trends arising from MLR fits to the observations that include Equivalent Effective Stratospheric Chlorine (EESC) as a proxy for ODS changes. The fitted EESC coefficients usually give a negative ozone trend while EESC increases from 1979 to 1997, and a positive ozone trend while EESC declines from 2000 to 2013. For the EESC, a mean age-of-air of three years and width of 1.5 years were assumed (Newman et al., 2007).

panel) indicates that instrumental uncertainties may play a role, since the different data sets diverge by about 1% in the last years. Also, due to the different lengths of the data sets (50 years ground-based, >30 years SBUV, <20 years GSG), accounting for the solar cycle in the regression may make some difference (see also Section 2.3.2). Uncertainties may also be underestimated (Vyushin et al., 2007, 2010). Discrepancies between simulated and observed total ozone column trends in the tropics, therefore, remain. Before 1997, the decline detected from observations was smaller than in the CCMs (WMO, 1999, 2003, 2007, 2011). Since 2000, the total-ozone increases in some data sets are larger than those simulated.

Figure 2-4 shows that the total ozone column at most latitudes has a positive trend since 2000, but in many regions this trend is not statistically different from zero. This is consistent with WMO (2011) and with more recent studies using station data (e.g., Steinbrecht et al., 2011; Nair et al., 2013; Tully et al., 2013) and global data (e.g., Ziemke and Chandra, 2012; Krzyścin, 2012). As indicated by the black dashed lines for EESC trends in the lower panel of Figure 2-4, ODS-related total ozone increases since 1997 to 2000 should be small, <1% per decade at most latitudes, and not yet be detectable with the large current uncertainty margins of observed trends (mostly > ±1%/decade). Figure 2-4, thus, shows that total ozone has not been decreasing further after the mid-1990s, confirming the effectiveness of the Montreal Protocol. However, a clear attribution of total ozone increases to declining ODSs is not yet possible. This is essentially the same conclusion as reached in the last Assessment (WMO, 2011).

2.2.4 Trends in Ozone Profiles

2.2.4.1 TIME SERIES

Like Figure 2-2 for total ozone, Figures 2-5 to 2-8 show time series of ozone profile annual mean anomalies at selected altitude or pressure levels. Section 2.2.1 and Table 2-2 summarize the profile data sets that were used. Data sets using altitude coordinates are for the altitudes given in the figures; data sets using pressure coordinates are at the given pressures. Ground-based station data are also included, although the number of stations in the tropical and southern midlatitude bands is very limited (see Figure 2A-1 of Appendix 2A). All data sets are normalized to their 1998 to 2008 average annual cycles (same as for total ozone in Section 2.2.3).

These updates and additions give a comprehensive picture of ozone profile variations, but they have not resulted in major changes of our understanding from the last Assessment (WMO, 2011). For the upper stratosphere near 42 km/2 hPa, Figure 2-5 shows the well known ozone decline due to increasing ODS from the 1970s to the mid-1990s (WMO, 1999, 2003). Since 1995 to 2000, the decline is followed by a leveling off, as expected from the turnaround of ODSs after 1997 (WMO, 2007, 2011). In the last years, in most panels, the ozone values are usually above the zero line (=1998 to 2008 climatology), and indicate an ozone increase from around 2000 to 2012 or 2013. This increase is most visible in the 35°N to 60°N and 60°S to 35°S latitude bands. In the tropical band, data in recent years indicate little or no increase, only elevated ozone around the solar-cycle maxima, near 2001 and 2012. For the 60°S to 60°N mean, data points since 2009 also lie above the zero line.

Ozone time series at lower levels (Figures 2-6 to 2-8) also show the ODS-related long-term decline until the mid-1990s, and are generally leveling off since around 2000. However, long-term changes at these lower levels are less pronounced than at 2 hPa. Several aspects of Figures 2-6 to 2-8 are worth mentioning:

- At 31 km/10 hPa and at 26 km/20 hPa (Figures 2-6 and 2-7), QBO-related variations are pronounced, especially in the tropics (Baldwin, 2001; Kirgis et al., 2013; Kramarova et al., 2013b; Gebhardt et al., 2014).
- Near 31 km/10 hPa in the tropics (Figure 2-6), fairly high ozone values are recorded by several instruments between 2000 and 2003, whereas ozone has often been low after 2005. Thus, trend analyses over this period, e.g., of ozone records from instruments on the Odin and Envisat satellites, tend to indicate a decadal decline in the tropics around 31 to 35 km/10 to 5 hPa (Kyrölä et al., 2013; Eckert et al., 2014; Gebhardt et al., 2014).

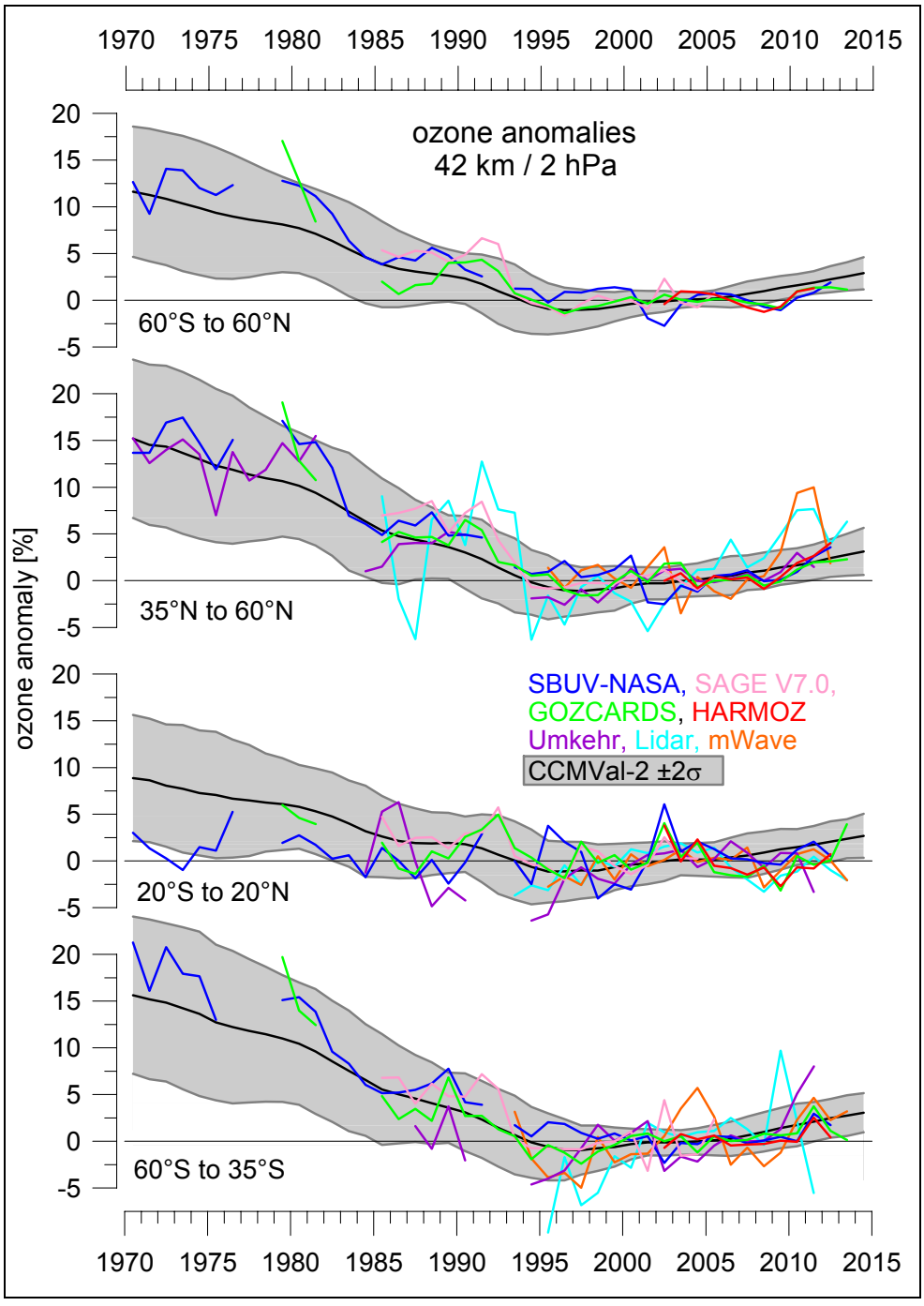

Figure 2-5. Annual mean ozone anomaly time series for different latitude bands, at 42 km altitude (for data sets using altitude coordinates) or at 2 hPa pressure (for data sets using pressure coordinates). Satellite data (see Table 2-2) are based on zonal means. NASA SBUV V8.6 (MOD V8.6) is given in blue, SAGE II V7.0 in pink, GOZCARDS in green, HARMOZ in red. Ground-based station data (Umkehr, lidar, microwave; see Table 2-3, and also Figure 2A-1 of Appendix 2A) are averaged over the zonal bands. Umkehr data in purple, lidar in cyan, microwave data in orange. The gray background gives the CCMVal-2 multi-model mean, and ±2 standard-deviation range of individual annual means, same as in Figure 2-2 for total ozone. All anomalies are with respect to the average annual cycle during 1998 to 2008, determined individually for each data set/instrument/model.

Table 2-3. Remote sensing stations used for ozone profile data sets in this report.

Station	Latitude / Longitude	FTIR	Lidar	Microwave	Umkehr
Lauder	45.0°S / 169.7°E	01/2001 to 12/2012	12/1994 to 06/2012	10/1992 to 10/2013	02/1987 to12/2011
Wollongong	34.4°S / 150.9°E	05/1996 to 12/2012			
Mauna Loa	19.5°N / 155.6°W		07/1993 to 08/2013	07/1995 to 10/2013	01/1984 to 12/2011
Izana	28.3°N / 16.5°W	03/1999 to 10/2012			
Table Mountain	34.4°N / 117.7°W		02/1988 to 08/2013		
Tateno Rikubetsu	36.0°N / 140.1°W 43.5°N / 143.8°E	05/1995 to 12/2009			08/1957 to 12/2011
Boulder	40.0°N / 105.3°W				05/1979 to 12/2011
Haute Provence	43.9°N / 5.7°E		07/1985 to 05/2013		01/1984 to 12/2011
Arosa Jungfraujoch	46.8°N / 9.7°E 46.6°N / 8.0°E	03/1995 to 12/2012			01/1956 to 12/2011
Bern Payerne	47.0°N / 7.5°E 46.8°N / 7.0°E			01/1994 to 12/2012 01/2004 to 12/2013	
Hohenpeissenberg	47.8°N / 11.0°E		09/1987 to 12/2013		

- Near 31 km/10 hPa and 26 km/20 hPa in the Southern Hemisphere (Figures 2-6 and 2-7), recent years indicate an ozone decrease from 2002 to 2005, and an increase from about 2005 to 2011, whereas in the Northern Hemisphere, ozone values were more or less constant over the last decade.
- Consistent with the high total column ozone observed in 2010 in the Northern Hemisphere (see Figures 2-2 and 2-3, and Section 2.2.3; Steinbrecht et al., 2011), the Northern Hemisphere profile data also report high ozone in 2010 from 19 to 31 km/70 to 10 hPa.
- In the tropical lower stratosphere (19 km/70 hPa, Figure 2-8), SAGE II data (V7.0), and the GOZCARDS record, which is based on SAGE II (V6.20), indicate a long-term decline from 1985 to about 2005 (Randel and Thompson, 2011; Sioris et al., 2014). However, also from Figure 2-8 it appears that this decline has not continued over the last decade (Gebhardt et al., 2014). Note further the importance of El Niño in the tropical lower stratosphere, i.e., low ozone values associated with El Niño events (e.g., 1998, 2010), and high values associated with La Niña events (e.g., 1985, 1989, 1999/2000, 2011). See Section 2.3.3 for further discussion.

Unlike the largely ODS-related ozone changes at most altitudes and latitudes, the ozone decline in the tropical lowermost stratosphere (19 km/70 hPa, Figure 2-8) has been attributed to a long-term increase of the mean meridional upwelling of the Brewer-Dobson circulation (BDC) (Randel and Thompson, 2011; Randel and Jensen, 2013), which enhances vertical transport of ozone-poor air in the tropics. CCMs predict such an increase and simulate a continuing ozone decline in the tropical lowermost stratosphere (Eyring et al., 2010; WMO, 2011). However, model simulations (black line and gray range in Figure 2-8) and observations also indicate substantial interannual and decadal variability, and no clear decline since 1997. Observational evidence for the long-term decline before 1997 relies substantially on the high ozone values reported by SAGE II from 1985 to 1990. SAGE II has only sparse sampling in the tropics, but is

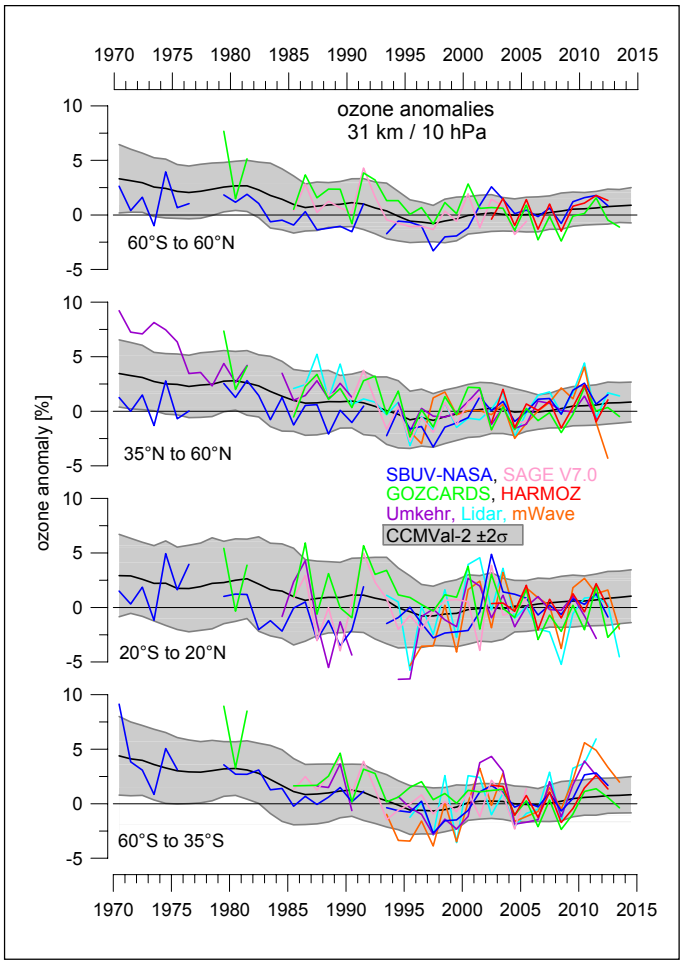

Figure 2-6. Same as Figure 2-5, but for the 31 km/10 hPa level.

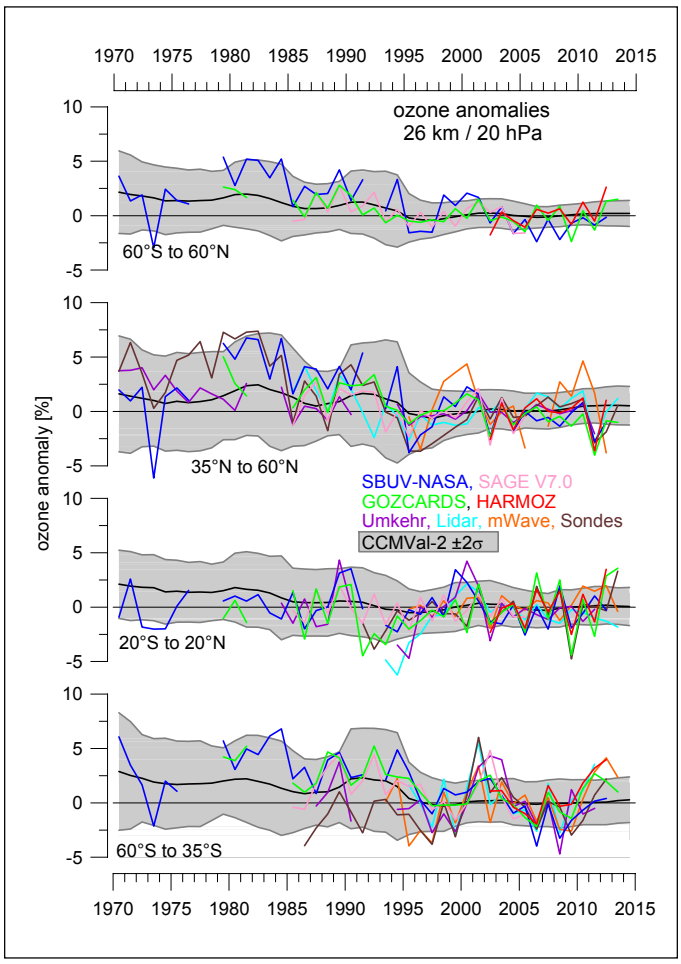

Figure 2-7. Same as Figures 2-5 and 2-6, but for the 26 km/20 hPa level. In addition, data from about 50 ozonesondes stations, averaged over the respective latitude bands are shown (see Figure 2-25). Note that SBUV NASA has only very coarse altitude resolution (10 to 15 km), and reports only one layer from the ground to ≈20 hPa/26 km for the 20°S to 20°N latitude belt.

the only credible observational data set for the tropical lowermost stratosphere before 1991. This, together with the leveling off of ozone in the tropical lowermost stratosphere since about 2000, suggested by multiple data sets in Figure 2-8, means that observational evidence for the modeled long-term ozone decline due to a strengthening BDC remains weak (see also Solomon et al., 2012). For further discussion see Section 2.4.2 and the more comprehensive discussion of the BDC in Chapter 4.

Figures 2-5 to 2-8 also contain information about uncertainty of the available ozone records and about possible drifts. Nearly all data sets show very similar ozone evolution, especially over the last 10–15 years (also due to normalization to the 1998 to 2008 period). The relative differences are larger in the early years (e.g., up to 15% between SBUV, Umkehr, and ozonesondes in the 1970s: Figures 2-6 and 2-7). Before 1985, and before 2000 at 19 km/70 hPa, there are not enough observations to determine ozone levels with a high level of confidence in the tropics and the SH. After 2000, the availability of multiple

and redundant data sets generally provides a higher level of confidence. Sampling issues also play a role, particularly when single station data are compared to zonal means (Gabriel et al., 2011a). This can be seen in the sometimes larger deviations of ground-based station data, such as lidars and microwave radiometers near 2 hPa in the 35°N to 60°N latitude band in 1986 and in 2010–2012 (Figure 2-5), or near 20 hPa from 1994 to 1996 for Umkehr and lidar data at Mauna Loa, which is located at 20°N near the edge of the tropics (Figure 2-8). Generally, however, Figures 2-5 to 2-8 confirm statements about data quality and drifts from Section 2.2.2.

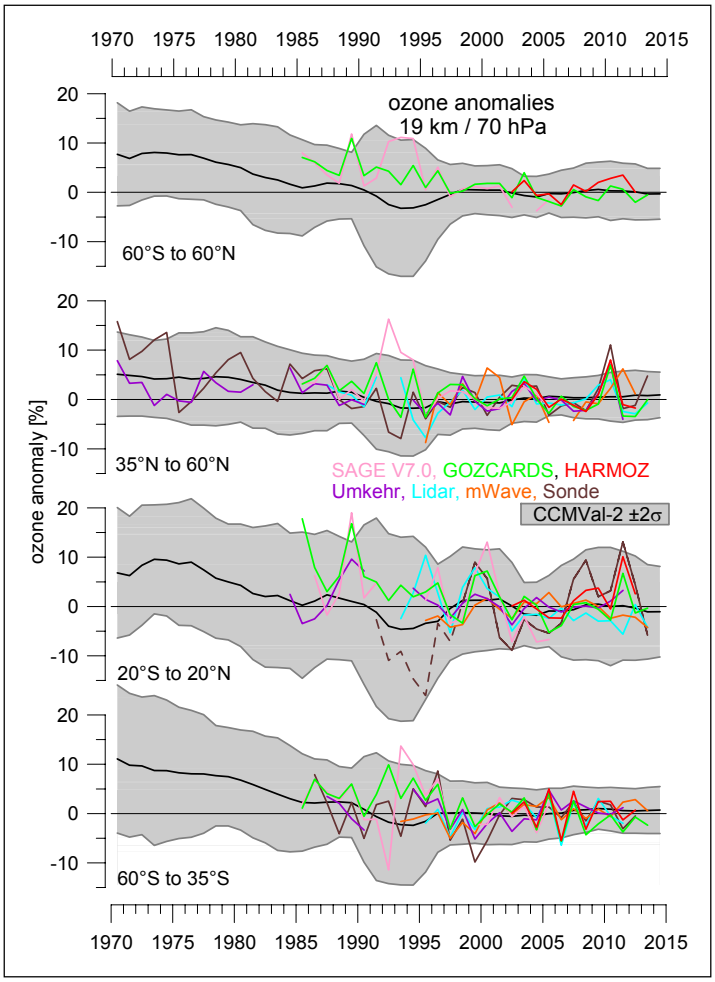

Figure 2-8. Same as Figure 2-7, but for the 19 km/70 hPa level. SBUV NASA data are not included because they have only very coarse altitude resolution, 10 to 15 km, in the lowermost stratosphere. The dashed line for the sonde data in the tropical belt indicates that before 1998 only data from the sonde station at Hilo, Hawaii (20°N), were used here. Umkehr, microwave and lidar data are also only from a few stations, e.g., Hawaii only in the tropical belt.

2.2.4.2 Ozone Trends up to 1997

Previous Assessments have established the latitude-altitude pattern of ozone decline due to increasing ODSs (WMO, 1999, 2003, 2007, 2011). The largest negative trends, −6 to −8% per decade, were found around 42 km/2 hPa (e.g., Figure 2-4 of WMO, 2011). This section briefly revisits the latitude-pressure pattern of ozone trends before the turnaround of stratospheric chlorine loading, i.e., before 1997, based on the new data sets, and based on the regression described in Section 2.2.3.3.

Figure 2-9 shows resulting linear ozone trends for the declining period up to 1997, for the GOZCARDS data set (in pressure coordinates), which is largely based on SAGE I and SAGE II (V6.20) over this trend period from 1978 to 1997, for the SBUV-NASA data set (trend period 1970 to 1997, in pressure coordinates), and for the SAGE II V7.0 data set (trend period 1984 to 1997, in altitude coordinates). The corresponding pattern from the CCMVal-2 model simulations (trend period 1970 to

1997) is shown as well. Note that small differences between trends can arise from the use of pressure or altitude in different observing systems (Box 2-1).

The observations all show the largest ozone decline near 42 km/2 hPa, between 30° and 70°, in both hemispheres. This highly significant (>3σ) decline is also simulated by the CCMVal-2 models, which show the largest loss near the poles, where SBUV and SAGE cannot observe during polar night. The trends from Figure 2-9 are consistent with previous Assessments (e.g., WMO, 2011), and with recent trend studies based on SAGE II V7.0 data (Remsberg, 2014), as well as the combined SAGE II – GOMOS (Kyrolä et al., 2013) data set. Below 22 km/50 hPa, all observational data sets also report significant ozone decline in both hemispheres. This decline is also largely due to ozone depletion through ODSs, especially near the poles (WMO, 2003, 2007, 2011).

In the tropical lowermost stratosphere below 22 km/50 hPa, the CCMVal-2 simulations indicate a long-term decline that is very pronounced in SAGE-II observations and captured in GOZCARDS, but is absent in the SBUV record. However, SBUV data have only very coarse altitude resolution below 25 km, where the retrieval mixes contributions from stratospheric and tropospheric ozone (Kramarova et al., 2013b).

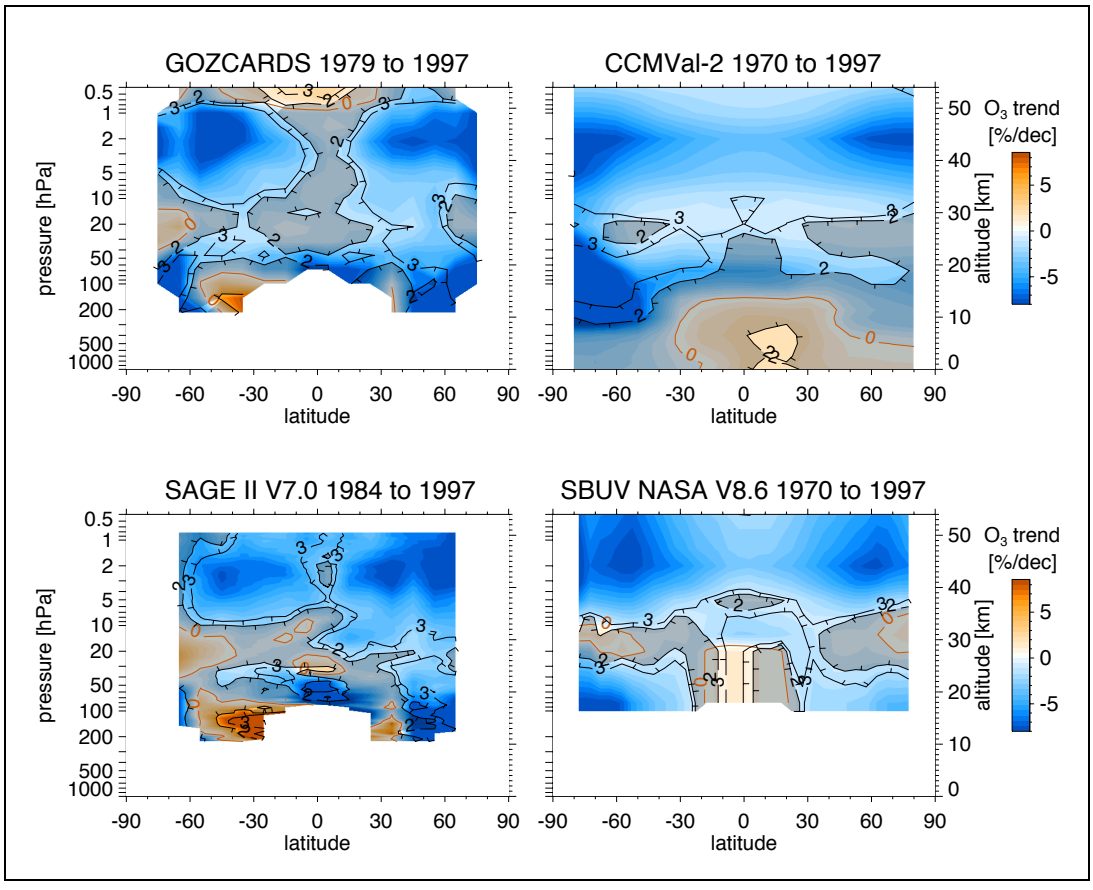

Figure 2-9. Ozone trends (in % per decade) before 1997 as a function of latitude and pressure. SAGE II altitude coordinates are converted to approximate pressure. Results are from multi-linear regression accounting for QBO, solar cycle, volcanic aerosol and ENSO related variations. See text for details. Top left: GOZCARDS record from 1979 to 1997. Top right: CCMVal-2 multi-model mean from 1970 to 1997 (REF-B1 runs, including volcanos and solar cycle, see text). Bottom left: SAGE II V7.0 from 1984 to 1997. Bottom right: BUV/SBUV/2 V8.6 NASA MOD data set from 1970 to 1997. See Table 2-2 for data sources. Trend magnitude is given by the color scale. The black contour lines give the ratio of trend to uncertainty, i.e., the statistical significance of the trends. The line labeled 3 corresponds to 3σ, 2 corresponds to 2σ. Gray shading indicates regions where the trends are not significant at the 2σ level. See text for details on the uncertainties.

2.2.4.3 OZONE TRENDS SINCE 2000

Upper stratospheric chlorine has been decreasing at a rate of 5–6%/decade since about 1997, following a strong increase in the early 1990s (Jones et al., 2011; see also Chapter 1). Despite the clear decline of upper stratospheric chlorine after 1997, a corresponding significant increase of upper stratospheric ozone had not been identified at the time of the last Assessment (WMO, 2011). There was, however, broad consensus that a significant change in the trend of midlatitude, upper stratospheric ozone had occurred in the second half of the 1990s (Reinsel et al., 2002; Newchurch et al., 2003; Miller et al., 2006; Steinbrecht et al., 2009; Jones et al., 2009), and that the negative trend of ozone had slowed down and eventually ended (WMO, 2007, 2011). Ozone time series are now longer and more data sets are available. Several studies have reported statistically significant increases of ozone in the upper stratosphere since 2001 (Kyrölä et al., 2013; Gebhardt et al., 2014; Eckert et al., 2014).

Confirming these studies, Figure 2-10 gives ozone trends since 2000 for three independent observational data sets and for the CCMVal-2 simulations. In the upper stratosphere, between 36 and 48

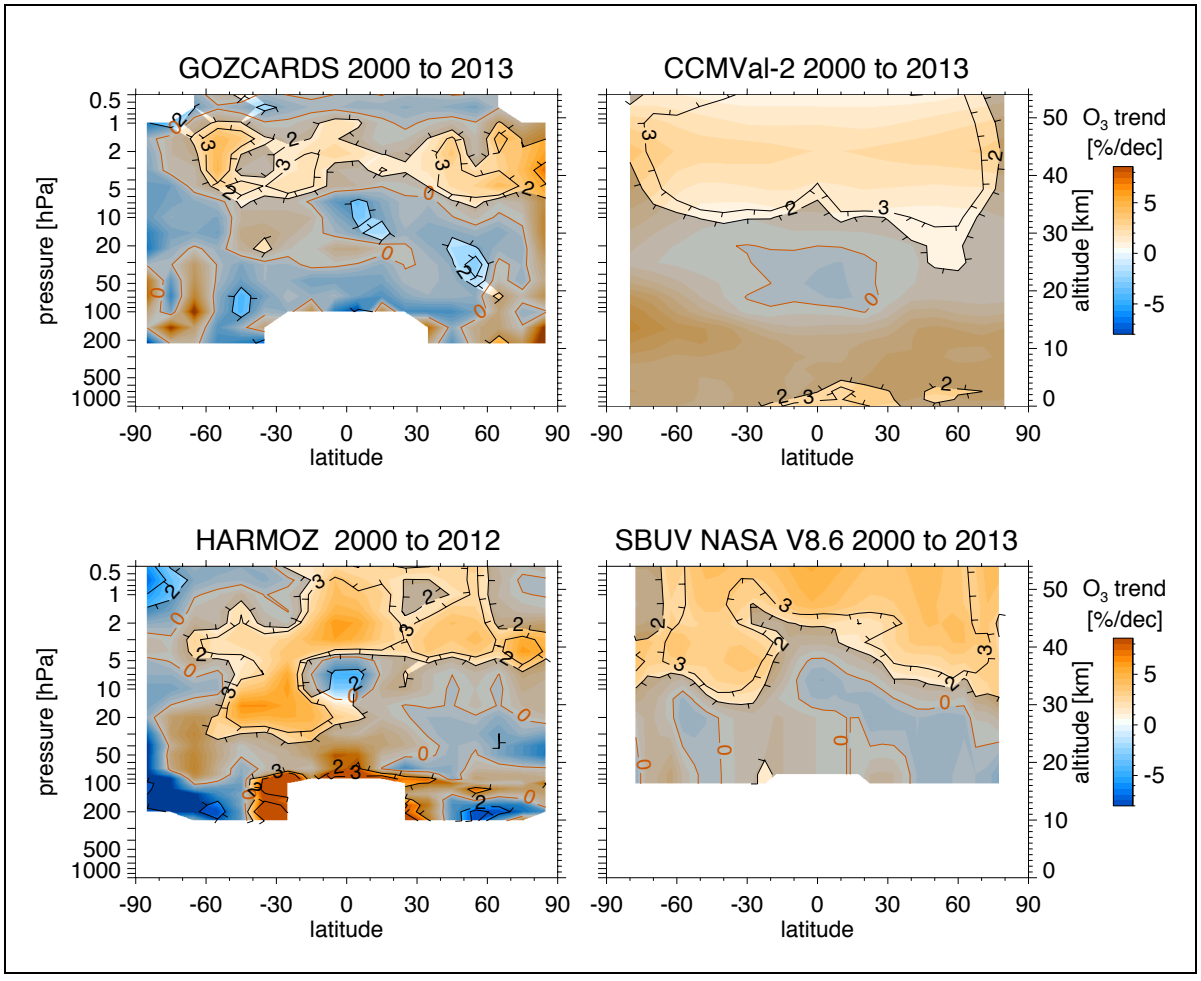

Figure 2-10. Same as Figure 2-9, but for ozone trends (in % per decade) since 2000. In the lower left panel, the trend derived from average ozone anomalies of the HARMOZ data set is given instead of SAGE II V7.0 trends. See Table 2-2 for details on the data sources. CCMVal-2 trend is for the REF-B2 simulations (not including volcanos and solar cycle, see text).

km/5 hPa and 1 hPa, all observations show significant ozone increases, up to 5% per decade, at most latitudes north of 60°S. Very similar increases are reported for individual instruments (Kyrölä et al., 2013; Gebhardt et al., 2014; Eckert et al., 2014). Here, ozone anomalies from these instruments have been averaged to obtain the HARMOZ trend in Figure 2-10. Upper stratospheric ozone increases since 2000, which have a peak near 2 hPa, are generally reproduced by the CCMVal-2 simulations (top right panel of Figure 2-10), although the simulated pattern is much smoother than the noisy observed pattern. Ozone increases in the upper stratosphere were mentioned in Figures 2-7 and 2-25 of WMO (2011). Four additional years of data, the new SBUV V8.6 data, and the additional GOZCARDS and HARMOZ data sets, now confirm these increases. In particular, the statistical significance of the increases is now higher ($>2\sigma$) than in WMO (2011).

In the mid- and lower stratosphere, ozone trends since 2000 are generally not significant. In the SH middle stratosphere (around 30 km/15 hPa), HARMOZ and SBUV show significant ozone increases, which are also evident, but not significant, in GOZCARDS. This increase was also reported for GOMOS, SCIAMACHY, and MIPAS by the studies mentioned above. In the NH, the observations show small ozone decreases between 30°N and 80°N at most levels below 32 km/10 hPa. These decreases are not statistically significant. At this point, the interhemispheric difference in Figure 2-10 is interesting, but not statistically significant.

In the tropical stratosphere, 20°S to 20°N, observations agree on decreases between 32 and 36 km/10 hPa and 5 hPa, largely due to high ozone values in the years 2000 to 2003 (see discussion of Figure 2-6; also Gebhardt et al., 2014; Eckert et al., 2014). In the lowermost tropical stratosphere, between 100 hPa and 50 hPa, 16 and 21 km, HARMOZ data indicate an increase, while GOZCARDS (and simulations) indicate a decrease: none of these are significant. There are substantial differences in trends since 2000 computed from individual instruments. Sioris et al. (2014) report a decline for OSIRIS data and Gebhardt et al. (2014) report an increase for SCIAMACHY and Aura MLS data. At this point, differences among trends computed from different data sets in the tropical lowermost stratosphere remain an open question.

2.2.4.4 TREND PROFILES

Trend profiles for the three latitude bands 60°S–35°S, 20°S–20°N, and 35°N–60°N are given in Figure 2-11. Results from the ground-based stations are averaged over available stations in each latitude belt, and are shown along with the satellite zonal mean data. CCMVal-2 model trends are given as gray background. In all three zonal bands, and at most pressure/altitude levels, the observed trends computed for the different observational data sets agree to within uncertainty bars, and for both periods (before 1997 and after 2000). The simulated trends also agree, within the uncertainty limits, with the observed trends. Some uncertainty bars are quite large, especially for the sparse ground-based data. There is only one station providing lidar, microwave, and Umkehr data in each of the tropical (Mauna Loa) and SH (Lauder) belts.

In addition to the individual trend estimates, the average trend of satellite and ground-based data sets is also plotted in Figure 2-11 (thick black line). This average trend is calculated as the weighted mean of the trends from all individual data sets, weighted by their inverse squared uncertainty. In order to account for possible instrumental drifts, a 2% per decade uncorrelated systematic uncertainty has been added to the individual trend uncertainties before building the weighted average. This results in more similar weights, and a larger and more conservative uncertainty estimate for the average trend. Table 2-4 summarizes these observed profile trends and compares them with the observed total column ozone trends from Figure 2-4.

Consistent with Figure 2-9 and previous Assessments (WMO, 1999, 2003, 2007, 2011), the left panel of Figure 2-11 shows significant ozone decline before 1997 at most levels. This decline peaks around 42 km/2 hPa at about −7% per decade in the Northern Hemisphere, at −4% per decade in the tropics, and at −8% per decade in the Southern Hemisphere. Near 26 km/20 hPa, the ozone decline

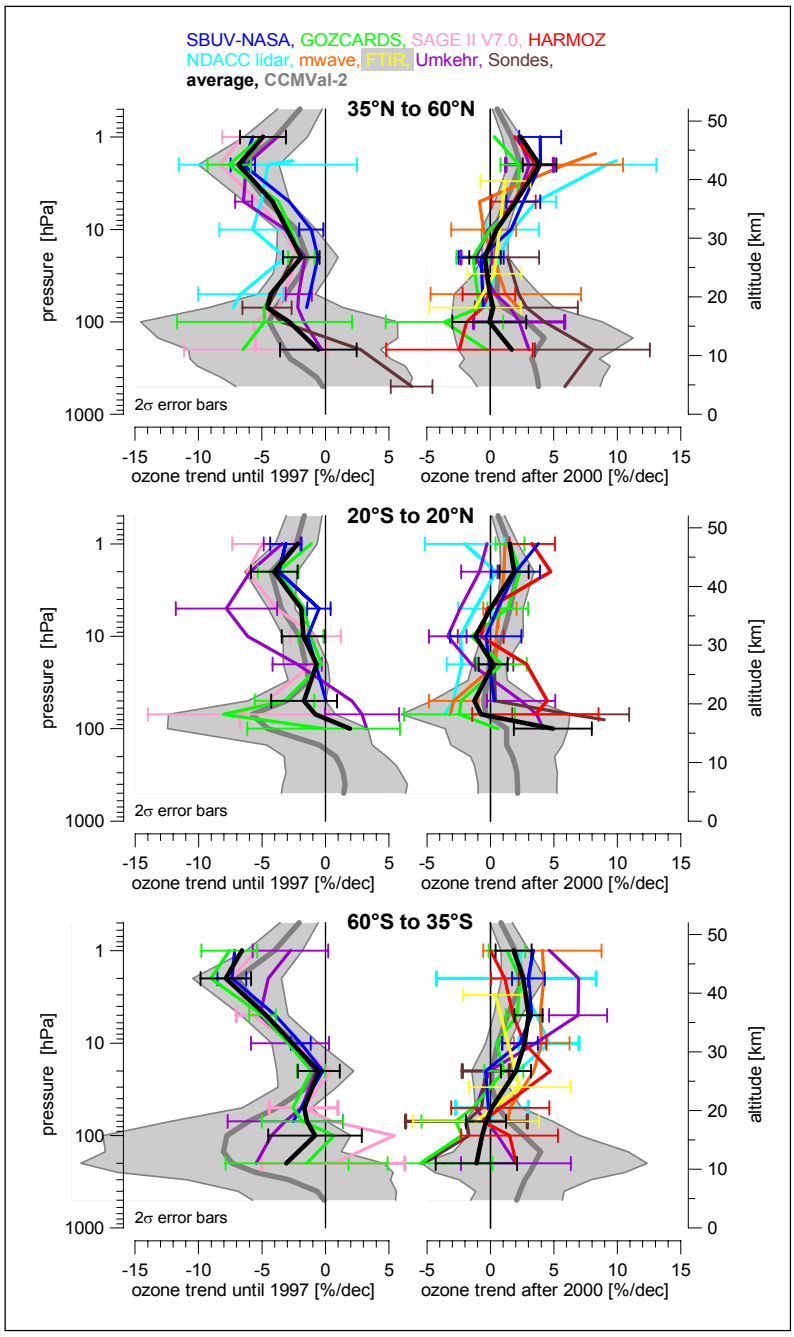

Figure 2-11. Ozone trends for the periods up to 1997 and after 2000 from various observed data sets and CCMVal-2 model simulations and for selected latitude bands. Length of period depends on length of data record for each system. See Tables 2-1 and 2-2. For CCMVal-2 simulations, the trend periods are 1979 to 1997 and 2000 to 2013. Data sets using pressure co-ordinates are plotted on the pressure axis, data sets using altitude coordinates are plotted on the altitude axis. Observed trends are from multi-linear regression accounting for QBO, solar cycle, volcanic aerosol and ENSO, same as in Figures 2-4, 2-9, and 2-10. Gray areas give multi-model average trend and ±2 standard deviation range of individual model trends from CCMVal-2 REF-B2 simulations (not including volcanos and solar cycle, see text).

before 1997 is small and barely significant. A second region with large declines before 1997, but also with large interannual variability and large uncertainty, occurs in the lower stratosphere, where trends peak around 100 hPa, and around −5% per decade. As in previous Assessments, trend uncertainties in the lowermost stratosphere are large, especially around the tropopause (10 km/200 hPa in the extratropics, 17 km/100 hPa in the tropics). This is due both to large natural variability and large gradients in this region (see also the large width of the gray range of model results), and due to less reliable observations at these altitudes.

The right-hand panels of Figure 2-11 indicate significant ozone increases since 2000 near 42 km/2 hPa, by about +3% per decade in Southern and Northern midlatitudes, and by about +2% per decade in the tropics. The CCMVal-2 simulations reproduce these observed increases (gray range in Figure 2-11). Between 16 and 31 km (100 to 10 hPa), ozone trends since 2000 are not significantly different from zero in the Northern Hemisphere, and in the tropics. In the Southern Hemisphere, they are significantly positive above 27 km/20 hPa. This hemispheric asymmetry has already been mentioned (see previous section, and Figure 2-10).

Table 2-4. Summary of ozone trends. Given uncertainty margins are ±2σ. Statistically significant trends are printed in bold. Trends are derived for 1979 to 1997 and 2000 to 2013, as described in Section 2.2.3 for total column ozone and in Section 2.2.4 for ozone profile trends.

Ozone Trends (% per decade)	60°S to 60°N		60°S to 35°S		20°S to 20°N		35°N to 60°N	
	up to 1997	since 2000	up to 1997	since 2000	up to 1997	since 2000	up to 1997	since 2000
Total column	**-2.0±0.7**	+1.1±1.7	**-3.8±1.2**	+1.6±1.7	-0.6±0.7	+1.1±2.1	**-3.3±1.4**	+0.8±2.3
70 hPa / 20 km	**-3.8±2.0**	-0.2±1.4	-1.5±2.9	-0.1±1.6	-0.8±4.0	-0.7±1.8	**-4.6±2.2**	+0.2±1.8
10 hPa / 30 km	**-2.9±1.4**	+0.1±1.1	**-2.6±1.9**	**+2.7±1.2**	-1.7±1.9	-1.2±1.3	**-3.0±1.5**	+0.5±1.2
2 hPa / 40 km	**-6.1±1.7**	**+3.6±1.2**	**-7.8±2.0**	**+2.6±1.3**	**-4.0±1.8**	**+1.9±1.2**	**-6.8±1.8**	**+3.9±1.3**

Positive ozone trends of about +3% per decade near 2 hPa since 1997 (or 2000) were already noted in Figures 2-7 and 2-25 of WMO (2011). Since then, these positive trends have now become clearer and statistically more significant. As discussed later (Section 2.4.2), the CCMVal-2 model simulations attribute this upper stratospheric ozone increase to declining ODSs and to stratospheric cooling by increasing GHGs.

2.2.4.5 CONSISTENCY BETWEEN TOTAL COLUMN TRENDS AND INTEGRATED PROFILE TRENDS

Although the long-term evolution of tropospheric ozone columns is only measured at a few sonde stations, and the vertical resolution and sampling of many instruments are limited in the lowermost stratosphere, it is useful and good practice from past Assessments to compare observed total ozone column trends with integrated profile trends. Generally, the profile ozone trends reported here (Figures 2-9 to 2-11) are consistent within uncertainty bars with the total column ozone trends reported in Figure 2-4. There are, however, two points worth noting:

Previous Assessments (WMO, 2003, 2007, 2011) have discussed that the large ozone decline reported in the tropical lowermost stratosphere from 1984 to 1997 by SAGE II (see Figure 2-8) is not consistent with the observed near constant total column ozone in the tropics. The observed, near-constant total ozone columns in the tropics were also not consistent with the long-term decline simulated by the CCMVal-2 models at these latitudes. New model results presented in Figure 2-12 now indicate that a long-term increase in tropospheric column ozone may resolve this long-standing discrepancy (Shepherd et al., 2014). The model simulation in Figure 2-12 shows good agreement between observed and simulated total ozone columns in the tropics, with little or no long-term decline (top panel). The middle panel shows good agreement also between observed stratospheric ozone columns from limb-sounding satellites and simulated stratospheric columns, both giving significant long-term decline. The new model simulations include a better simulation of tropospheric ozone changes. Figure 2-12 (bottom panel) indicates that a long-term increase of tropospheric ozone columns may have occurred. This could resolve the long-standing discrepancy mentioned above. Unfortunately, reliable long-term observations of tropospheric column ozone in the tropics are not available before 1998, precluding direct observational confirmation of this new model result.

Total ozone column increases of 2% per decade reported from 2000 to 2013 by several data sets (Figure 2-4) are larger than the vertically integrated ozone profile changes between 20°S and 30°N (from Figures 2-10 and 2-11). There, the vertically integrated trends give only small and insignificant column increases of 0–1% per decade, with error bars of about 1% per decade. These vertically integrated changes are, however, consistent with the small total column changes reported by SBUV V8.6 (and TOMS/SBUV V8.0) between 30°S and 30°N (see Figure 2-4). Reasons for the larger total column trends

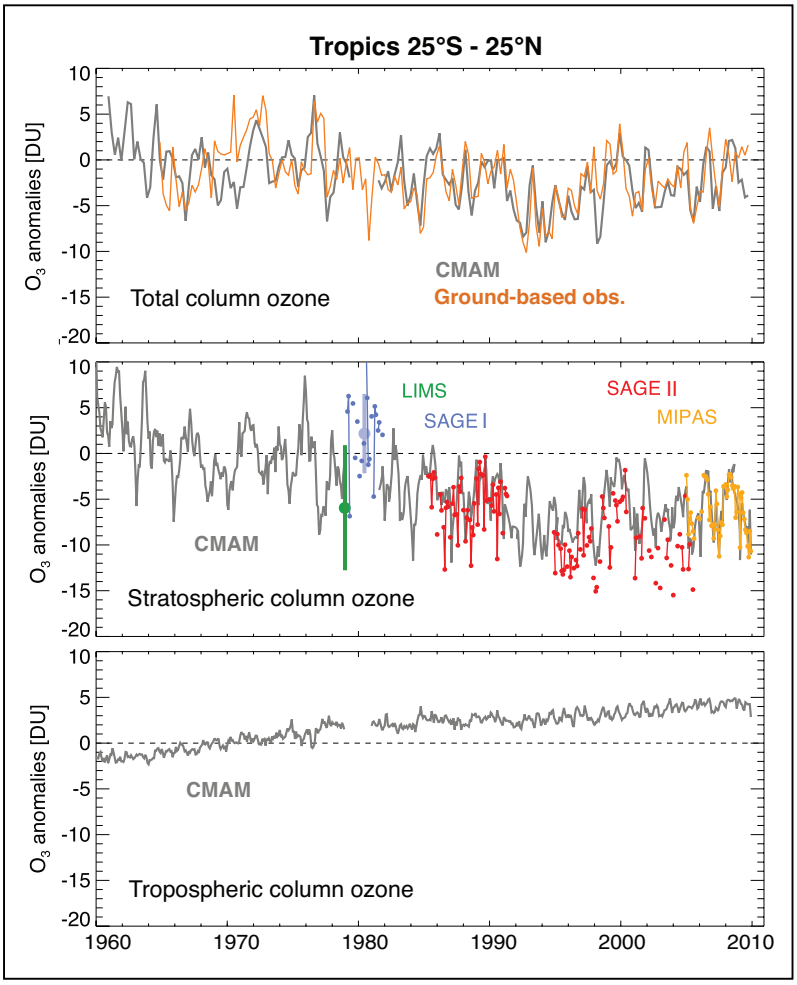

Figure 2-12. Total ozone columns in the tropical belt (top panel), and partial ozone columns for the stratosphere (middle panel) and troposphere (bottom panel). For total column and stratospheric column ozone, results from observations (colored lines) are compared to simulations by one chemistry-climate model (CCM), driven by observed meteorology (gray lines). For the troposphere, a consistent long-term observational record is not available. CCM simulations are from the Canadian Middle Atmosphere Model (CMAM) and are driven by meteorological conditions from the ERA-40 and ERA-Interim reanalyses. Figure adapted from Shepherd et al. (2014).

from some data sets are currently not known. However, as mentioned in the discussion of Figure 2-4, systematic uncertainties in the total column data of the order of 1% have to be considered as well.

2.3 UPDATES ON NATURAL OZONE VARIATIONS

This section discusses recent advances in understanding of ozone variability in the upper troposphere and stratosphere. An assessment of recent advances in diurnal ozone variations (Section 2.3.1) is included to demonstrate the importance of time-of-day sampling in sun-synchronous (and other) satellite observations. This is followed by discussions of recent advances in understanding of low-frequency ozone variability caused by the solar cycle and ENSO. It is well known that these two factors impact stratospheric composition, through their effects on chemistry and transport. As reported again by Kirgis et al. (2013) and Nair et al. (2013), the QBO is also an important contributor to interannual variability, both in the tropics and at higher latitudes (see also Figure 2-3). Dynamical feedbacks in the Earth System lead to effects of originally tropical phenomena, such as the QBO and ENSO, on midlatitude wave structures and wave propagation. This affects the Brewer-Dobson circulation and ozone transport in the stratosphere. Many variations thus impact detection and attribution of long-term changes. Finally, effects of volcanic and other aerosols are discussed in Section 2.3.4, since variations of such aerosols and their impacts on ozone chemistry must also be quantified.

2.3.1 Diurnal Ozone Variations and Their Impacts on Evaluating Long-Term Trends

The diurnal variation of ozone is large and well established in the mesosphere and lower thermosphere, i.e., above 50 km (e.g., Huang et al., 1997; Schneider et al., 2005; Dikty et al., 2010a; Huang et al., 2008, 2010). Since WMO (2011), several studies have improved our understanding of diurnal ozone variations, demonstrating in particular that substantial diurnal variations occur also between 20 km and 50 km and even in the total column (e.g., Sakazaki et al., 2013; Studer et al., 2014).

Diurnal variations of ozone in the tropics and midlatitudes can be obtained from measurements by satellites with non-sun-synchronous orbit. Figure 2-13 shows tropical (10°S–10°N) diurnal ozone variations derived from data from the Superconducting Submillimeter-Wave Limb-Emission Sounder (SMILES) during Northern Hemisphere winter from October 2009 to April 2010 (Sakazaki et al., 2013). At 20–30 km, ozone levels have a maximum in the morning and a minimum in the late afternoon with typical variations of 1% above and below the daily mean. At 30–40 km, ozone levels are smallest after dawn and highest in the afternoon with variations of 2–3% above and below the daily mean. At 40–50 km, ozone concentrations are minimum during daytime and maximum in the late afternoon with variations of 4% above and below the daily mean. UARS MLS and Sounding of the Atmosphere using Broadband Emission Radiometry (SABER) data show a similar altitude and local time dependence in the tropics (Huang et al., 1997, 2010) but there is disagreement about the size of the diurnal variation between the three instruments, particularly in the lower stratosphere.

Measurements of the diurnal cycle in ozone from ground-based microwave radiometers located in the extratropics are consistent with the results from satellites in the middle and upper stratosphere (Haefele et al., 2008; Studer et al., 2014). The vertical resolution of these radiometers is reported to be 6–20 km. The diurnal cycle of ozone levels above two stations in Switzerland (Payerne (47°N, 7°E) and Bern (48°N, 7°E)) and a station at Mauna Loa (20°N, 116°E) shows an afternoon maximum at 30–40 km (approximately 2–4% larger than the nighttime value) and daytime depletion above 40 km. Haefele et al. (2008) and Studer et al. (2013) also noted a seasonal dependence of the diurnal cycle, with the largest amplitude in summer. Figure 2-14 shows their seasonal variations of the diurnal ozone cycle at 5.8 hPa (~35 km in altitude) at 48°N. The peak-to-peak difference is 6% in summer and 3% in winter.

Generally, there is good agreement between the diurnal cycle of ozone in measurements and in CCMs and CTMs (Haefele et al., 2008; Sakazaki et al., 2013; Studer et al., 2014). Figure 2-13, for example, indicates good agreement between SMILES observations and model results for the whole tropical stratosphere. CTMs and CCMs show seasonal variations in the amplitude of the diurnal cycle that are, at least qualitatively, in agreement with space- and ground-based measurements.

The CTM simulations by Sakazaki et al. (2013) show that diurnal ozone variations in the stratosphere can be explained by a combination of photochemical processes (in the altitude region above 30 km) and dynamical processes in association with vertical ozone transport by atmospheric tides.

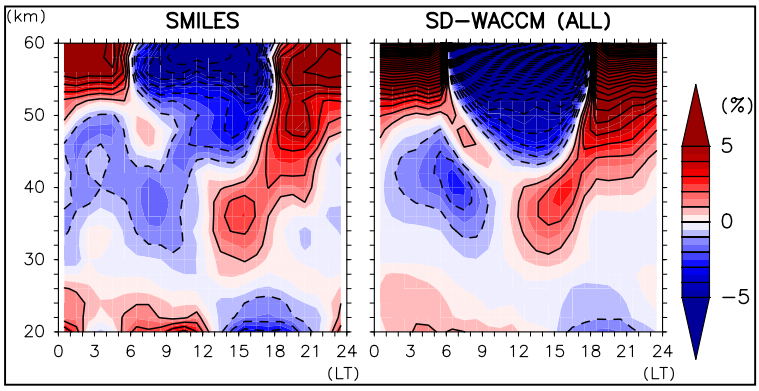

Figure 2-13. Diurnal ozone variations, relative to the daily mean, and averaged over 10°S–10°N, as a function of local time and altitude. Left panel: SMILES observations. Right panel: Specified Dynamics-Whole-Atmosphere Community Climate Model (SD-WACCM) simulation. A low-pass filter (three-point running mean in both time and vertical domains) was applied to the SMILES observations. The WACCM simulation is given for the full grid, not subsampled to the SMILES observation points. Adapted from Sakazaki et al. (2013).

Dynamical processes are important at 20–30 km and at 40–50 km where the vertical ozone gradient is large. Photochemical contributions are important at all latitudes, while the dynamical contributions are important only in the tropics. The latter means that the diurnal variations are enhanced in the tropics, at 20–30 km and at 40–50 km. The combined effect of these dynamical/photochemical changes results in a peak-to-peak difference of up to 1% in the total ozone column in the tropics (Sakazaki et al., 2013). Semidiurnal variations are seen with maxima at 01:00 local time (LT) and 15:00 LT. The former maximum is caused by the variations at 20–30 km due to dynamics, while the latter is caused by the variations at 30–40 km due to photochemistry. In CTM simulations, the diurnal cycle in total ozone is large at high latitudes in the summer hemisphere (e.g., the peak-to-peak difference is up to 6 DU (1.5%) at 70°S and <1 DU (<0.2%) at 70°N in January).

Diurnal variations are important for ozone trend analyses because data from satellite measurements have biases due to the difference in local time of measurements. It is well known that data from solar occultation satellite sensors show a sunset-sunrise bias. The SAGE II sunset profiles exhibit, for example, up to 10% more ozone than the sunrise profiles between 35 km and 55 km in the tropics (McLinden et al., 2009; Kyrölä et al., 2013). The results presented here suggest that at least half of the sunset-sunrise bias in SAGE II can be attributed to diurnal variations. Second, the diurnal variation of ozone should be considered when creating merged ozone time series that combine data from different satellites measuring at different local solar times. Furthermore, the local solar time of satellite measurements may change as their orbits drift. For example, the local time of measurements by Solar Backscatter Ultraviolet (SBUV) instruments on several NOAA satellites changed from early afternoon to late afternoon over a few years (e.g., McPeters et al., 2013). None of the (merged) data sets at this time tries to correct for such diurnal effects. The results presented here indicate that, in severe cases, systematic differences due to changing local times could reach 5% even below 45 km altitude, and more at higher altitudes. Depending on the timescale of satellite changes or local time drifts, trend uncertainties of several percent per decade could result. For instruments with nearly fixed local time sampling, the effects should be substantially smaller, but the need to combine data from several instruments with different sampling complicates the issues.

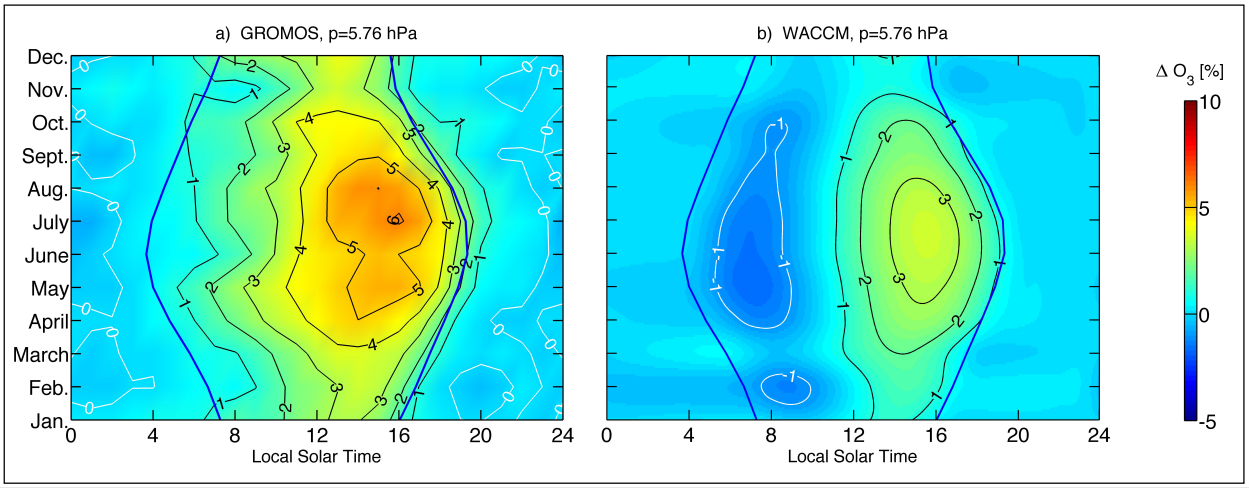

Figure 2-14. (a) Seasonal variation of diurnal ozone cycle with respect to the mean nighttime value (22:30–01:30) at 5.76 hPa/35 km as derived from the Ground-Based Millimeter-Wave Ozone Spectrometer (GROMOS) radiometer measurements at Berne (48°N, 7°E) during 1994–2011. (b) As for (a) but from WACCM free-running simulation. Color bar is shown at the right. Contour interval is 1%. The thick lines near 4 to 8 local time and near 16 to 19 local time give the sunrise and sunset times for Berne, Switzerland. Adapted from Studer et al. (2014).

2.3.2 Solar Variability

WMO (2011) reported a solar cycle effect on upper and lower stratospheric ozone of 2% to 4% between solar minimum and solar maximum. In the tropical middle stratosphere the observed solar cycle response is weaker and statistically insignificant (Soukharev and Hood, 2006; Randel and Wu, 2007). The solar cycle effect on upper stratospheric ozone is a direct radiative effect of heating and photochemistry. The lower stratospheric response in ozone (and also in total column ozone), however, occurs predominantly through a dynamical response to solar ultraviolet variations (e.g., Sitnov, 2009; Hood and Soukharev, 2012). The exact mechanism of the dynamical response to solar cycle variations is not fully understood and cannot be reproduced fully by CCMs (Gray et al., 2010). Ozone changes in the middle and upper stratosphere are also in phase with 27-day sun-rotation UV variation (Fioletov, 2009; Gruzdev et al., 2009; Dikty et al., 2010b; Kubin et al., 2012).

Remsberg and Lingenfelser (2010) and Remsberg (2014) found a stratospheric 11-year solar ozone response of around 2% for HALOE data and a response of up to 4% for SAGE II data. The differences between HALOE and SAGE II in the upper stratosphere solar response can be in part explained by the conversion between pressure and height coordinates that are used by the two data sets (see also Box 2-1). A minimum ozone response to the solar cycle in the middle stratosphere reported by Randel and Wu (2007) was not confirmed by Remsberg and Lingenfelser (2010). From a combined SAGE II/GOMOS data set, a solar cycle-induced stratospheric ozone response of 1–3% was derived (Kyrölä et al., 2013). These values are all in accord with WMO (2011).

Regarding total column ozone, in line with earlier studies (e.g., WMO, 2007, 2011), Hood and Soukharev (2012) confirmed a solar-induced 3% change in total column ozone from the SBUV/TOMS data set. This solar total ozone response is visible in the time-series of Figure 2-2, particularly in the tropics. The solar modulation of total ozone is likely driven by decadal variations of the Brewer-Dobson circulation (BDC) (Hood and Soukharev, 2012). Model simulations show that zonal asymmetries in the ozone, water vapor, and temperature fields are modulated by the 11-year solar cycle (Gabriel et al., 2011b). This provides a direct link between the solar cycle, zonal asymmetries, planetary waves, and the BDC, all of which affect stratospheric ozone.

Based on a CTM driven by analyzed meteorological fields, a double-peak profile with a minimum in the middle stratosphere was found in the tropical solar cycle (Dhomse et al., 2011), in agreement with Randel and Wu (2007). This modeled solar response was in better agreement with HALOE than with SAGE-corrected SBUV (McLinden et al., 2009) or SAGE II. However, uncertainties in analyzed upper stratospheric temperatures and in the various ozone data sets still complicate the assessment of solar responses in models and observations (Dhomse et al., 2011).

Since solar irradiance variations over the 11-year solar cycle are the main driver of the corresponding ozone variation, data from the Solar Radiation and Climate Experiment (SORCE) satellite, suggesting a significantly stronger variability by a factor of 4–6 in the ultraviolet (UV) spectral range compared to other solar data (Harder et al., 2009; Haigh et al., 2010; Figure 2-15), have received a lot of attention. Most spectral solar irradiance (SSI) observations and solar models, with the exception of SORCE, had so far provided a qualitatively consistent picture of SSI variability over the 11-year solar cycle.

In order to preserve total solar irradiance (TSI or solar constant), which is SSI integrated over the entire wavelength range, the large UV variability reported for SORCE data by Harder et al. (2009) requires that the visible SSI from SORCE has to decrease from solar minimum to solar maximum. Most solar models and other observations, however, indicate a positive (but weak) change in the visible (Ermolli et al., 2013; Figure 2-15). A careful analysis of the green spectral channel of VIRGO (Variability of solar IRradiance and Gravity Oscillations) confirmed a positive SSI change in the visible toward solar maximum (Wehrli et al., 2013). DeLand and Cebula (2012) and Lean and DeLand (2012) provide arguments that the SORCE data may be affected by optical degradation during the first years of the mission, near solar maximum. An additional investigation on the SORCE SSI variability closer to

solar minimum came to the conclusion that the SORCE UV SSI variability is about halved from the original studies but still higher than other observations and solar models (Ermolli et al., 2013; see Figure 2-15).

The large UV variation from SORCE has triggered several reinvestigations, comparing CCM runs using both the SORCE SSI and Naval Research Laboratory Solar Spectral Irradiance Model (NRLSSI) reconstructions. NRLSSI is representative for typical SSI variations assumed before SORCE data become available, and is commonly used in CCM simulations (e.g., Morgenstern et al., 2010). The CCMs generally showed a larger in-phase solar ozone response in the lower and middle stratosphere and out-of-phase (opposite) response above 37 to 45 km for simulations using SORCE SSI compared to simulations using NRLSSI (Haigh et al., 2010; Merkel et al., 2011; Swartz et al., 2012; Ermolli et al., 2013; see Figure 2-16a). SABER (2002–2010) and Aura MLS (2004–2007) daytime ozone observations seem to confirm the anti-cyclic ozone behavior in the mesosphere (Haigh et al., 2010; Merkel et al., 2011). Other results remain inconclusive as to which CCM simulations fit the observations better (Swartz et al., 2012; Shapiro et al., 2013; see Figure 2-15a). CTM simulations with different SSI implementations, including SORCE SSI, also provide very similar ozone responses in the middle atmosphere (Dhomse et al., 2013).

In the upper stratosphere and mesosphere, ozone is influenced substantially by odd-hydrogen (HO_x) chemistry. The observed decadal variability of hydroxyl (OH) total columns above 21 hPa, on the order of 7%, matches CCM results using SORCE SSI better than using NRLSSI (S. Wang et al., 2013). Many CCMs and general circulation models (GCMs) also show larger stratospheric temperature and shortwave heating rate responses for the SORCE SSI (Cahalan et al., 2010; Oberländer et al., 2012; Swartz et al., 2012; Ermolli et al., 2013). The modeled solar response of total ozone using SORCE SSI agrees better with SBUV/TOMS satellite data, but the run with NRLSSI agrees better with ground-based data (Swartz et al., 2012; Figure 2-16b).

In summary, recent studies have confirmed a 2–4% variation of stratospheric ozone (3% in total ozone) in phase with the 11-year solar cycle. However, the exact shape of the solar response profile depends on the type of data and/or analysis, the length of data records, and the time periods under investigation. There is evidence that SORCE SSI strongly overestimates UV solar cycle variability. However, a clear conclusion on which SSI fits ozone observations best can currently not be drawn, because (1) available ozone records are too short (only a few solar cycles), and have limited accuracy, (2) spectral resolution of the radiation schemes in global models is not sufficient (Oberländer et al., 2012; Swartz et al., 2012), and (3) solar cycle induced changes in atmospheric transport compete with the direct radiative effects (Shapiro et al., 2013; Dhomse et al., 2013).

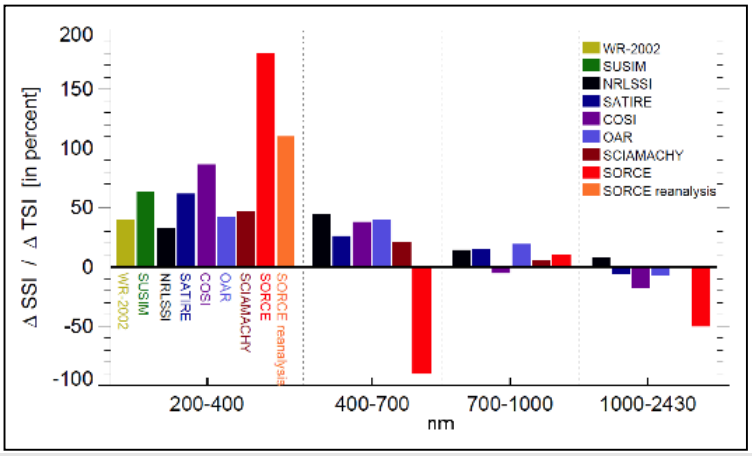

Figure 2-15. Spectral solar irradiance (SSI) changes over a solar cycle and in various spectral regions. SSI changes are normalized to total solar irradiance changes (TSI, solar constant), and are given for several data sets. WR-2002 (Woods and Rottman, 2002), SORCE, Solar Ultraviolet Spectral Irradiance Monitor (SUSIM), and SCIAMACHY are derived from observations. SATIRE, COSI, and OAR are solar models. NRLSSI is a solar reconstruction from Lean (2000). Except for SORCE (2004–2008) all values were derived from solar maximum to minimum conditions. As reported in Ermolli et al. (2013) a reanalysis of SORCE data close to solar minimum in 2009 revealed a weaker sensitivity in the UV, shown as SORCE reanalysis here. Adapted from Ermolli et al. (2013).

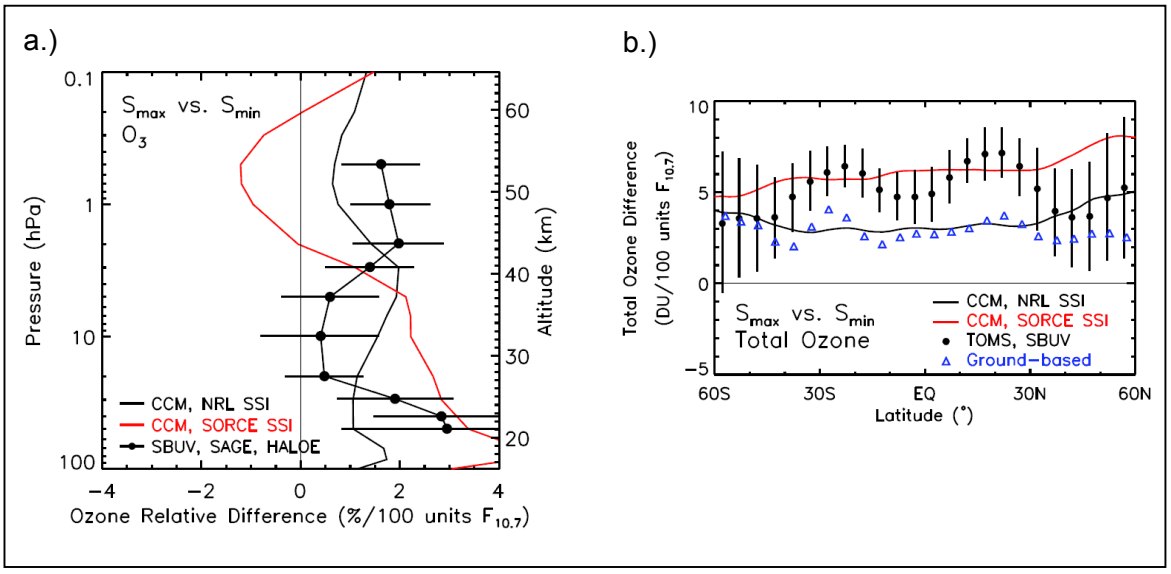

Figure 2-16. Solar cycle response of ozone from Goddard Earth Observing System Chemistry-Climate Model (GEOSCCM) simulations using SORCE SSI (red line) and NRLSSI (black, Lean and DeLand, 2012). a.) Comparison to profile response in SAGE II data from Randel and Wu (2007). b.) Comparison to response in zonal mean total ozone from SBUV/TOMS data and from ground-based Dobson and Brewer data. Both panels from Swartz et al. (2012).

2.3.3 Variations Associated with El Niño-Southern Oscillation

The El Niño-Southern Oscillation (ENSO) is an important mode of interannual variability in the tropical ocean and atmosphere. ENSO-forced variations in tropical upwelling lead to temperature and water vapor variations in the tropical lower stratosphere and have impacts on the chemistry and transport of ozone (e.g., Randel et al., 2009). Atmospheric teleconnections lead to ENSO-related impacts on the strength of planetary waves and the Brewer-Dobson circulation. Both affect stratospheric ozone distributions in middle and high latitudes.

Since WMO (2011), several studies have refined our understanding of ozone variations associated with ENSO. Randel and Thompson (2011) describe ENSO-related variations of tropical ozone found in the SAGE II and Southern Hemisphere Additional Ozonesondes (SHADOZ) data sets. In the tropical lower stratosphere (17–21 km), ENSO warm events lead to enhanced tropical upwelling that results in a reduction of zonal-mean ozone concentrations. A similar analysis using combined SAGE II and OSIRIS ozone data (Sioris et al., 2014) demonstrates that ENSO cold events (La Niña) in 1988–1989 and 1999–2000 led to positive anomalies in lower stratospheric ozone, see also Figure 2-8. Oman et al. (2013) used the spatially dense MLS and Tropospheric Emission Spectrometer (TES) observations to demonstrate the zonal symmetry of the ENSO signal in stratospheric ozone. ENSO-related signals (Figure 2-17) are strongest just above the tropical tropopause; at higher levels they appear with a one- to two-month delay and are weaker than QBO-related signals in ozone.

In contrast to the zonal-mean response in the lower stratosphere, these studies (Randel and Thompson, 2011; Oman et al., 2013) isolate a strong longitudinal dependence of the ENSO influence on tropical tropospheric ozone, which peaks in the upper troposphere (11–16km). It is also detected in total column ozone (Ziemke et al., 2010). This spatial structure is defined by an out-of-phase relationship between the Indonesian/western Pacific (high upper tropospheric ozone during ENSO warm events) and eastern Pacific regions (low ozone during ENSO warm events). Simulations using GEOSCCM (Oman et al., 2011, 2013), which include no year-to-year variations in biomass-burning emissions of ozone

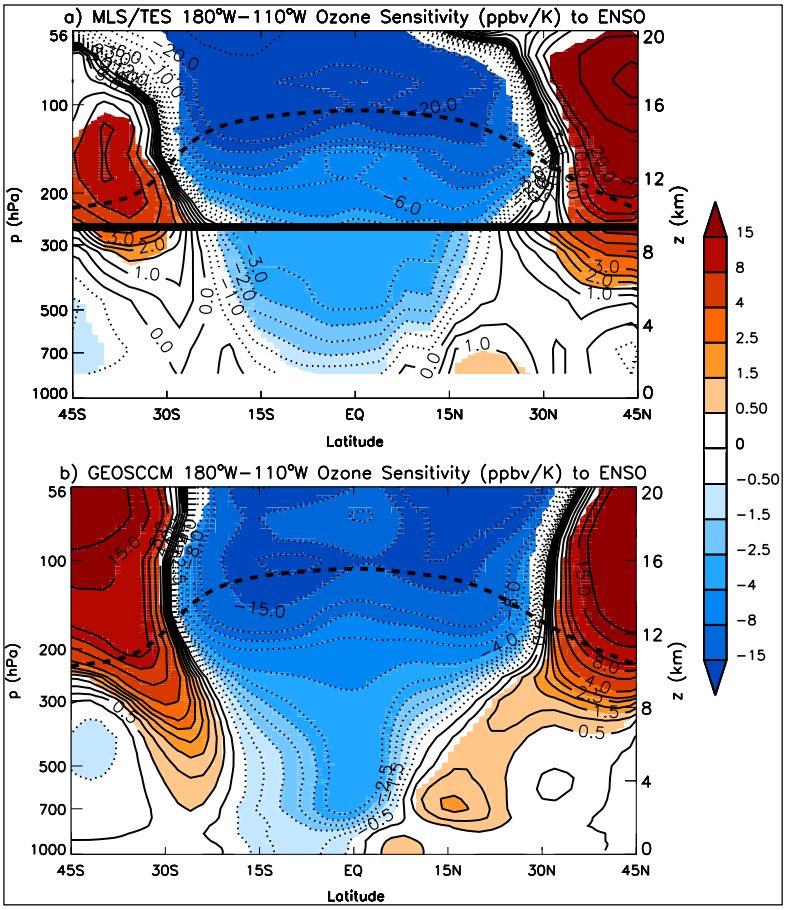

Figure 2-17. Sensitivity coefficient of ozone over the eastern Pacific (longitudinal average from 180°W to 110°W) to sea surface temperature anomalies in the Niño 3.4 region of the tropical Pacific (parts per billion by volume (ppbv) per Kelvin). Results of multiple linear regression analysis by Oman et al. (2013). Top panel: Observation results from Microwave Limb Sounder (MLS) and Tropospheric Emission Spectrometer (TES). The thick black line at 260 hPa separates MLS data used above from TES data used below. Bottom panel: Same for model simulations by the GEOSCCM model. Only regions that are significant at the 2σ level are colored. The dashed black line gives the mean model tropopause. From Oman et al. (2013).

precursors, demonstrate that the ENSO-related longitudinal structure is mainly caused by changes in atmospheric circulation that impact transport and photochemistry. Impacts of ENSO-related variations of biomass-burning emissions might have additional effects (e.g., Ott et al., 2010).

Several studies have examined the sensitivity of midlatitude ozone columns to the occurrence of ENSO through changes in planetary waves and their propagation and damping in the middle atmosphere (e.g., Hood et al., 2010; Gabriel et al., 2011b). Extratropical ozone variations due to ENSO are opposite to the tropical effects (Figure 2-17). There is also some evidence for hemispheric asymmetry, especially in the West Pacific (70°E–140°E). Smaller or negative sensitivity of ozone to ENSO is found in the SH midlatitude lower stratosphere, at least in these short records since 2004. Rieder et al. (2013) show a spatially complex relationship between midlatitude ozone column and ENSO index in both hemispheres during December-January-February and March-April-May between 30° and 50°N. Brönnimann et al. (2013) showed a similar zonal mean response to ENSO using an assimilated ozone data set covering much of the 20th century.

2.3.4 Effects of Increased Stratospheric Aerosol Loading

Previous Assessments have described how stratospheric sulfate aerosols impact ozone concentrations through both direct impacts on heterogeneous chemical processes and indirect impacts on temperature and transport. Figure 2-18 (Trickl et al., 2013) shows the well-documented, rapid increases in sulfate aerosol loading associated with the El Chichón (1982) and Mt. Pinatubo (1991) volcanic eruptions

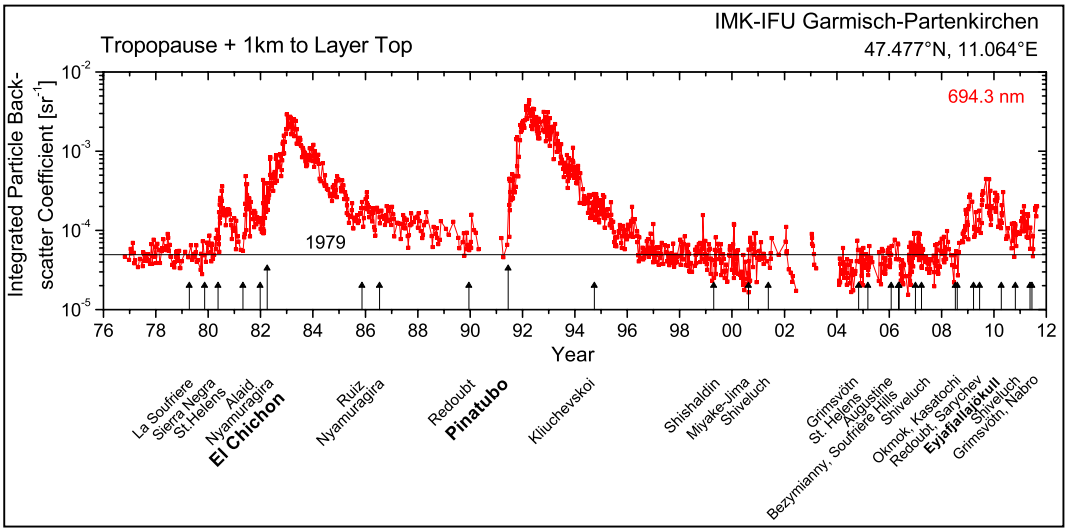

Figure 2-18. Aerosol backscatter coefficient measured since 1976 by lidar at Garmisch-Partenkirchen (47.5°N, 11.0°E) as a measure of stratospheric aerosol loading. Backscatter coefficient is integrated over the stratospheric aerosol layer, from 1 km above the tropopause to above 30 km altitude. Arrows mark the eruption of volcanoes that have, most likely, resulted in the observed aerosol enhancements. Note the recent aerosol enhancement after 2008. From Trickl et al. (2013).

followed by several years of gradual reductions. The figure also reveals an increase in the stratospheric aerosol burden after 2006 to 2008.

The recent aerosol increases are likely to impact stratospheric ozone. The 4–10% increase in the stratospheric aerosol burden is about twice as large in the tropics as in the middle latitudes (Vernier et al., 2011; Trickl et al., 2013). While Hofmann et al. (2009) hypothesized that this aerosol increase could come from increasing Asian fossil-fuel emissions, other studies (Nagai et al., 2010; Vernier et al., 2011; Neely et al., 2013; Trickl et al., 2013) show that volcanic sulfate aerosols are the likely cause. Most volcanic sulfates are injected directly into the lowermost stratosphere, but some may also be transported there via monsoonal circulations from the upper troposphere (Bourassa et al., 2012; 2013). The exact path of aerosols and precursors is not always clear (Vernier et al., 2013; Fromm et al., 2013; Bourassa et al., 2013). Quantitative assessments of the impact on ozone of this observed stratospheric aerosol increase are needed, especially in the context of other changes in the tropical lower stratosphere. Most likely, given the current (high) stratospheric chlorine and bromine burden, heterogeneous reactions on the increased aerosol surface area will result in some lower-stratospheric ozone destruction. Using a total column depletion of typically 2%, maximum 5%, after Mt. Pinatubo as a reference (Telford et al., 2009; see also Figure 2-2, WMO, 1999), the current effect on the total column should be below 0.2 to 0.5%, since aerosol loading is about a factor of 10 smaller, and chlorine levels are comparable. Major stratospheric aerosol perturbations, however, are likely to lead to substantial ozone loss until stratospheric halogen loading falls to values expected in about 2030–2050 (Pitari et al., 2014). Note that bromine released from very short-lived halocarbons that are transported into the lowermost stratosphere contributes substantially, up to 50%, to the aerosol-related ozone destruction (Salawitch et al., 2005; Sinnhuber et al., 2009). These very short-lived halocarbon sources are not expected to decrease in the future, providing potential for ozone loss due to enhanced stratospheric aerosol even when controlled ODSs have largely disappeared from the stratosphere.

Mt. Pinatubo was the most recent major volcanic eruption to increase global stratospheric aerosol levels by an order of magnitude or more, injecting about 17 teragrams (Tg) of sulfur dioxide into the stratosphere, which oxidized into about 30 Tg of sulfate aerosol (WMO, 1995, 1999). This aerosol

remained in the stratosphere for several years (see Figure 2-18) and was transported in approximately equal amounts to both hemispheres. The observed sudden depletion of stratospheric nitrogen dioxide (NO_2) in both hemispheres (WMO, 1995, 1999) provided evidence that the volcanic aerosol had enhanced heterogeneous chemistry at all latitudes. However, while observations showed enhanced ozone depletion in the NH, a small increase of the ozone column was detected, surprisingly, in the SH during the year following the eruption (see Figure 2-2). This remained unexplained in WMO (2011). Recent studies have now provided explanations. Poberaj et al. (2011) suggested that in the SH, enhanced ozone transport in late 1991 and early 1992 more than compensated the aerosol-induced chemical ozone loss. The enhanced transport was related to enhanced wave forcing of the SH stratosphere. A set of CCM simulations by Aquila et al. (2013) demonstrated that aerosol-induced longwave heating in the lower stratosphere would increase tropical upwelling, leading in turn to an enhanced BDC. This also increases ozone in the southern midlatitudes. Both mechanisms have likely acted together, and can explain the lack of a clear ozone decline in the SH after the Mt. Pinatubo eruption.

2.3.5 Impacts of Ozone-Depleting Substances and Greenhouse Gas Changes on Ozone Trends

Although the concentrations of ozone-depleting substances (ODSs) in the stratosphere continue to decrease, the detection of ozone recovery from ODSs remains a challenging scientific task. Essentially it is a statistical problem, complicated by the fact that influences other than ODSs, such as greenhouse gas (GHG) concentration increases, atmospheric dynamical variability, solar irradiance variations, and volcanic aerosol all affect stratospheric ozone (see previous sections). In the lower stratosphere and for total ozone, dynamical variability influences ozone directly, via changes in transport. Ozone is also affected indirectly by dynamical temperature changes, which affect rates of chemical production and destruction of ozone.

In the following we report how our capability to connect observed changes in total column ozone, and ozone in the upper stratosphere, to changes in ODSs and GHGs has improved. We also report on recent studies that examine observational evidence, from ozone in the lowermost tropical stratosphere, for an acceleration of the mean meridional Brewer-Dobson circulation (BDC). This acceleration has been simulated by most chemistry-climate model (CCM) simulations. These remain the major tool for estimating contributions from different processes, which usually cannot be separated on the basis of observations alone.

2.3.5.1 Changes in Total and Lower Stratospheric Ozone and ODS and GHG Changes

To detect the influence of ODSs on ozone changes, WMO (2011) relied on multiple-linear regression analysis. Equivalent Effective Stratospheric Chlorine (EESC) or piecewise linear trends (PWLT), both closely resembling the increase and the beginning of the decline of ODSs, were used as proxies describing the effect of ODSs (see also Section 2.2.3.3). In addition chemical transport models (CTMs) forced with winds and temperatures from meteorological analyses have been used to separate the influences of ODSs and dynamical variability. WMO (2007) attributed about 30% of the observed negative total ozone column trend from 1979 to the mid-1990s to changes in the lower stratospheric circulation. WMO (2011) also found that total ozone column increases observed since mid-1990 were significantly larger than expected from ODS decreases, and that dynamical variability contributed to these increases. Several new studies, reviewed below, follow the same approach.

Kiesewetter et al. (2010), for example, used a CTM and attributed at least 50% of the linear negative trend in total ozone from 1979 to 1999 to gas-phase chemistry. They found that insignificant ozone increases over the period 2000–2009 were dominated by changes in transport (see also Section 2.2.3.3). This is expected since stratospheric halogen loading has not yet decreased substantially over the last decade (compare EESC lines in Figure 2-4, or see Chapter 1). Kobayashi and Shibata (2011) also

used a CTM driven with observed meteorological conditions and pointed out that, in the northern midlatitudes, meteorological changes drive ozone changes on interannual to decadal timescales in the lower stratosphere, whereas upper stratospheric ozone decreases until the mid-1990s were dominated by changes in halogen loading, in agreement with previous studies.

Several studies assessed by WMO (2011) (e.g., Li et al., 2009; Waugh et al., 2009) used CCM model simulations driven by individual forcings to separately detect the influence of ODSs and GHGs on the past ozone trends. These results, corroborated by Plummer et al. (2010) and Fleming et al. (2011), have shown that ODS-induced changes dominated ozone during recent decades everywhere except for the lower tropical stratosphere (where little change has been observed; see Figure 2-8). However, none of these studies tested specifically whether observed ozone changes are consistent with responses to each of the forcings taking into account both the temporal evolution and spatial distribution of the changes. Such a test was performed by Gillett et al. (2011), who applied detection and attribution techniques common in other branches of climate science (e.g., Hegerl et al., 1996) to simulations from the CCMVal-2 ensemble, including simulations driven by all forcing, anthropogenic-only forcing, and GHG and ODS changes only over the period 1979–2005. Figure 2-19 (adapted from Gillett et al., 2011) shows a good agreement between observed total ozone trends and those simulated in response to the combined natural and anthropogenic forcing as well as to ODS changes alone. This suggests that the ODS changes are the dominant cause of the global ozone trends from 1979 to 2005, as concluded in WMO (2011). By applying optimal regression, Gillett et al. (2011) showed that the response of total column ozone to ODSs as well as to natural forcing (i.e., volcanoes and solar cycle) is detectable in observations. Furthermore, the observed and simulated responses to these forcings are of comparable magnitude. They also showed that the response of total ozone to GHG forcing is not yet detectable using this method. Note, however, that Gillett et al. (2011) attributed overall ozone changes over the entire 1979 to 2005 period to ODS and GHG changes, without considering a possible change in the trend since around 2000.

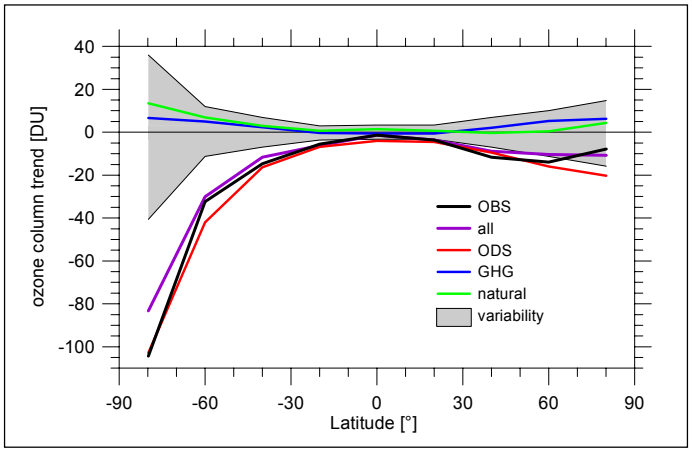

Figure 2-19. Comparison of observed (black line, OBS) and simulated linear trends in zonal mean total column ozone in Dobson units (DU) over the 27-year period 1979–2005. Observed total column ozone is taken from the merged TOMS/SBUV V8.0 data set. Simulated trends are from CCMVal-2 simulations and are shown for separate responses to ODS, GHG, and natural forcing, and all forcings combined (all, purple line). Gray band shows the estimated 5 to 95 percentile ranges of internal variability. Adapted from Gillett et al. (2011).

2.3.5.2 Changes in Upper Stratospheric Ozone and ODS and GHG Changes

As shown in previous Assessments (WMO, 1999, 2003, 2007, 2011), and reaffirmed by recent studies (e.g., Gillett et al., 2011), the large increase of ODSs from the 1970s to the late 1990s has been the main driver of the negative trend in upper stratospheric ozone until the late 1990s (see also Section 2.2, Figures 2-5, 2-9, 2-11). Model simulations have indicated that stratospheric cooling due to increasing GHGs is another important driver of the ozone evolution in the upper stratosphere (WMO, 1999; Jonsson et al., 2009; Eyring et al., 2010; Oman et al., 2010b; Gillett et al., 2011; Fleming et al., 2011; WMO, 2011; Stolarski et al., 2012).

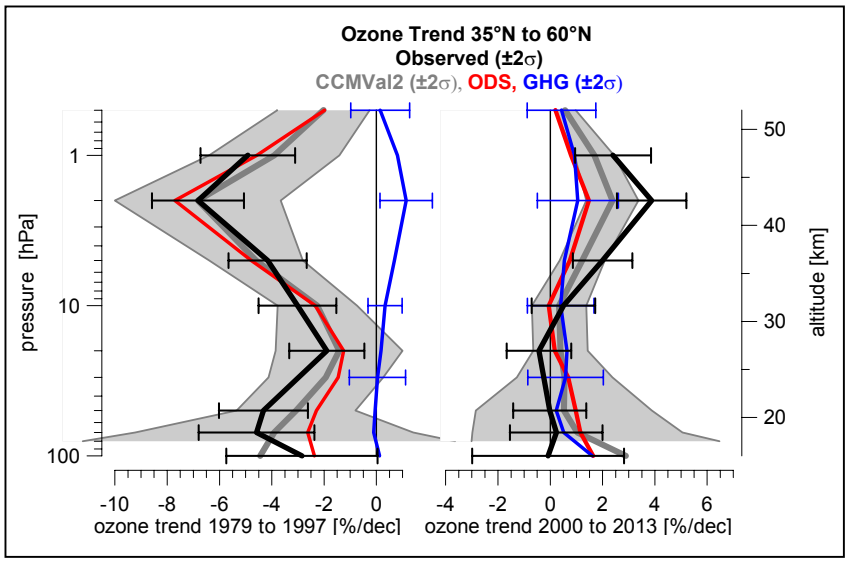

Figure 2-20. Observed and modeled ozone trend profiles. Left panel: For the period 1979 to 1997. Right panel: For the period 2000 to 2013. Black line: Average of all available observations in the 35°N to 60°N latitude band (same as in Figure 2-11). Gray line with shading: Corresponding mean trends from CCMVal-2 model simulations (same as Figure 2-11, but only for the subset of 7 models that did simulations with fixed GHGs), with uncertainty range given by ±2 standard deviations of individual model trends. Red line: Trend attributed to ODS changes alone, from CCMVal-2 simulations with fixed GHG concentrations (7 models). Blue line: Trend attributed to increasing GHGs alone, from CCMVal-2 simulations with fixed ODS concentrations (9 models). See Tables 1 and 2 of Eyring et al. (2010) or Tables 3-1 and 3-2 of WMO (2011) for details on CCMVal-2 fixed GHG and fixed ODS simulations.

The left panel of Figure 2-20 illustrates the influences of ODS and GHG changes on midlatitude ozone amounts during the period of ozone decline. The figure compares the observed ozone trend profiles (already shown in Figure 2-11; see also Figure 2-25 of WMO, 2011) to simulations from models in the CCMVal-2 ensemble forced by ODSs (red) and GHGs (blue) concentrations alone, in addition to simulations with all forcings (gray line and shading). Consistent with Oman et al. (2010a), simulations forced with ODS changes alone and with all forcings produce a large decline (−7% per decade) in ozone at 2 hPa until the mid-1990s. Within observational and model uncertainty these changes are consistent with the observed decline. Ozone increases due to GHG-driven cooling are smaller at around 1% per decade and also peak around 2 hPa.

The more recent impacts of declining ODSs and increasing GHGs in the early 21st century are illustrated in the right panel of Figure 2-20. Since 2000, declining chlorine and the continued slowing of gas-phase ozone destruction cycles due to declining temperatures both act to increase upper stratospheric ozone. Each factor contributes about one-half to the simulated upper stratospheric ozone increases (Eyring et al., 2010; Oman et al., 2010b; Fleming et al., 2011; Shepherd and Jonsson, 2011; WMO, 2011). The simulations also indicate that the contributions from ODSs and GHGs add linearly to produce the overall ozone change over this period (WMO, 2011).

Figure 2-20 indicates that this combined effect of GHG and ODS on upper stratospheric ozone can already be observed in the NH midlatitude upper stratosphere. Around 42 km (2 hPa), both ODS and GHG forced simulations each indicate a trend of 1–2% per decade in ozone concentration, compared to a mean observed trend of 2.5–5% per decade. Only when models are forced with both ODS and GHG changes are they able to capture trends as large as observed at these levels.

Since WMO (2011), four years of additional observations and the availability of more data sets have decreased the uncertainty margins for the observed trends. There are now stronger indications that a significant ozone increase is detectable in the upper stratosphere since 2000, and that about half of this increase is due to declining ODSs, with another half coming from the photochemical response to the cooling of the upper stratosphere by increasing GHGs.

2.3.5.3 TROPICAL OZONE CHANGES

WMO (2011) reported negative ozone trends in the tropical lower stratosphere (about 18–19 km) for 1985–2005, based on SAGE II data. While the uncertainty in this trend was large, the ozone decrease was consistent with that simulated by CCMs. These simulations indicate a long-term increase in tropical upwelling and an increased Brewer-Dobson circulation (BDC), resulting in declining ozone in the tropical lowermost stratosphere. New studies that merge SAGE II data for 1984 to 2005 with either SHADOZ ozonesonde data for 1998–2009 (Randel and Thompson, 2011) or OSIRIS satellite data for 2001–2012 (Sioris et al., 2014) seem to confirm a negative long-term ozone trend in the lowermost tropical stratosphere, −2% to −4% per decade for the 17 to 21 km altitude range, see also Figure 2-8. The magnitude and vertical profile of this ozone decline from 1984 to around 2000 are similar to the results from twelve different CCMVal-2 simulations (Eyring et al., 2010; WMO, 2011; Randel and Thompson, 2011).

However, as discussed in Section 2.2, recent analyses of shorter satellite data sets, between 2002 and 2012, do not show significant lower stratospheric ozone trends. This is the case for both SCIAMACHY (Gebhardt et al., 2014) and MIPAS data (Eckert et al., 2014). Analysis of a combined SAGE II-GOMOS data set for 1984–2011 (Kyrölä et al., 2013) shows a significant negative trend between 20-22 km for the period 1984–1997 but an insignificant trend for 1997–2011. Examination of the tropical ozone time series near 70 hPa in Figure 2-8 reveals the large year-to-year variations of ozone in this region, and variations around a relatively constant level since 1997. The CCMVal-2 simulations in Figure 2-8 also do not indicate a clear decline over the last 10–15 years in the tropical belt. The absence of a significant trend in the most recent observations is therefore not unexpected.

Overall these new results indicate substantial decadal variability of ozone in the tropical lowermost stratosphere. Based on existing tropical ozone records, there is little evidence for a continuing ozone decline in the tropical lowermost stratosphere since around 2000 that would be driven by a strengthening BDC. In agreement with WMO (2011), ozone values appear to have declined between 1984 and about 2000. Chapter 4 of this Assessment examines the BDC and its possible long-term change in more detail. The general expectation from model simulations is that, in the long term, ozone in the tropical lowermost stratosphere will continue to decrease due to enhanced upwelling and increases of the BDC driven by increasing GHGs (WMO, 2011).

2.4 UPDATE ON FUTURE OZONE CHANGES

2.4.1 Expected Return to 1960 or 1980 Levels and Ozone Recovery

The past two Ozone Assessments (WMO, 2007; 2011) have used chemistry-climate models (CCMs) as the primary tool for future ozone projections. WMO (2011) based their future projections on the simulations of 17 models, all of which participated in CCMVal-2 (Eyring et al., 2010). This ensemble remains the most comprehensive set of coordinated simulations of past and future stratospheric ozone changes. It is therefore the basis of future projections in the current Assessment. These CCMs have been extensively evaluated by CCMVal and the results are documented in the SPARC CCMVal Report (2010). Recent new simulations by four CCMVal-2 models using the revised estimates of ODS lifetimes (SPARC, 2013; also Chapter 1) are shown in Figure 2-21. These simulations indicate that the expected future evolution of near-global total ozone columns changes very little when using the revised ODS lifetimes. Changes in expected recovery dates to 1980 levels, for example, are typically less than a few years and are usually not significant given the large interannual variability and the intermodel differences. The estimates of return dates in different regions (Table 2-5) are not updated from WMO (2011). At this point there is not enough new evidence to motivate a revision of the estimates of ozone recovery presented in the previous Assessment.

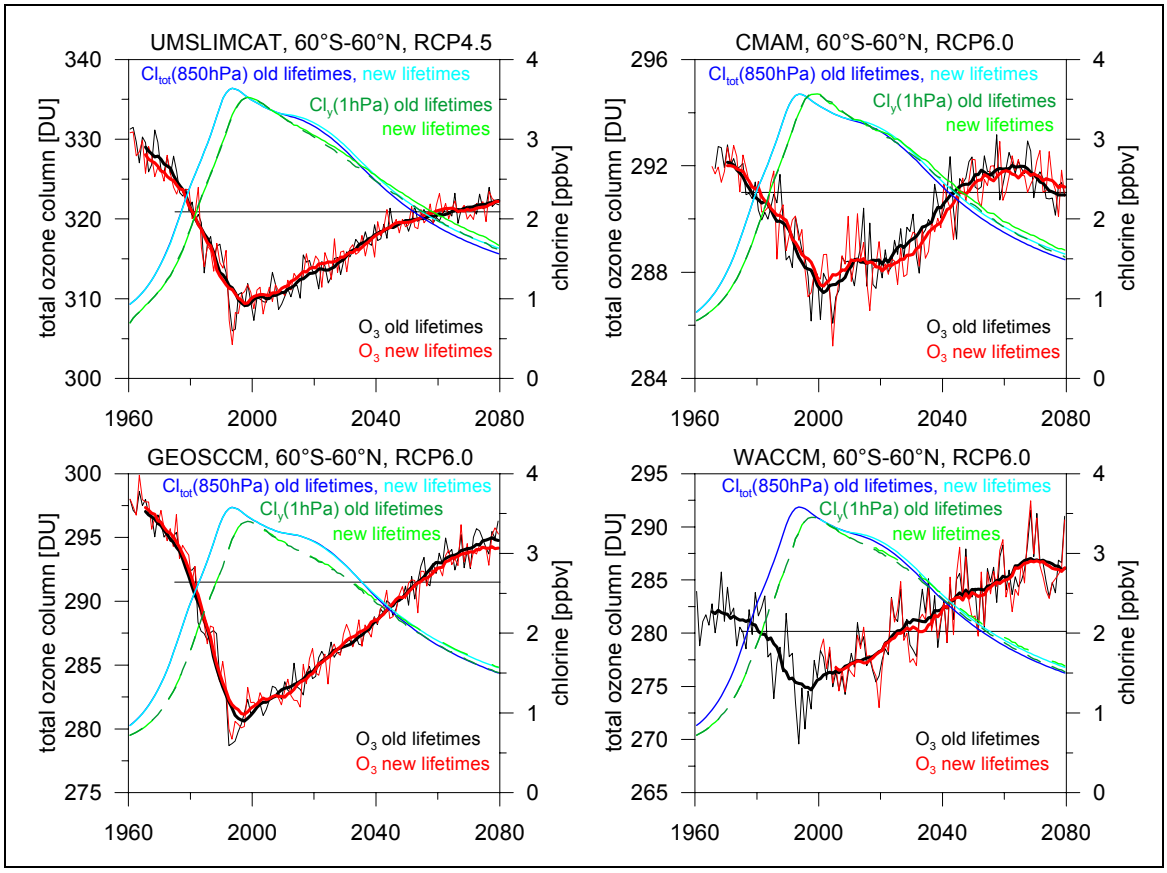

Figure 2-21. Comparison of total ozone column evolutions simulated using "old" ODS lifetimes from WMO (2010), black lines, and simulations using updated "new" ODS lifetimes from SPARC (2013), red lines. Also shown, on the axes on the right, are total organic chlorine at 850 hPa in the troposphere (Cl_{tot}, blue and cyan lines) and chlorine in the upper stratosphere at 1 hPa (Cl_y, dark green and light green lines). Annual means, averaged from 60°S to 60°N, are used. Results are from simulations with the chemistry-climate models UMSLIMCAT (Unified Model Single-Layer Isentropic Model of Chemistry and Transport; top left), CMAM (top right), GEOSCCM (bottom left, Oman and Douglass, 2014), and WACCM (bottom right). All models are described in Eyring et al. (2010) and WMO (2011). For greenhouse gases (GHGs) the simulations use the Representative Concentration Pathway (RCP) 6.0 scenario, except for UMSLIMCAT, which uses the RCP4.5 scenario. WACCM is coupled to an interactive ocean; the other simulations use prescribed sea surface temperatures. For total ozone, sliding 11-year averages are also plotted (thick lines).

WMO (2011) constructed its ozone projections by combining all available simulations from chemistry-climate model ensembles. WMO (2011) also gave equal weights to all simulations, and used multi-model means as the best estimate of future ozone and intermodel spread as a measure of uncertainty. This mean estimate of the CCMVal-2 ensemble can be seen in the black line in Figure 2-23, which will be discussed later in Section 2.4.3.1.

Table 2-5 shows that the simulations predict a later return date for SH midlatitudes than for the NH. This is the opposite of the currently observed total column trends in Figure 2-4, or profile trends in Figures 2-10 and 2-11, which tend to indicate slightly more increase since 2000 in the SH. The differences are not very significant though. As mentioned (e.g., in Sections 2.2.3 and 2.2.4) decadal changes in transport play an important role. WMO (2011) assumes that long-term changes in transport, i.e., in the Brewer-Dobson circulation (BDC), cause the earlier NH return dates. Garny et al. (2013)

suggest other possible reasons for the asymmetry in return dates between NH and SH midlatitudes. They hypothesize that transport effects play only a small role in this asymmetry and that differences in column return dates are related to less efficient destruction of ozone by nitrogen-oxides (NO_x) cycles in the NH and more efficient destruction of ozone by total inorganic chlorine (Cl_y) in the SH due to the larger polar vortex. These results should be interpreted cautiously because they rely on attribution of ozone changes in a single CCM and use a relatively novel and complex attribution method.

Since WMO (2011) there has been discussion about the possibility of using prior physical constraints to weight ozone projections from different models in order to reduce the significant uncertainty in current multi-model ozone projections. Challenges associated with combining projections from multi-model ensembles are common in all areas of climate science. Several weighting methods have been proposed. An overview of strategies for analyzing model ensembles and recommendations for good practice in applying multi-model ensembles is given in Knutti et al. (2010). Moreover, for CCMs the SPARC CCMVal Report (2010) presented a comprehensive set of diagnostics of model performance that are useful for model discrimination.

Several recent studies demonstrate that, at least for some regions, the performance-based weighting may give a more realistic ozone projection than the multi-model mean approach used by WMO (2011). Strahan et al. (2011) argued that in the tropical lower stratosphere the spread of ozone projections from the full set of models is unrealistically large. They evaluated CCM performance based on several transport diagnostics and found that tropical ozone agreed best with observations in the models whose transport was the most realistic. They further demonstrated that models with the most realistic transport in the tropical stratosphere produced a smaller spread of ozone projections compared to the full set of models. Douglass et al. (2014) demonstrate that selecting models based on their realistic performance can reduce the intermodel spread in the ensemble of projected ozone changes, although this comes at the expense of severely reducing the sample size.

Douglass et al. (2012) showed that, in agreement with expectation based on photochemical theory of upper stratospheric ozone, models with cold biases in upper stratospheric temperatures have higher ozone levels and stronger ozone sensitivity to chlorine changes. Thus, intermodel spread is not always an appropriate measure of uncertainty in future upper stratospheric ozone projections, but is also indicative of systematic errors that depend on model biases in simulated temperature, ozone, and reactive nitrogen climatologies.

Table 2-5. Expected return years when ozone columns will return to 1960 or 1980 values. Results from multi-model projections from the entire CCMVal-2 model simulation ensemble are repeated here from WMO (2011). Four new simulations using the recently updated longer ODS lifetimes from SPARC (2013; see also Chapter 1) indicate insignificant delays, about 2 years, in these return years (see Figure 2-21). Interannual variability of ozone columns, systematic differences between models, and uncertainty about future emissions (see Figure 2-23) cause larger uncertainty in the estimated return years.

Region	Date of Return	Mean Estimate	Lower Bound	Upper Bound
Global annual mean	1960	2053	2046	2064
	1980	2032	2027	2038
Tropics annual mean	1960	---	---	---
	1980	2042	2028	---
Northern midlatitude annual mean	1960	2029	2024	2036
	1980	2021	2017	2026
Southern midlatitude annual mean	1960	2055	2049	2064
	1980	2035	2030	2040

Karpechko et al. (2013) used the dependence of Antarctic ozone projections on simulated biases in present-day transport to constrain future projections. They showed that constraining projections resulted in a slightly delayed ozone recovery compared to the multi-model mean; however the difference between the two estimates was within the uncertainty limits. Waugh and Eyring (2008) and WMO (2011) also reported little difference between weighted and unweighted ozone projections, providing some support for using multi-model mean projections, as done in Section 2.2. The agreement between weighted and unweighted projections can be expected if models have opposite biases that nearly compensate each other within the ensemble. However when the models tend to have common biases, weighted projections can differ considerably from the multi-model mean.

These studies suggest that physically based model weighting approaches may help to reduce uncertainty in future ozone projections for regions where ozone is dominated by a small number of well understood processes, which are poorly simulated by some models. For consistency with the last Assessment, however, this chapter uses unweighted multi-model mean and intermodel spread from all relevant CCMVal-2 models, as in Eyring et al. (2010) and WMO (2011), as discussed in Section 2.2.3.1. Further, as shown in Douglass et al. (2014), performance metrics based on observations of meteorology and transport do not currently reduce the ensemble spread of the impacts of climate change on ozone in the late 21st century because the response of any model to climate change is not closely related to its transport skill.

2.4.2 Effects of Future Stratospheric Temperature and Circulation Changes

Future increases in greenhouse gases (GHGs), especially carbon dioxide (CO_2) are important for global ozone because they result in stratospheric cooling, slowing some chemical ozone destruction rates in the middle and upper stratosphere (e.g., Stolarski et al., 2012). According to model simulations, GHG-forced climate change leads to increased upwelling in the tropics and to changes in planetary waves that drive an increase in the strength of the BDC, which in turn affects the distribution of ozone in the stratosphere and the transport of ODSs, nitrous oxide (N_2O), methane (CH_4), and water vapor (H_2O) between the stratosphere and troposphere. For a mid-range GHG emission scenario, such as SRES A1B used in CCMVal-2, the dominant impact on stratospheric temperatures is from CO_2 changes. Future changes in transport due to the BDC, however, depend more on the amount of tropospheric warming, which will reflect the radiative forcing of the total mixture of future GHGs. Projecting future changes in the BDC is more difficult since the processes involved span the troposphere and stratosphere and are not well constrained in climate models. Observational evidence for changes in stratospheric temperatures and circulation is discussed in Chapter 4 of this Assessment.

Figure 2-22 shows a simple, illustrative experiment using the Solar-Climate-Ozone Links (SOCOL) CCM (Zubov et al., 2013) that separates the direct effects of GHG-induced temperature change on ozone from those resulting from stratospheric circulation change. This is achieved by performing timeslice experiments in which GHG and sea surface temperature and sea ice are varied independently. In the lower tropical stratosphere, large negative percentage changes of ozone below 20 hPa (Figure 2-22d) are driven almost completely by increased sea surface temperatures driven by tropospheric warming due to GHG increases (Figure 2-22c). As described in detail in WMO (2011), or Oberländer et al. (2013), the increased surface temperatures result in enhanced upward transport, especially in the tropics, and planetary wave driven increases in the mean meridional BDC. In midlatitudes, the same process is responsible for the enhancement of ozone in the lower stratosphere as ozone-rich air is transported from above. WMO (2011) concluded that CCMs consistently predict a strengthening of the BDC of around 2% per decade between 1960 and 2100, but that this strengthening had not been confirmed in observations (see also Section 2.3.5.3 and Figure 2-8). Recent work (see Chapter 4) separately considers changes in the shallow and deep branches of the BDC. Lin and Fu (2013) show that for the CCMVal-2 models, less than one-quarter of the predicted increase in tropical mass flux can be attributed to changes in the deep branch. CCM projections of changes to the shallow branch of the

BDC are sensitive to changes in the strength of the tropospheric subtropical jets and warming in the tropical upper troposphere (Lin and Fu, 2013), following the mechanism described by Shepherd and McLandress (2011). As well as the transport-induced impacts on lower stratospheric ozone concentrations, Meul et al. (2014) demonstrate using a CCM that the increased upwelling also leads to changes in chemical production and loss of tropical stratospheric ozone. The projected changes in lower stratospheric ozone concentrations in the late 21st century are thus caused by a combination of direct transport-induced changes and various chemical impacts that vary considerably with altitude in the low stratosphere.

In the upper stratosphere, above 10 hPa, the local cooling effect of CO_2 on ozone amounts (Figure 2-22b) is dominant, with little contribution from changes in transport. It is of comparable size to the increases in ozone driven by ODS reduction (Figure 2-22a; see also Figure 2-20 and Section 2.3.5.2). In midlatitudes, the upper stratospheric ozone increase from CO_2 cooling is roughly similar to that in the tropics, whereas the ODS-driven ozone increases are larger at midlatitudes. These upper stratospheric increases, combined with enhanced transport, drive an increase in ozone also in the lower stratosphere, resulting in increases in total column amounts (with a stronger signal expected in the NH; see also Shepherd, 2008; Li et al., 2009).

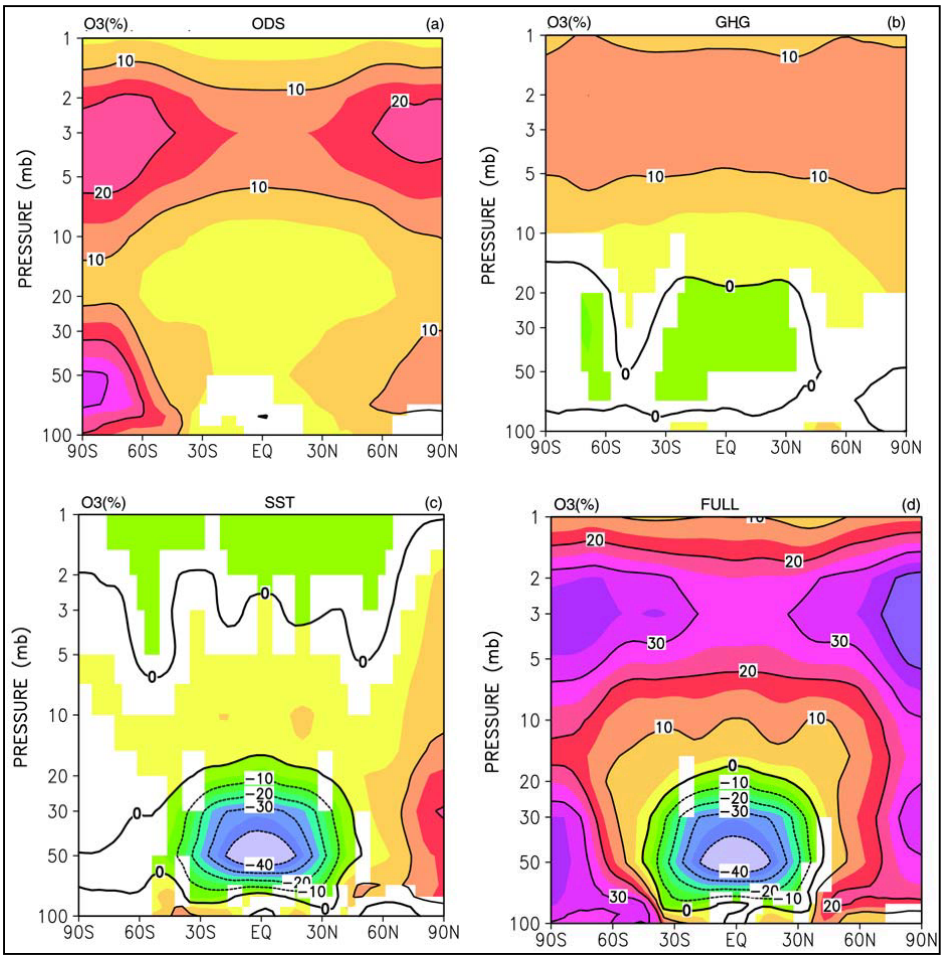

Figure 2-22. Zonal, annual and ensemble mean percentage changes of the ozone mixing ratio between different timeslice integrations of the SOCOL CCM for 2100 and for 2000 conditions.
(a) Ozone changes from 2000 to 2100 when only ODSs are changed.
(b) Ozone changes from 2000 to 2100 due to GHG changes only.
(c) Ozone changes due to changes in sea surface temperature and sea ice, driven by tropospheric warming.
(d) Ozone changes when ODS, GHG, sea surface temperature, and sea ice are all changed together. White regions indicate nonsignificant changes at the 5% confidence level. Adapted from Zubov et al. (2013).

2.4.3 Sensitivity to the Specification of Different Future Scenarios

As recognized in WMO (2011), numerous factors other than ODSs, including concentrations of CO_2, N_2O, and CH_4, will affect the future evolution of ozone in the stratosphere. In addition, changes in stratospheric water vapor are important for HO_x and NO_x chemistry, as reviewed by WMO (2011). Apart from methane oxidation, stratospheric water vapor concentrations are strongly influenced by stratospheric and tropospheric temperature and circulation changes. All are reviewed in detail in Chapter 4, Section 4.2.2 of this Assessment. Both natural and anthropogenic influences on the stratospheric aerosol layer also have the potential to influence ozone in the next decades, while ODS levels remain high. Since WMO (2011) our understanding of the influence of the 1991 Mt. Pinatubo eruption on ozone has increased, enhancing confidence in predictions of the future effects of these changes (Section 2.3.4).

Assessing the impact on ozone of future changes in CO_2, N_2O, and CH_4 is complicated by the significant, nonlinear interactions between them (Portmann et al., 2012). The following subsections address impacts on ozone of various future scenarios, and the complex effects of changes in N_2O and CH_4.

2.4.3.1 Effects of Different Representative Concentration Pathways (RCP) Scenarios

Quantifying the combined influence of CO_2, CH_4, and N_2O increases on ozone over the 21st century requires an estimate of the potential range of future anthropogenic emissions of these gases and subsequent calculations of the effect of these changes on ozone abundance using CCMs. Given the computational complexity and cost of CCMs, the number of simulations available for these calculations is limited.

As introduced in WMO (2011) the scenarios used for the latest Climate Model Intercomparison Project experiment (CMIP5) are the so-called Representative Concentration Pathways (RCPs, van Vuuren et al., 2011). These scenarios will also be the basis for most future runs of the next generation of CCMs, so they are reviewed here. It is important to note that the RCPs are chosen to represent some of the many different potential future emissions pathways and are produced using a complex chain of different Integrated Assessment Models (IAMs). RCPs are named to reflect their total radiative forcing in 2100. The evolution of emissions of CO_2, CH_4, N_2O, and other GHGs in each scenario is complex and the ordering of emissions of each gas as a function of scenario changes with respect to time over the 21st century. Key points to note are that CH_4 emissions are much larger (by a factor of more than 2) in the RCP8.5 scenario than the other three scenarios and that N_2O emissions in the RCP6.0 and 8.5 scenarios are much larger than those of the RCP2.6 and 4.5 scenarios by midcentury. Since the emissions trajectories for GHGs in the RCP scenarios are complex and have differing rates of change over time, this will lead to differing rates of change for key processes in CCMs, both in the stratosphere and in the troposphere.

WMO (2011) reported early calculations of the sensitivity of future ozone to the GHG scenario and concluded that the GHG scenarios had a measurable impact on future ozone concentrations in the stratosphere and troposphere, particularly during the latter half of the 21st century, but that model uncertainty was at least as large as scenario uncertainty for all regions.

More recently, Eyring et al. (2013) considered the sensitivity of ozone projections to GHG scenario for those models submitted to CMIP5 that had a representation of stratospheric ozone chemistry. The results of Eyring et al. (2013) are qualitatively consistent with WMO (2011), increasing confidence in our understanding of the scenario uncertainty associated with future ozone projections. However, the CMIP5 results from Eyring et al. (2013) deviate quantitatively from the projections made by the CCMVal-2 models (WMO, 2011). As shown in Figure 2-23, the multi-model mean of the CCMVal-2 models assessed by WMO (2011), and used in this Assessment, differs in timing of minimum total ozone columns and in other aspects from the CMIP5 model projections. Most noteworthy are the differences between CCMVal-2 simulations using the SRES A1B intermediate radiative forcing (6 W

m^{-2}) scenario from IPCC (2007), and CMIP5 simulations using the similar RCP6.0 scenario. These deviations may be due to differences in the models used in each ensemble, in the ensemble sizes, and differences in the scenarios themselves. It should also be noted that the RCP scenarios do not sample all possible future emission changes relevant to ozone, for example different ODS scenarios. As noted in WMO (2011), it will only be possible to refine estimates of scenario uncertainty by comparing a large number of CCM integrations forced with different emissions scenarios.

Given these caveats, all simulations in Figure 2-23 project substantial changes in total ozone columns in the future. Outside of the tropics, simulations for the scenarios with higher radiative forcing project a recovery of total ozone columns to 1980 values or even larger columns, with contributions from declining ODS, continued stratospheric cooling, and strengthening of the BDC (see previous sections). Future increases in tropospheric column ozone also contribute to the expected larger columns. In the tropics, projected future increases of tropospheric ozone column are particularly large in the RCP8.5 scenario, where they more than compensate the projected decline of tropical stratospheric column ozone. Depending on the assumed scenario, total ozone columns in 2100 could vary by up to 10 DU or 4% in the tropics, by up to 20 DU or 7% in the global mean, and by up to 40 DU or 12% at midlatitudes. This large variation shows that, apart from the expected decline of ODS, future emissions of GHGs will have a substantial influence on ozone levels.

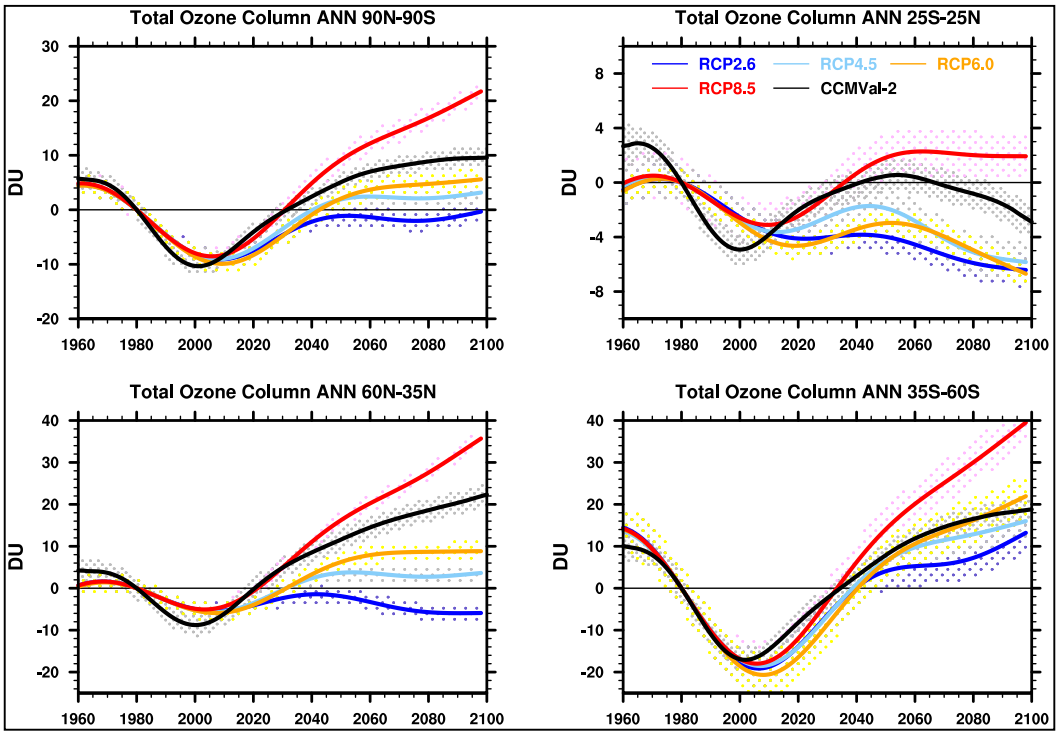

Figure 2-23. 1980-baseline adjusted total column (tropospheric plus stratospheric) ozone time series for CMIP5 runs of models that follow four RCP scenarios for GHGs, and the A1 scenario from WMO (2003) for ODS. The RCP2.6 scenario is shown in the solid blue line with the 95% confidence interval for the mean of 5 models shown in blue stippling. The RCP4.5 scenario is shown in the light blue line and averages 6 models. The RCP6.0 scenario is shown in the orange line and averages 5 models. The RCP8.5 scenario is shown in the red line and averages 6 models. Five models are common to all scenarios. Also included is the CCMVal-2 multi-model mean (black line), which is based on different models, the SRES A1B scenario for GHGs, and the adjusted A1 scenario from WMO (2007) for ODS (see Section 2.2.3). Adapted from Eyring et al. (2013).

2.4.3.2 INFLUENCES OF NITROUS OXIDE AND METHANE

As well as being important GHGs, N_2O and CH_4 are key source gases for the NO_x and HO_x chemical cycles, which directly impact ozone amounts. About 90% of stratospheric NO_x arises from N_2O oxidation (Vitt and Jackman, 1996). At low halogen levels, chemical ozone destruction is dominated by the NO_x loss cycle in the middle stratosphere and by the HO_x loss cycle below 20 km and above ~50 km (in the mesosphere). As the ODS burden declines over the 21st century, ozone changes will depend strongly on the N_2O and CH_4 burdens, which are assumed to change in very different ways in the RCP scenarios. These impacts are considered in this section.

In the global mean, for a mid-range N_2O emissions scenario, simulations compute a total ozone reduction by around ~5 DU by 2050, compared to preindustrial values. Similar changes are computed by both 2-D (Fleming et al., 2011; Portmann et al., 2012) and 3-D (Revell et al., 2012a, b) models. This reduction, shown by the green line in Figure 2-24, is about one-quarter of the isolated maximum effect of the ODS changes in 2000 (blue line in Figure 2-24), and comparable to the increases in total column ozone due to the isolated effects of CO_2 and of CH_4 through the 21st century (red and yellow lines in Figure 2-24). These studies found that the depletion of the total column due to the isolated effect of N_2O does not exceed that due to ODSs until ~2080. The efficiency of N_2O in destroying ozone can be compared to ODSs by computing the Ozone Depletion Potential for these gases (Ravishankara et al., 2009; Daniel et al., 2010). This is discussed further in Chapter 5 (Sections 5.3–5.4), along with policy-relevant information about future N_2O increases.

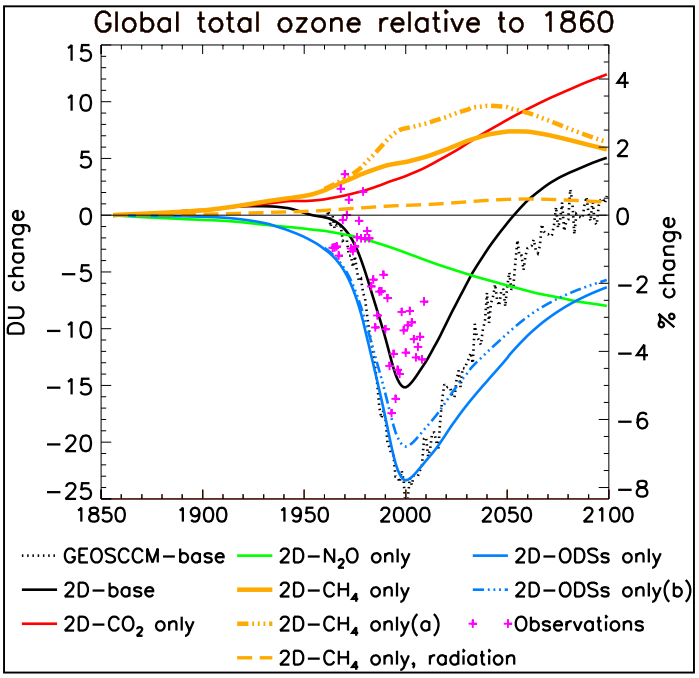

Figure 2-24. Global and annual average total ozone time series relative to 1860 values from model simulations (lines) and ground-based data (pink crosses, updated from from Fioletov et al., 2002). The black dotted line shows a base simulation of the 3-D chemistry-climate model GEOSCCM with the A1 scenario of WMO (2007) for ODS concentrations and the SRES A1B scenario for GHG concentrations (same as for the CCMVal-2 simulations). The black solid line shows the simulation of a 2-D chemical transport model that uses the same forcings. The other colored lines show additional scenarios of the 2-D model in which only selected forcings are varied in time (while keeping the others at 1850 levels). The experiments are as follows: Red-line: Only CO_2 varies. Green line: Only N_2O varies. Yellow solid line: Only CH_4 varies. Blue solid line: Only ODSs vary. Also shown are experiments in which both ODSs and CH_4 are varied. The orange dot dashed line shows the effects of CH_4 in the presence of time-dependent ODS changes (difference between simulation with CH_4 and ODSs changing and simulation with only ODSs changing). The blue dot dashed line shows the effects of ODSs in the presence of time-dependent CH_4 changes (difference between simulation with CH_4 and ODSs changing and simulation with only CH_4 changing). Finally, the orange dashed line shows the impact of CH_4 on ozone when its effects are confined to impacts on the radiation budget only. Adapted from Fleming et al. (2011).

Revell et al. (2012a) provided a study of the sensitivity to N_2O/NO_x by comparing three RCP scenarios, bounded by RCP2.6 (lower N_2O growth) and RCP8.5 (higher N_2O growth). They performed a suite of CCM simulations in which each of the gases is varied in isolation along four different future N_2O and CH_4 pathways. Their results demonstrate clear links between the assumed GHG scenario and stratospheric ozone. Increased N_2O emissions lead to higher NO_x concentrations and faster chemical ozone destruction in the middle stratosphere. Middle stratospheric ozone concentrations in the late 21st century are thus substantially lower for the RCP8.5 N_2O scenario than for the RCP2.6 scenario (Figure 2-25a, b). In the lower tropical stratosphere the differences are of opposite sign because of enhanced ozone production following CH_4 oxidation caused in the troposphere by the higher NO_x concentrations in the RCP8.5 scenario (this mechanism is discussed below). Some of this lower stratospheric ozone increase could also be due to "self-healing" wherein the ozone decreases in the middle and upper stratosphere allow more solar UV radiation to penetrate to lower altitudes, leading to ozone enhancements in the lower stratosphere (Mills et al., 2008).

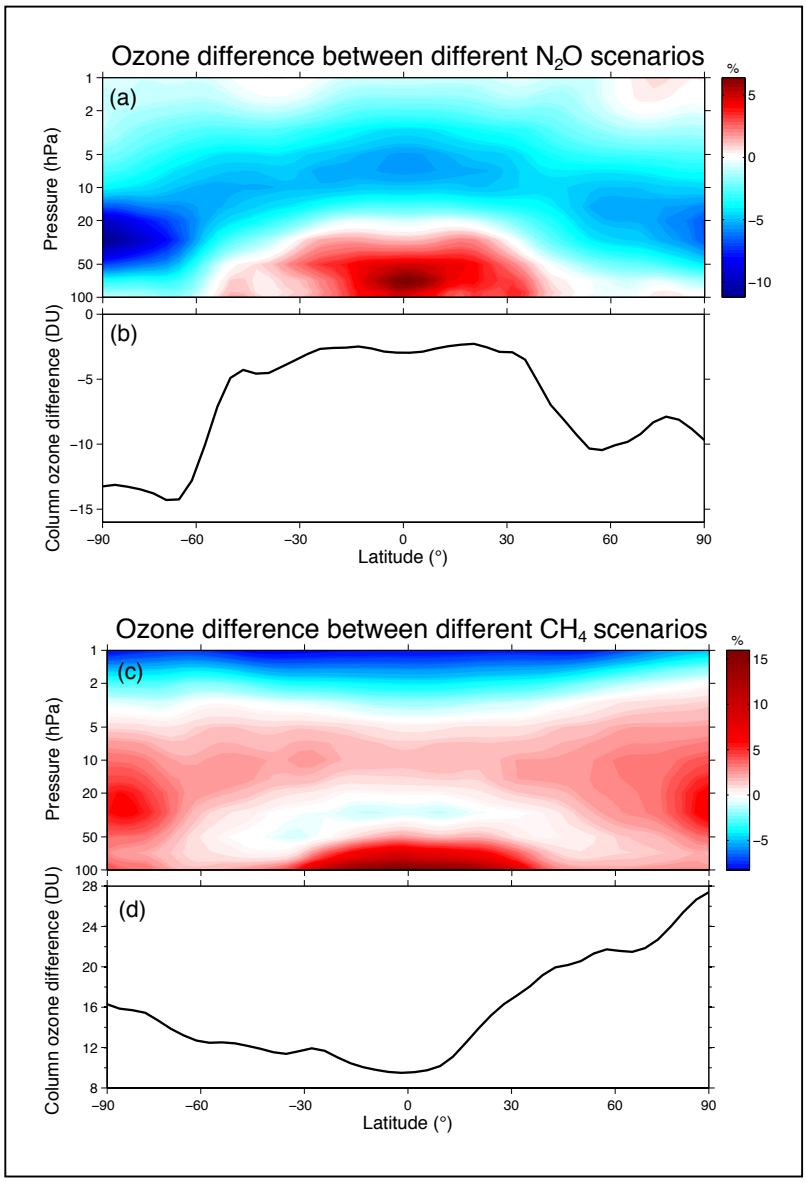

Figure 2-25. Ozone changes in the 2090s due to different N_2O and CH_4 scenarios, computed with the National Institute of Water and Atmospheric Research (NIWA)-SOCOL chemistry-climate model. (a) Difference between ozone in the 2090s under the N_2O-RCP8.5 scenario and ozone under the N_2O-RCP2.6 scenario, calculated as a per-centage of N_2O-RCP2.6 ozone, as a function of latitude and pressure. In 2100, N_2O mixing ratio is 340 parts per billion by volume (ppbv) for the RCP2.6 scenario, and 430 ppbV for the RCP8.5 scenario, com-pared to 320 ppbv in 2010. (b) Same but for the change in total column ozone (in Dobson units). Both simulations use the same scenario for CH_4 and CO_2 (IPCC SRES A1B), and the adjusted A1 scenario from WMO (2007) for the halocarbons. (c, d) same but for CH_4-RCP8.5 ozone minus CH_4-RCP2.6 ozone in the 2090s decade, otherwise using the same scenario for N_2O and CO_2 (IPCC SRES A1B), and the adjusted A1 scenario from WMO (2007) for the halocarbons. In 2100, the CH_4 mixing ratio is 1.25 parts per million by volume (ppmv) for the RCP2.6 scenario, and 3.75 ppmv for the RCP8.5 scenario; com-pared to 1.8 ppmv in 2010. Adapted from Revell et al. (2012a).

Various feedbacks are also important. The recovering ozone layer will reduce the penetration of UV radiation to the middle stratosphere and reduce the photolytic production of $O(^1D)$ (Rosenfield and Douglass, 1998; Fleming et al., 2011; Chipperfield et al., 2014), thereby reducing the production of NO_y via N_2O oxidation. Upper stratospheric cooling caused by GHG increases leads to enhanced conversion of NO_y to N_2 and less ozone destruction (Rosenfield and Douglass, 1998; Plummer et al., 2010). Portmann et al. (2012) computed that in 2100, the ozone destruction caused by increased N_2O was reduced by roughly 20% when the CO_2-induced stratospheric cooling effects on NO_y were included in the model simulations. Oman et al. (2010a) showed that the upper stratospheric cooling was greater when CCM simulations used the SRES A2 scenario than when they used the SRES A1b scenario. This enhanced cooling moderated the NO_y increase relative to the N_2O growth in the A2 scenario. Climate change-induced changes to the circulation, including an enhancement of the BDC, also modify the photochemical breakdown of N_2O (Rosenfield and Douglass, 1998; Plummer et al., 2010). A stronger Brewer-Dobson circulation will increase the loss of NO_y by increasing the rate of NO_y transport to the extratropical troposphere, where it is removed via nitric acid (HNO_3) washout. By comparing CCM simulations of N_2O increases, with and without the radiative and dynamical impacts of GHGs, Plummer et al. (2010) showed that GHG-induced cooling and circulation changes reduced the N_2O-induced increase of stratospheric NO_y by more than 50% by the end of the century.

The sensitivity of ozone to CH_4 is also complex, arising from a combination of direct and indirect effects (e.g., Brasseur and Solomon, 2005). Ozone is decreased through the direct impact of enhanced HO_x–ozone loss cycles as CH_4 is oxidized to H_2O. This mechanism dominates above ~45 km, so that the net impact of CH_4 is to reduce ozone in the very upper stratosphere and mesosphere. Figure 2-25c, d show the sensitivity of ozone in the late 21st century to the choice of high (RCP8.5) or low (RCP2.6) CH_4 scenarios. Below 45 km, and in the total column, increased CH_4 loading leads to increases in ozone via several mechanisms:

1) CH_4 converts active chlorine to the reservoir HCl via the reaction:
   $CH_4 + Cl \rightarrow HCl + CH_3$. This reduces the chlorine-catalyzed ozone loss, as long as chlorine levels are high (red areas around 20 hPa near the poles in Figure 2-25c).
2) CH_4 oxidation (mainly CH_4 + OH) leads to enhanced NO_x-induced ozone production in the troposphere and lowermost stratosphere ("photochemical smog chemistry," red area below 50 hPa in Figure 2-25c).
3) Increased H_2O, from methane oxidation, enhances stratospheric cooling and reduces chemical ozone loss rates (shown by the red area in Figure 2-25c around 10 to 20 hPa in the tropics and midlatitudes, and around 20 hPa near the poles).

For present-day chlorine loading, roughly two-thirds of the total column increase due to methane loading can be attributed to mechanism (1), but this will be much less important by the late 21st century. The process also reduces the effectiveness of present-day chlorine in depleting ozone by 15–20% (Fleming et al., 2011; Portmann et al., 2012). Mechanism (3) is most important in the middle stratosphere to lower mesosphere (30–60 km); it contributes about 20% to the total projected CH_4-induced increase in total column ozone during the 21st century (Figure 2-25d). By 2100, mechanism (2) will likely have the greatest impact. Methane oxidation (mechanism 2) is also affected by lower stratospheric NO_x produced by N_2O oxidation (e.g., Portmann and Solomon, 2007), as seen in Figure 2-25a. Also, CH_4 loading will increase stratospheric HO_x, which can (a) sequester NO_x in the reservoir HNO_3 (Nevison et al., 1999; Randeniya et al., 2002), and (b) enhance the HO_x-ozone loss, thereby reducing atomic oxygen abundance which in turn will reduce the NO_x-ozone loss cycles (Revell et al., 2012b).

Based on the SRES A1B GHG scenario, 2-D model calculations show that the total column response of ozone to CH_4 is around half to two-thirds that of N_2O at the end of the 21st century, with a CH_4-induced increase in the global ozone column of between 3 DU (Portmann et al., 2012) and 5 DU (Fleming et al., 2011) by 2100 (see Figure 2-24). However, quantifying the impact of CH_4 on ozone amounts toward the end of the century will have a large uncertainty due to the wide variation among the

RCP CH_4 scenarios, especially RCP8.5 (Section 2.4.3.1). Finally, uncertainties in the kinetic and photolytic loss rate parameters of both CH_4 and N_2O will have significant impacts on future ozone amounts (SPARC, 2013).

2.5 HIGHLIGHTS FOR POLICYMAKERS

This Assessment confirms the success of the international Montreal Protocol for the protection of the ozone layer.

As reported in previous Assessments, the decline of stratospheric ozone has been stopped in the late 1990s. Since about 2000, ozone levels in most parts of the stratosphere have remained approximately constant, or have been increasing slightly. Assessment of the most recent ozone observations since 2010 confirms these overall trends.

In the upper stratosphere, around 40 km altitude, ozone levels have been increasing in the last 10 years, and at a statistically significant rate. This increase is expected and is consistent with scientific understanding. About half of the ozone increase is due to declining ozone-depleting substances (ODSs, declining due to the Montreal Protocol). The other half is due to cooling of the stratosphere due to carbon dioxide (CO_2) increases, which slows chemical ozone destruction cycles in the upper stratosphere.

Not only ozone-depleting substances, but also increasing greenhouse gases affect the ozone layer.

Radiatively active greenhouse gases (GHGs) absorb thermal infrared radiation in the troposphere (global warming). Less thermal radiation reaches the stratosphere. In addition, GHGs, especially CO_2, emit radiation from the stratosphere to space. Both effects result in cooling of the stratosphere with increasing GHG levels. It is expected that GHG levels will increase throughout this century, and that the cooling of the stratosphere will continue.

A small acceleration of the global stratospheric Brewer-Dobson circulation (BDC) over the next century is expected from model simulations. This change is caused by GHG-induced warming of the troposphere and cooling of the stratosphere. Acceleration of the BDC will reduce ozone in the tropics and enhance ozone at higher latitudes.

As shown in previous Assessments, the continuing slow decline of ODSs, and the expected further increase of CO_2, will contribute to a recovery of stratospheric ozone. Model simulations indicate that total column ozone outside of the tropics will recover to 1980s values by 2020 to 2050 and to 1960s values by 2025 to 2060, later in the Antarctic. The recovery dates will depend on future GHG emissions but are expected to remain in this range for different plausible emission scenarios. In the second half of the century, ozone columns may even exceed historical levels. Figure 2-26 shows the expected range of near global (60°S to 60°N) annual mean total column ozone anomalies. In the tropics, ozone columns will probably not recover to 1960 values, but past ozone decline in the tropics has also been small.

Importance of future nitrous oxide and methane emissions

Since the last Assessment, model simulations have confirmed that not only ODSs and CO_2, but also future levels of nitrous oxide (N_2O) and methane (CH_4) will play a significant role in the recovery of stratospheric ozone over this century. By itself, increasing N_2O will increase ozone loss. This would delay and negate part of the expected ozone recovery (due to declining ODSs and stratospheric cooling).

Increasing methane, on the other hand, will generally increase ozone levels by tying up chlorine and by enhancing ozone production in the lower stratosphere. In the second half of the century, lower chlorine levels, stratospheric cooling, and other factors will reduce the efficiency by which CH_4 and N_2O emissions affect ozone.

Continued monitoring

Apart from future ODS levels, future levels of GHGs, especially carbon dioxide (CO_2), nitrous oxide (N_2O), methane (CH_4), and water vapor (H_2O) are expected to have important effects on the evolution of stratospheric ozone. Although most scenarios predict a recovery of stratospheric ozone, only continued measurements of ozone and these trace gases, and the combination of observations and model simulations, can verify that the ozone layer is recovering.

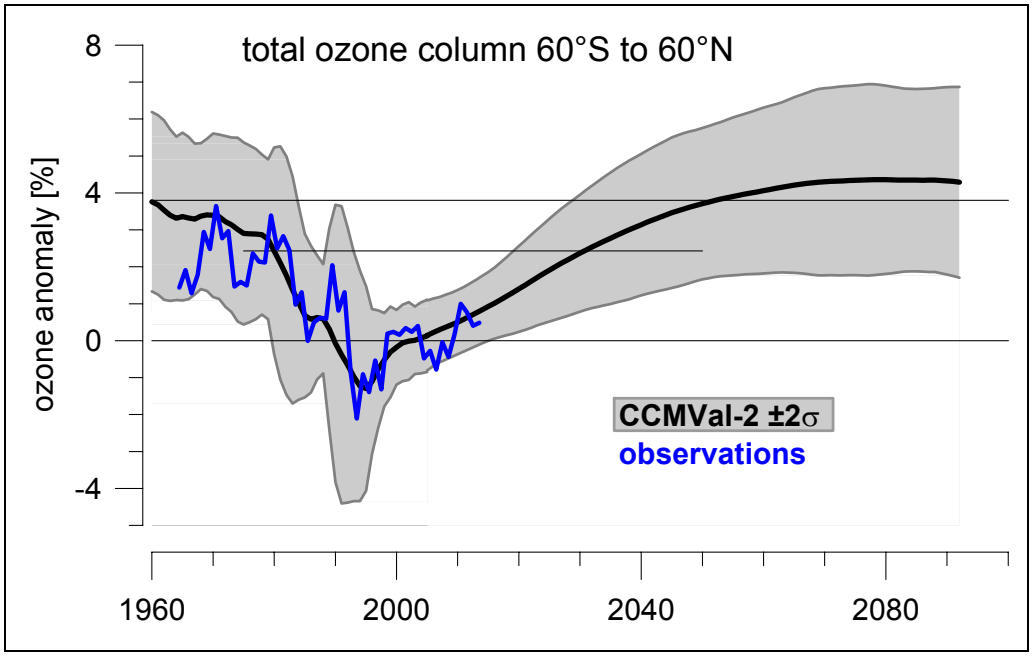

Figure 2-26. Simulated and observed evolution of the near global total ozone column. Observations are annual mean anomalies averaged over all available ground- and satellite-based measurements (blue line). Black line and gray range give multi-model mean and ±2 standard deviations of simulated individual model annual mean anomalies for the CCMVal-2 simulations already used in WMO (2011). Only the subset of 9 models performing runs for fixed ODS and for all forcings is used. All data are referenced to the 1998 to 2008 period. Up to 2000, the simulations account for changing ODSs, GHGs, observed sea surface temperatures and sea ice, volcanic aerosol, the 11-year solar-cycle, and the QBO (REF-B1 scenario, Eyring et al., 2010; WMO, 2011). After 2000 the adjusted A1 scenario of WMO (2007) is used for ODSs, the SRES A1B scenario is used for GHGs, sea surface temperatures and sea ice are from other models, the QBO is generated internally, there is no volcanic aerosol, and most models, except for 3, do not include the solar cycle (REF-B2 scenario, Eyring et al., 2010; WMO, 2011).

REFERENCES

Adams, C., A.E. Bourassa, A.F. Bathgate, C.A. McLinden, N.D. Lloyd, C.Z. Roth, E.J. Llewellyn, J.M. Zawodny, D.E. Flittner, G.L. Manney, W.H. Daffer, and D.A. Degenstein, Characterization of Odin-OSIRIS ozone profiles with the SAGE II dataset, *Atmos. Meas. Tech.*, *6* (5), 1447-1459, doi: 10.5194/amt-6-1447-2013, 2013.

Adams, C., A.E. Bourassa, V. Sofieva, L. Froidevaux, C.A. McLinden, D. Hubert, J.-C. Lambert, C.E. Sioris, and D.A. Degenstein, Assessment of Odin-OSIRIS ozone measurements from 2001 to the present using MLS, GOMOS, and ozonesondes, *Atmos. Meas. Tech.*, *7* (1), 49-64, doi: 10.5194/amt-7-49-2014, 2014.

Antón, M., M. Kroon, M. López, J.M. Vilaplana, M. Bañón, R. van der A, J.P. Veefkind, P. Stammes, and L. Alados-Arboledas, Total ozone column derived from GOME and SCIAMACHY using KNMI retrieval algorithms: Validation against Brewer measurements at the Iberian Peninsula, *J. Geophys. Res.*, *116* (D22), D22303, doi: 10.1029/2011JD016436, 2011.

Aquila, V., L.D. Oman, R. Stolarski, A.R. Douglass, and P.A. Newman, The response of ozone and nitrogen dioxide to the eruption of Mt. Pinatubo at southern and northern midlatitudes, *J. Atmos. Sci.*, *70* (3), 894-900, doi: 10.1175/JAS-D-12-0143.1, 2013.

Baldwin, M.P., L.J. Gray, T.J. Dunkerton, K. Hamilton, P.H. Haynes, W.J. Randel, J.R. Holton, M.J. Alexander, I. Hirota, T. Horinouchi, D.B.A. Jones, J.S. Kinnersley, C. Marquardt, K. Sato, and M. Takahashi, The quasi-biennial oscillation, *Rev. Geophys.*, *39* (2), 179-229, doi: 10.1029/1999RG000073, 2001.

Barath, F.T., M.C. Chavez, R.E. Cofield, D.A. Flower, M.A. Frerking, M.B. Gram, W.M. Harris, J.R. Holden, R.F. Jarnot, W.G. Kloezeman, G.J. Klose, G.K. Lau, M.S. Loo, B.J. Maddison, R.J. Mattauch, R.P. McKinney, G.E. Peckham, H.M. Pickett, G. Siebes, F.S. Soltis, R.A. Suttie, J.A. Tarsala, J.W. Waters, and W.J. Wilson, The Upper Atmosphere Research Satellite microwave limb sounder instrument, *J. Geophys. Res.*, *98* (D6), 10751-10762, doi: 10.1029/93JD00798, 1993.

Bertaux, J.L., E. Kyrölä, D. Fussen, A, Hauchecorne, F. Dalaudier, V. Sofieva, J. Tamminen, F. Vanhellemont, O. Fanton d'Andon, G. Barrot, A. Mangin, L. Blanot, J.C. Lebrun, K. Pérot, T. Fehr, L. Saavedra, G.W. Leppelmeier, and R. Fraisse, Global ozone monitoring by occultation of stars: An overview of GOMOS measurements on ENVISAT, *Atmos. Chem. Phys.*, *10* (24), 12091-12148, doi: 10.5194/acp-10-12091-2010, 2010.

Bhartia, P.K., R.D. McPeters, L.E. Flynn, S. Taylor, N.A. Kramarova, S. Frith, B. Fisher, and M. DeLand, Solar Backscatter UV (SBUV) total ozone and profile algorithm, *Atmos. Meas. Tech.*, *6* (10), 2533-2548, doi: 10.5194/amt-6-2533-2013, 2013.

Bodeker, G.E., B. Hassler, P.J. Young, and R.W. Portmann, A vertically resolved, global, gap-free ozone database for assessing or constraining global climate model simulations, *Earth Syst. Sci. Data*, *5* (1), 31-43, doi: 10.5194/essd-5-31-2013, 2013.

Bojkov, R.D., V.E. Fioletov, and A.M. Shalamjansky, Total ozone changes over Eurasia since 1973 based on reevaluated filter ozonometer data, *J. Geophys. Res.*, *99* (D11), 22985-22999, doi: 10.1029/94JD02006, 1994.

Bourassa, A.E., A. Robock, W.J. Randel, T. Deshler, L.A. Rieger, N.D Lloyd, E.J. Llewellyn, and D.A. Degenstein, Large volcanic aerosol load in the stratosphere linked to Asian Monsoon transport, *Science*, *337* (6090), 78-81, doi: 10.1126/science.1219371, 2012.

Bourassa, A.E., A. Robock, W.J. Randel, T. Deshler, L.A. Rieger, N.D Lloyd, E.J. Llewellyn, and D.A. Degenstein, Response to comments on "Large volcanic aerosol load in the stratosphere linked to Asian Monsoon transport," *Science*, *339* (6120), 647, doi: 10.1126/science.1227961, 2013.

Boyd, I.S., A.D. Parrish, L. Froidevaux, T. von Clarmann, E. Kyrölä, J.M. Russell III, and J.M. Zawodny, Ground-based microwave ozone radiometer measurements compared with Aura-MLS v2.2 and other instruments at two Network for Detection of Atmospheric Composition Change sites, *J. Geophys. Res.*, *112* (D24), D24S33, doi: 10.1029/2007JD008720, 2007.

Brasseur, G., and S. Solomon, *Aeronomy of the Middle Atmosphere*, 3rd ed., Dordrecht, The Netherlands, 2005.

Brönnimann, S., J. Bhend, J. Franke, S. Flückiger, A.M. Fischer, R. Bleisch, G. Bodeker, B. Hassler, E. Rozanov, and M. Schraner, A global historical ozone data set and prominent features of stratospheric variability prior to 1979, *Atmos. Chem. Phys.*, *13* (18), 9623-9639, doi: 10.5194/acp-13-9623-2013, 2013.

Cahalan, R.F., G. Wen, J.W. Harder, and P. Pilewskie, Temperature responses to spectral solar variability on decadal time scales, *Geophys. Res. Lett.*, *37* (7), L07705, doi: 10.1029/2009GL041898, 2010.

Charlton-Perez, A.J., E. Hawkins, V. Eyring, I. Cionni, G.E. Bodeker, D.E. Kinnison, H. Akiyoshi, S.M. Frith, R. Garcia, A. Gettelman, J.F. Lamarque, T. Nakamura, S. Pawson, Y. Yamashita, S. Bekki, P. Braesicke, M.P.

Chipperfield, S. Dhomse, M. Marchand, E. Mancini, O. Morgenstern, G. Pitari, D. Plummer, J.A. Pyle, E. Rozanov, J. Scinocca, K. Shibata, T.G. Shepherd, W. Tian, and D.W. Waugh, The potential to narrow uncertainty in projections of stratospheric ozone over the 21st century, *Atmos. Chem. Phys.*, *10*, 9473-9486, doi: 10.5194/acp-10-9473-2010, 2010.

Chehade, W., M. Weber, and J.P. Burrows, Total ozone trends and variability during 1979-2012 from merged data sets of various satellites, *Atmos. Chem. Phys.*, *14* (13), 7059-7074, doi: 10.5194/acp-14-7059-2014, 2014.

Chiou, E.W., P.K. Bhartia, R.D. McPeters, D.G. Loyola, M. Coldewey-Egbers, V.E. Fioletov, M. Van Roozendael, R. Spurr, C. Lerot, and S.M. Frith, Comparison of profile total ozone from SBUV (v8.6) with GOME-type and ground-based total ozone for the 16-year period (1996 to 2011), *Atmos. Meas. Tech.*, *7* (6), 1681-1692, doi: 10.5194/amt-7-1681-2014, 2014.

Chipperfield, M.P., Q. Liang, S.E. Strahan, O. Morgenstern, S.S. Dhomse, N.L. Abraham, A.T. Archibald, S. Bekki, P. Braesicke, G. Di Genova, E.L. Fleming, S.C. Hardiman, D. Iachetti, C.H. Jackman, D.E. Kinnison, M. Marchand, G. Pitari, J.A. Pyle, E. Rozanov, A. Stenke, and F. Tummon, Multimodel estimates of atmospheric lifetimes of long-lived ozone-depleting substances: Present and future, *J. Geophys. Res.*, *119* (5), 2555-2573, doi: 10.1002/2013JD021097, 2014.

Coldewey-Egbers, M., M. Weber, L.N. Lamsal, R. deBeck, M. Buchwitz, and J.P. Burrows, Total ozone retrieval from GOME UV spectral data using the weighting function DOAS approach, *Atmos. Chem. Phys.*, *5* (4), 1015-1025, doi: 10.5194/acp-5-1015-2005, 2005.

Damadeo, R.P., J.M. Zawodny, L.W. Thomason, and N. Iyer, SAGE version 7.0 algorithm: Application to SAGE II, *Atmos. Meas. Tech.*, *6* (12), 3539-3561, doi: 10.5194/amt-6-3539-2013, 2013.

Daniel, J.S., E.L. Fleming, R.W. Portmann, G.J.M. Velders, C.H. Jackman, and A.R. Ravishankara, Options to accelerate ozone recovery: Ozone and climate benefits, *Atmos. Chem. Phys.*, *10* (16), 7697-7707, doi: 10.5194/acp-10-7697-2010, 2010.

DeLand, M.T., and R.P. Cebula, Solar UV variations during the decline of Cycle 23, *J. Atmos. Sol. Terr. Phys.*, *77*, 225-234, doi: 10.1016/j.jastp.2012.01.007, 2012.

DeLand, M.T., S.L. Taylor, L.K. Huang, and B.L. Fisher, Calibration of the SBUV version 8.6 ozone data product, *Atmos. Meas. Tech.*, *5* (11), 2951-2967, doi: 10.5194/amt-5-2951-2012, 2012.

Deshler, T., J.L. Mercer, H.G.J. Smit, R. Stubi, G. Levrat, B.J. Johnson, S.J. Oltmans, R. Kivi, A.M. Thompson, J. Witte, J. Davies, F.J. Schmidlin, G. Brothers, and T. Sasaki, Atmospheric comparison of electrochemical cell ozonesondes from different manufacturers, and with different cathode solution strengths: The Balloon Experiment on Standards for Ozonesondes, *J. Geophys. Res.*, *113*, D04307, doi: 10.1029/2007JD008975, 2008.

Dhomse, S., M.P. Chipperfield, W. Feng, and J.D. Haigh, Solar response in tropical stratospheric ozone: A 3-D chemical transport model study using ERA reanalyses, *Atmos. Chem. Phys.*, *11* (24), 12773-12786, doi: 10.5194/acp-11-12773-2011, 2011.

Dhomse, S.S., M.P. Chipperfield, W. Feng, W.T. Ball, Y.C. Unruh, J.D. Haigh, N.A. Krivova, S.K. Solanki, and A.K. Smith, Stratospheric O_3 changes during 2001-2010: The small role of solar flux variations in a chemical transport model, *Atmos. Chem. Phys.*, *13* (19), 10113-10123, doi: 10.5194/acp-13-10113-2013, 2013.

Dikty, S., H. Schmidt, M. Weber, C. von Savigny, and M.G. Mlynczak, Daytime ozone and temperature variations in the mesosphere: A comparison between SABER observations and HAMMONIA model, *Atmos. Chem. Phys.*, *10* (17), 8331-8339, doi: 10.5194/acp-10-8331-2010, 2010a.

Dikty, S., M. Weber, C. von Savigny, T. Sonkaew, A. Rozanov, and J.P. Burrows, Modulations of the 27 day solar rotation signal in stratospheric ozone from Scanning Imaging Absorption Spectrometer for Atmospheric Cartography (SCIAMACHY) (2003-2008), *J. Geophys. Res.*, *115*, D00I15, doi: 10.1029/2009JD012379, 2010b.

Douglass, A.R., R.S. Stolarski, S.E. Strahan, and L.D. Oman, Understanding differences in upper stratospheric ozone response to changes in chlorine and temperature as computed using CCMVal-2 models, *J. Geophys. Res.*, *117*, D16306, doi: 10.1029/2012JD017483, 2012.

Douglass, A.R., S.E. Strahan, L.D. Oman, and R.S. Stolarski, Understanding differences in chemistry climate model projections of stratospheric ozone, *J. Geophys. Res.*, *119* (8), 4922-4939, doi: 10.1002/2013JD021159, 2014.

Eckert, E., T. von Clarmann, M. Kiefer, G.P. Stiller, S. Lossow, N. Glatthor, D.A. Degenstein, L. Froidevaux, S. Godin-Beekmann, T. Leblanc, S. McDermid, M. Pastel, W. Steinbrecht, D.P.J. Swart, K.A. Walker, and P.F. Bernath, Drift-corrected trends and periodic variations in MIPAS IMK/IAA ozone measurements, *Atmos. Chem. Phys.*, *14* (5), 2571-2589, doi: 10.5194/acp-14-2571-2014, 2014.

Ermolli, I., K. Matthes, T. Dudok de Wit, N.A. Krivova, K. Tourpali, M. Weber, Y.C. Unruh, L. Gray, U. Langematz, P. Pilewskie, E. Rozanov, W. Schmutz, A. Shapiro, S.K. Solanki, and T.N. Woods, Recent variability of the solar spectral irradiance and its impact on climate modelling, *Atmos. Chem. Phys.*, *13* (8), 3945-3977, doi: 10.5194/acp-13-3945-2013, 2013.

Eyring, V., I. Cionni, G.E. Bodeker, A.J. Charlton-Perez, D.E. Kinnison, J.F. Scinocca, D.W. Waugh, H. Akiyoshi, S. Bekki, M.P. Chipperfield, M. Dameris, S. Dhomse, S.M. Frith, H. Garny, A. Gettelman, A. Kubin, U. Langematz, E. Mancini, M. Marchand, T. Nakamura, L.D. Oman, S. Pawson, G. Pitari, D.A. Plummer, E. Rozanov, T.G. Shepherd, K. Shibata, W. Tian, P. Braesicke, S.C. Hardiman, J.F. Lamarque, O. Morgenstern, J.A. Pyle, D. Smale, and Y. Yamashita, Multi-model assessment of stratospheric ozone return dates and ozone recovery in CCMVal-2 models, *Atmos. Chem. Phys.*, *10*, 9451-9472, doi: 10.5194/acp-10-9451-2010, 2010.

Eyring, V., J.M. Arblaster, I. Cionni, J. Sedláček, J. Perlwitz, P.J. Young, S. Bekki, D. Bergmann, P. Cameron-Smith, W.J. Collins, G. Faluvegi, K.-D. Gottschaldt, L.W. Horowitz, D.E. Kinnison, J.-F. Lamarque, D.R. Marsh, D. Saint-Martin, D.T. Shindell, K. Sudo, S. Szopa, and S. Watanabe, Long-term ozone changes and associated climate impacts in CMIP5 simulations, *J. Geophys. Res.*, *118* (10), 5029-5060, doi: 10.1002/jgrd. 50316, 2013.

Fioletov, V.E., Estimating the 27-day and 11-year solar cycle variations in tropical upper stratospheric ozone, *J. Geophys. Res.*, *114*, D02302, doi: 10.1029/2008JD010499, 2009.

Fioletov, V.E., G.E. Bodeker, A.J. Miller, R.D. McPeters, and R. Stolarski, Global and zonal total ozone variations estimated from ground-based and satellite measurements: 1964–2000, *J. Geophys. Res.*, *107* (D22), 4647, doi: 10.1029/2001JD001350, 2002.

Fioletov, V.E., G. Labow, R. Evans, E.W. Hare, U. Köhler, C.T. McElroy, K. Miyagawa, A. Redondas, V. Savastiouk, A.M. Shalamyansky, J. Staehelin, K. Vanicek, and M. Weber, Performance of ground-based total ozone network assessed using satellite data, *J. Geophys. Res.*, *113*, D14313, doi: 10.1029/2008JD009809, 2008.

Fleming, E.L., C.H. Jackman, R.S. Stolarski, and A.R. Douglass, A model study of the impact of source gas changes on the stratosphere for 1850-2100, *Atmos. Chem. Phys.*, *11* (16), 8515-8541, doi: 10.5194/acp-11-8515-2011, 2011.

Froidevaux, L., Y.B. Jiang, A. Lambert, N.J. Livesey, W.G. Read, J.W. Waters, E.V. Browell, J.W. Hair, M.A. Avery, T.J. McGee, L.W. Twigg, G.K. Sumnicht, K.W. Jucks, J.J. Margitan, B. Sen, R.A. Stachnik, G.C. Toon, P.F. Bernath, C.D. Boone, K.A. Walker, M.J. Filipiak, R.S. Harwood, R.A. Fuller, G.L. Manney, M.J. Schwartz, W.H. Daffer, B.J. Drouin, R.E. Cofield, D.T. Cuddy, R.F. Jarnot, B.W. Knosp, V.S. Perun, W.V. Snyder, P.C. Stek, R.P. Thurstans, and P.A. Wagner, Validation of Aura Microwave Limb Sounder stratospheric ozone measurements, *J. Geophys. Res.*, *113* (D15), D15S20, doi: 10.1029/2007JD008771, 2008.

Fromm, M., G. Nedoluha, and Z. Charvát, Comment on "Large volcanic aerosol load in the stratosphere linked to Asian monsoon transport," *Science*, *339* (6120), 647, doi: 10.1126/science.1228605, 2013.

Frossard, L., H.E. Rieder, M. Ribatet, J. Staehelin, J.A. Maeder, S. Di Rocco, A.C. Davison, and T. Peter, On the relationship between total ozone and atmospheric dynamics and chemistry at mid-latitudes – Part 1: Statistical models and spatial fingerprints of atmospheric dynamics and chemistry, *Atmos. Chem. Phys.*, *13* (1), 147-164, doi: 10.5194/acp-13-147-2013, 2013.

Gabriel, A., H. Körnich, S. Lossow, D.H.W. Peters, J. Urban, and D. Murtagh, Zonal asymmetries in middle atmospheric ozone and water vapour derived from Odin satellite data 2001-2010, *Atmos. Chem. Phys.*, *11* (18), 9865-9885, doi: 10.5194/acp-11-9865-2011, 2011a.

Gabriel, A., H. Schmidt, and D.H.W. Peters, Effects of the 11 year solar cycle on middle atmospheric stationary wave patterns in temperature, ozone, and water vapor, *J. Geophys. Res.*, *116*, D23301, doi: 10.1029/2011 JD015825, 2011b.

Garny, H., G.E. Bodeker, D. Smale, M. Dameris, and V. Grewe, Drivers of hemispheric differences in return dates of mid-latitude stratospheric ozone to historical levels, *Atmos. Chem. Phys.*, *13* (15), 7279-7300, doi: 10.5194/acp-13-7279-2013, 2013.

Gebhardt, C., A. Rozanov, R. Hommel, M. Weber, H. Bovensmann, J.P. Burrows, D. Degenstein, L. Froidevaux, and A.M. Thompson, Stratospheric ozone trends and variability as seen by SCIAMACHY from 2002 to 2012, *Atmos. Chem. Phys.*, *14* (2), 831-846, doi: 10.5194/acp-14-831-2014, 2014.

Gillett, N.P., H. Akiyoshi, S. Bekki, P. Braesicke, V. Eyring, R. Garcia, A.Yu. Karpechko, C.A. McLinden, O. Morgenstern, D.A. Plummer, J.A. Pyle, E. Rozanov, J. Scinocca, and K. Shibata, Attribution of observed changes in stratospheric ozone and temperature, *Atmos. Chem. Phys.*, *11* (2), 599-609, doi: 10.5194/acp-11-599-2011, 2011.

Gottwald, M., and H. Bovensmann, *SCIAMACHY - Exploring the Changing Earth's Atmosphere*, Dordrecht Heidelberg London New York, doi: 10.1007/978-90-481-9896-2, 2011.

Gray, L.J., J. Beer, M. Geller, J.D. Haigh, M. Lockwood, K. Matthes, U. Cubasch, D. Fleitmann, G. Harrison, L. Hood, J. Luterbacher, G.A. Meehl, D. Shindell, B. van Geel, and W. White, Solar influence on climate, *Rev. Geophys.*, *48*, RG4001, doi: 10.1029/2009RG000282, 2010.

Gruzdev, A.N., H. Schmidt, and G.P. Brasseur, The effect of the solar rotational irradiance variation on the middle and upper atmosphere calculated by a three-dimensional chemistry-climate model, *Atmos. Chem. Phys.*, *9* (2), 595-614, doi: 10.5194/acp-9-595-2009, 2009.

Haefele, A., K. Hocke, N. Kämpfer, P. Keckhut, M. Marchand, S. Bekki, B. Morel, T. Egorova, and E. Rozanov, Diurnal changes in middle atmospheric H_2O and O_3: Observations in the Alpine region and climate models, *J. Geophys. Res.*, *113* (D17), D17303, doi: 10.1029/2008JD009892, 2008.

Haigh, J.D., A.R. Winning, R. Toumi, and J.W. Harder, An influence of solar spectral variations on radiative forcing of climate, *Nature*, *467*, 696-699, doi: 10.1038/nature09426, 2010.

Harder, J.W., J.M. Fontenla, P. Pilewskie, E.C. Richard, and T.N. Woods, Trends in solar spectral irradiance variability in the visible and infrared, *Geophys. Res. Lett.*, *36*, L07801, doi: 10.1029/2008GL036797, 2009.

Harris, N.R.P., E. Kyrö, J. Staehelin, D. Brunner, S.-B. Andersen, S. Godin-Beekmann, S. Dhomse, P. Hadjinicolaou, G. Hansen, I. Isaksen, A. Jrrar, A. Karpetchko, R. Kivi, B. Knudsen, P. Krizan, J. Lastovicka, J. Maeder, Y. Orsolini, J.A. Pyle, M. Rex, K. Vanicek, M. Weber, I. Wohltmann, P. Zanis, and C. Zerefos, Ozone trends at northern mid- and high latitudes – a European perspective, *Ann. Geophys.*, *26*, 1207-1220, 2008.

Hassler, B., G.E. Bodeker, I. Cionni, and M. Dameris, A vertically resolved, monthly mean, ozone database from 1979 to 2100 for constraining global climate model simulations, *Int. J. Remote Sens.*, *30* (15-16), 4009-4018, doi: 10.1080/01431160902821874, 2009.

Hassler, B., I. Petropavlovskikh, J. Staehelin, T. August, P.K. Bhartia, C. Clerbaux, D. Degenstein, M. De Mazière, B.M. Dinelli, A. Dudhia, G. Dufour, S.M. Frith, L. Froidevaux, S. Godin-Beekmann, J. Granville, N.R.P. Harris, K. Hoppel, D. Hubert, Y. Kasai, M.J. Kurylo, E. Kyrölä, J.-C. Lambert, P.F. Levelt, C.T. McElroy, R.D. McPeters, R. Munro, H. Nakajima, A. Parrish, P. Raspollini, E.E. Remsberg, K.H. Rosenlof, A. Rozanov, T. Sano, Y. Sasano, M. Shiotani, H.G.J. Smit, G. Stiller, J. Tamminen, D.W. Tarasick, J. Urban, R.J. van der A, J.P. Veefkind, C. Vigouroux, T. von Clarmann, C. von Savigny, K.A. Walker, M. Weber, J. Wild, and J. Zawodny, SI2N overview paper: Ozone profile measurements: Techniques, uncertainties and availability, *Atmos. Meas. Tech.*, 7, 1395-1427, doi: 10.5194/amt-7-1395-2014, 2014.

Hegerl G.C., H. von Storch, K. Hasselmann, B.D. Santer, U. Cubasch, and P.D. Jones, Detecting greenhouse-gas-induced climate change with an optimal fingerprint method, *J. Clim.*, *9* (10), 2281-2306, doi: 10.1175/1520-0442(1996)009<2281:DGGICC>2.0.CO;2, 1996.

Hendrick, F., J.-P. Pommereau, F. Goutail, R.D. Evans, D. Ionov, A. Pazmino, E. Kyrö, G. Held, P. Eriksen, V. Dorokhov, M. Gil, and M. Van Roozendael, NDACC/SAOZ UV-visible total ozone measurements: Improved retrieval and comparison with correlative ground-based and satellite observations, *Atmos. Chem. Phys.*, *11* (12), 5975-5995, doi: 10.5194/acp-11-5975-2011, 2011.

Hofmann, D., J. Barnes, M. O'Neill, M. Trudeau, and R. Neely, Increase in background stratospheric aerosol observed with lidar at Mauna Loa Observatory and Boulder, Colorado, *Geophys. Res. Lett.*, *36*, L15808, doi: 10.1029/2009GL039008, 2009.

Hood, L.L., and B.E. Soukharev, The lower-stratospheric response to 11-yr solar forcing: Coupling to the troposphere-ocean response, *J. Atmos. Sci.*, *69* (6), 1841-1864, doi: 10.1175/JAS-D-11-086.1, 2012.

Hood, L.L., B.E. Soukharev, and J.P. McCormack, Decadal variability of the tropical stratosphere: Secondary influence of the El Niño-Southern Oscillation, *J. Geophys. Res.*, *115* (D11), D11113, doi: 10.1029/2009 JD012291, 2010.

Huang, F.T., C.A. Reber, and J. Austin, Ozone diurnal variations observed by UARS and their model simulation, *J. Geophys. Res.*, *102* (D11), 12971-12985, doi: 10.1029/97JD00461, 1997.

Huang, F.T., H.G. Mayr, J.M. Russell III, M.G. Mlynczak, and C.A. Reber, Ozone diurnal variations and mean profiles in the mesosphere, lower thermosphere, and stratosphere, based on measurements from SABER on TIMED, *J. Geophys. Res.*, *113* (A4), A04307, doi: 10.1029/2007JA012739, 2008.

Huang, F.T., H.G. Mayr, J.M. Russell III, and M.G. Mlynczak, Ozone diurnal variations in the stratosphere and lower mesosphere, based on measurements from SABER on TIMED, *J. Geophys. Res.*, *115* (D24), D24308, doi: 10.1029/2010JD014484, 2010.

IPCC (Intergovernmental Panel on Climate Change), *Climate Change 2007: The Physical Science Basis: Contribution of Working Group I to the Fourth Assessment Report of the Intergovernmental Panel on Climate Change*, edited by Solomon, S., D. Qin, M. Manning, Z. Chen, M. Marquis, K.B. Averyt, M. Tignor, and H.L. Miller, 996 pp., Cambridge University Press, Cambridge, U.K., and New York, NY, U.S.A., 2007.

IPCC (Intergovernmental Panel on Climate Change), *Climate Change 2013: The Physical Science Basis: Contribution of Working Group I to the Fifth Assessment Report of the Intergovernmental Panel on Climate Change*, edited by T.F. Stocker, D. Qin, G.-K. Plattner, M. Tignor, S.K. Allen, J. Boschung, A. Nauels, Y. Xia, V. Bex, and P.M. Midgley, 1535 pp., Cambridge University Press, Cambridge, UK, and New York, NY, USA, 2013.

Jones, A., J. Urban, D.P. Murtagh, P. Eriksson, S. Brohede, C. Haley, D. Degenstein, A. Bourassa, C. von Savigny, T. Sonkaew, A. Rozanov, H. Bovensmann, and J. Burrows, Evolution of stratospheric ozone and water vapour time series studied with satellite measurements, *Atmos. Chem. Phys.*, *9* (16), 6055-6075, doi: 10.5194/acp-9-6055-2009, 2009.

Jones, A., J. Urban, D.P. Murtagh, C. Sanchez, K.A. Walker, N.J. Livesey, L. Froidevaux, and M.L. Santee, Analysis of HCl and ClO time series in the upper stratosphere using satellite data sets, *Atmos. Chem. Phys.*, *11* (11), 5321-5333, doi: 10.5194/acp-11-5321-2011, 2011.

Jonsson, A.I., V.I. Fomichev, and T.G. Shepherd, The effect of nonlinearity in CO_2 heating rates on the attribution of stratospheric ozone and temperature changes. *Atmos. Chem. Phys.*, *9*, 8447-8452, doi: 10.5194/acp-9-8447-2009, 2009.

Karpechko, A.Y., D. Maraun, and V. Eyring, Improving Antarctic total ozone projections by a process-oriented multiple diagnostic ensemble regression, *J. Atmos. Sci.*, *70* (12), 3959-3976, doi: 10.1175/JAS-D-13-071.1, 2013.

Kiesewetter, G., B.-M., Sinnhuber, M. Weber, and J.P. Burrows, Attribution of stratospheric ozone trends to chemistry and transport: A modelling study, *Atmos. Chem. Phys.*, *10* (24), 12073-12089, doi: 10.5194/acp-10-12073-2010, 2010.

Kirgis, G., T. Leblanc, I.S. McDermid, and T.D. Walsh, Stratospheric ozone interannual variability (1995-2011) as observed by lidar and satellite at Mauna Loa Observatory, HI and Table Mountain Facility, CA, *Atmos. Chem. Phys.*, *13* (9), 5033-5047, doi: 10.5194/acp-13-5033-2013, 2013.

Knutti, R., G. Abramowitz, M. Collins, V. Eyring, P.J. Gleckler, B. Hewitson, and L. Mearns, Good practice guidance paper on assessing and combining multi model climate projections, *IPCC Expert Meeting on Assessing and Combining Multi Model Climate Projections*, edited by T. Stocker, D. Qin, G.-K. Plattner, M. Tignor, and P.M. Midgley, 13 pp., University of Bern, Bern, Switzerland, 2010.

Kobayashi C., and K. Shibata, Evaluation of dynamical contribution to lower stratospheric ozone trends in northern mid-latitudes over the last three decades (1980–2006) using a Chemical Transport Model, *J. Meteorol. Soc. Japan.*, *89* (4), 363-376, doi: 10.2151/jmsj.2011-405, 2011.

Koukouli, M.E., D.S. Balis, D. Loyola, P. Valks, W. Zimmer, N. Hao, J.-C. Lambert, M. Van Roozendael, C. Lerot, and R.J.D. Spurr, Geophysical validation and long-term consistency between GOME-2/MetOp-A total ozone column and measurements from the sensors GOME/ERS-2, SCIAMACHY/ENVISAT and OMI/Aura, *Atmos. Meas. Tech.*, *5* (9), 2169-2181, doi: 10.5194/amt-5-2169-2012, 2012.

Kramarova, N.A., S.M. Frith, P.K. Bhartia, R.D. McPeters, S.L. Taylor, B.L. Fisher, G.J. Labow, and M.T. DeLand, Validation of ozone monthly zonal mean profiles obtained from the version 8.6 Solar Backscatter Ultraviolet algorithm, *Atmos. Chem. Phys.*, *13* (14), 6887-6905, doi: 10.5194/acp-13-6887-2013, 2013a.

Kramarova, N.A., P.K. Bhartia, S.M. Frith, R.D. McPeters, and R.S. Stolarski, Interpreting SBUV smoothing errors: An example using the quasi-biennial oscillation, *Atmos. Meas. Tech.*, *6* (8), 2089-2099, doi: 10.5194/amt-6-2089-2013, 2013b.

Kramarova, N.A., E.R. Nash, P.A. Newman, P.K. Bhartia, R.D. McPeters, D.F. Rault, C.J. Seftor, P.Q. Xu, and G.J. Labow, Measuring the Antarctic ozone hole with the new Ozone Mapping and Profiler Suite (OMPS), *Atmos. Chem. Phys.*, *14* (5), 2353-2361, doi: 10.5194/acp-14-2353-2014, 2014.

Kroon, M., J.P. Veefkind, M. Sneep, R.D. McPeters, P.K. Bhartia, and P.F. Levelt, Comparing OMI-TOMS and OMI-DOAS total ozone column data, *J. Geophys. Res.*, *113* (D16), D16S28, doi: 10.1029/2007JD008798, 2008.

Kroon, M., J.F. de Haan, J.P. Veefkind, L. Froidevaux, R. Wang, R. Kivi, and J.J. Hakkarainen, Validation of operational ozone profiles from the Ozone Monitoring Instrument, *J. Geophys. Res.*, *116* (D18), D18305, doi: 10.1029/2010JD015100, 2011.

Krzyścin, J.W., Onset of the total ozone increase based on statistical analyses of global ground-based data for the period 1964–2008, *Int. J. Clim.*, *32* (2), 240-246, doi: 10.1002/joc.2264, 2012.

Kubin, A., U. Langematz, and C. Brühl, Chemistry climate model simulations of the effect of the 27 day solar rotational cycle on ozone, *J. Geophys. Res*., *116* (D15), D15301, doi: 10.1029/2011JD015665, 2011.

Kyrölä, E., J. Tamminen, V. Sofieva, J.L. Bertaux, A. Hauchecorne, F. Dalaudier, D. Fussen, F. Vanhellemont, O. Fanton d'Andon, G. Barrot, M. Guirlet, T. Fehr, and L. Saavedra de Miguel, GOMOS O_3, NO_2, and NO_3 observations in 2002–2008, *Atmos. Chem. Phys.*, *10* (16), 7723-7738, doi: 10.5194/acp-10-7723-2010, 2010.

Kyrölä, E., M. Laine, V. Sofieva, J. Tamminen, S.-M. Päivärinta, S. Tukiainen, J. Zawodny, and L. Thomason, Combined SAGE II-GOMOS ozone profile data set for 1984-2011 and trend analysis of the vertical distribution of ozone, *Atmos. Chem. Phys.*, *13* (21), 10645-10658, doi: 10.5194/acp-13-10645-2013, 2013.

Labow, G.J., R.D. McPeters, P.K. Bhartia, and N. Kramarova, A comparison of 40 years of SBUV measurements of column ozone with data from the Dobson/Brewer network, *J. Geophys. Res.*, *118* (13), 7370-7378, doi: 10.1002/jgrd.50503, 2013.

Lamarque, J.-F., D.T. Shindell, B. Josse, P.J. Young, I. Cionni, V. Eyring, D. Bergmann, P. Cameron-Smith, W.J. Collins, R. Doherty, S. Dalsoren, G. Faluvegi, G. Folberth, S.J. Ghan, L.W. Horowitz, Y.H. Lee, I.A. MacKenzie, T. Nagashima, V. Naik, D. Plummer, M. Righi, S.T. Rumbold, M. Schulz, R.B. Skeie, D.S. Stevenson, S. Strode, K. Sudo, S. Szopa, A. Voulgarakis, and G. Zeng, The Atmospheric Chemistry and Climate Model Intercomparison Project (ACCMIP): Overview and description of models, simulations and climate diagnostics, *Geosci. Model Dev.*, *6* (1), 179-206, doi: 10.5194/gmd-6-179-2013, 2013.

Lean, J., Evolution of the sun's spectral irradiance since the Maunder Minimum, *Geophys. Res. Lett*., *27* (16), 2425-2428, doi: 10.1029/2000GL000043, 2000.

Lean, J.L., and M.T. DeLand, How does the sun's spectrum vary?, *J. Clim.*, *25* (7), 2555-2560, doi: 10.1175/JCLI-D-11-00571.1, 2012.

Lerot, C., M. Van Roozendael, R. Spurr, D. Loyola, M. Coldewey-Egbers, S. Kochenova, J. van Gent, M. Koukouli, D. Balis, J.-C. Lambert, J. Granville, and C. Zehner, Homogenized total ozone data records from the European sensors GOME/ERS-2, SCIAMACHY/Envisat, and GOME-2/MetOp-A, *J. Geophys. Res.*, *119* (3), 1639-1662, doi: 10.1002/2013JD020831, 2014.

Li, F., R.S. Stolarski, and P.A. Newman, Stratospheric ozone in the post-CFC era, *Atmos. Chem. Phys.*, *9* (6), 2207-2213, doi: 10.5194/acp-9-2207-2009, 2009.

Lin, P., and Q. Fu, Changes in various branches of the Brewer-Dobson circulation from an ensemble of chemistry climate models, *J. Geophys. Res.*, *118*, 73-84, doi: 10.1029/2012JD018813, 2013.

Liu, J., D.W. Tarasick, V.E. Fioletov, C. McLinden, T. Zhao, S. Gong, C. Sioris, J.J. Jin, G. Liu, and O. Moeini, A global ozone climatology from ozone soundings via trajectory mapping: A stratospheric perspective, *Atmos. Chem. Phys.*, *13* (22), 11441-11464, doi: 10.5194/acp-13-11441-2013, 2013.

Livesey, N.J., W. Van Snyder, W.G. Read, and P.A. Wagner, Retrieval algorithms for the EOS Microwave Limb Sounder (MLS), *IEEE Trans. Geosci. Rem. Sens.*, *44* (5), 1144-1155, doi: 10.1109/TGRS.2006.872327, 2006.

Loyola, D.G., R.M. Coldewey-Egbers, M. Dameris, H. Garny, A. Stenke, M. Van Roozendael, C. Lerot, D. Balis, and M. Koukouli, Global long-term monitoring of the ozone layer — a prerequisite for predictions, *Int. J. Remote Sens.*, *30*, 4295-4318, doi: 10.1080/01431160902825016, 2009.

Manney, G.L., M.L. Santee, M. Rex, N.J. Livesey, M.C. Pitts, P. Veefkind, E.R. Nash, I. Wohltmann, R. Lehmann, L. Froidevaux, L.R. Poole, M.R. Schoeberl, D.P. Haffner, J. Davies, V. Dorokhov, H. Gernandt, B. Johnson, R. Kivi, E. Kyrö, N. Larsen, P.F. Levelt, A. Makshtas, C.T. McElroy, H. Nakajima, M.C. Parrondo, D.W. Tarasick, P. von der Gathen, K.A. Walker, and N.S. Zinoviev, Unprecedented Arctic ozone loss in 2011, *Nature*, *478*, 469-475, doi: 10.1038/nature10556, 2011.

Mäder, J.A., J. Staehelin, T. Peter, D. Brunner, H.E. Rieder, and W.A. Stahel, Evidence for the effectiveness of the Montreal Protocol to protect the ozone layer, *Atmos. Chem. Phys.*, *10* (24), 12161-12171, doi: 10.5194/acp-10-12161-2010, 2010.

McLinden, C.A., and V. Fioletov, Quantifying stratospheric ozone trends: Complications due to stratospheric cooling, *Geophys. Res. Lett.*, *38* (3), L03808, doi: 10.1029/2010GL046012, 2011.

McLinden, C.A., S. Tegtmeier, and V. Fioletov, Technical note: A SAGE-corrected SBUV zonal-mean ozone data set, *Atmos. Chem. Phys.*, *9* (20), 7963-7972, doi: 10.5194/acp-9-7963-2009, 2009.

McLinden, C.A., A.E. Bourassa, S. Brohede, M. Cooper, D.A. Degenstein, W.J.F. Evans, R.L. Gattinger, C.S. Haley, E.J. Llewellyn, N.D. Lloyd, P. Loewen, R.V. Martin, J.C. McConnell, I.C. McDade, D. Murtagh, L. Rieger, C. von Savigny, P.E. Sheese, C.E. Sioris, B. Solheim, and K. Strong, OSIRIS: A decade of scattered light, *Bull. Am. Meteorol. Soc.*, *93* (12), 1845-1863, doi: 10.1175/BAMS-D-11-00135.1, 2012.

McPeters, R.D., P.K. Bhartia, D. Haffner, G.J. Labow, and L. Flynn, The version 8.6 SBUV ozone data record: An overview, *J. Geophys. Res.*, *118* (14), 8032-8039, doi: 10.1002/jgrd.50597, 2013.

Meehl, G.A., C. Covey, T. Delworth, M. Latif, B. McAvaney, J.F.B. Mitchell, R.J. Stouffer, and K.E. Taylor, The WCRP CMIP3 multi-model dataset: A new era in climate change research, *Bull. Amer. Meteorol. Soc.*, *88* (9), 1383-1394, doi: 10.1175/BAMS-88-9-1383, 2007.

Merkel, A.W., J.W. Harder, D.R. Marsh, A.K. Smith, J.M. Fontenla, and T.N. Woods, The impact of solar spectral irradiance variability on middle atmospheric ozone, *Geophys. Res. Lett.*, *38* (13), L13802, doi: 10.1029/2011 GL047561, 2011.

Meul, S., U. Langematz, S. Oberländer, H. Garny, and P. Jöckel, Chemical contribution to future tropical ozone change in the lower stratosphere, *Atmos. Chem. Phys*., *14*, 2959-2971, doi: 10.5194/acp-14-2959-2014, 2014.

Michou, M., D. Saint-Martin, H. Teyssèdre, A. Alias, F. Karcher, D. Olivié, A. Voldoire, B. Josse, V.-H. Peuch, H. Clark, J.N. Lee, and F. Chéroux, A new version of the CNRM Chemistry-Climate Model, CNRM-CCM: Description and improvements from the CCMVal-2 simulations, *Geosci. Model Dev.*, *4* (4), 873-900, doi: 10.5194/gmd-4-873-2011, 2011.

Miller, A.J., A. Cai, G. Taio, D.J. Wuebbles, L.E. Flynn, S.-K. Yang, E.C. Weatherhead, V. Fioletov, I. Petropavlovskikh, X.-L. Meng, S. Guillas, R.M. Nagatani, and G.C. Reinsel, Examination of ozonesonde data for trends and trend changes incorporating solar and Arctic oscillation signals, *J. Geophys. Res.*, *111*, D13305, doi: 10.1029/2005JD006684, 2006.

Mills, M.J., O.B. Toon, R.P. Turco, D.E. Kinnison, and R.R. Garcia, Massive global ozone loss predicted following regional nuclear conflict, *Proc. Nat. Acad. Sci.*, *105* (14), 5307-5312, doi: 10.1073/pnas.0710058105, 2008.

Morgenstern, O., M.A. Giorgetta, K. Shibata, V. Eyring, D.W. Waugh, T.G. Shepherd, H. Akiyoshi, J. Austin, A.J.G. Baumgaertner, S. Bekki, P. Braesicke, C. Brühl, M.P. Chipperfield, D. Cugnet, M. Dameris, S. Dhomse, S.M. Frith, H. Garny, A. Gettelman, S.C. Hardiman, M.I. Hegglin, P. Jöckel, D.E. Kinnison, J.-F. Lamarque, E. Mancini, E. Manzini, M. Marchand, M. Michou, T. Nakamura, J.E. Nielsen, D. Olivié, G. Pitari, D.A. Plummer, E. Rozanov, J.F. Scinocca, D. Smale, H. Teyssèdre, M. Toohey, W. Tian, and Y. Yamashita, Review of the formulation of present-generation stratospheric chemistry-climate models and associated external forcings, *J. Geophys. Res.*, *115*, D00M02, doi: 10.1029/2009JD013728, 2010.

Nagai, T., B. Liley, T. Sakai, T. Shibata, and O. Uchino, Post-pinatubo evolution and subsequent trend of the stratospheric aerosol layer observed by mid-latitude lidars in both hemispheres, *Sola*, *6*, 69-72, doi: 10.2151/sola.2010-018, 2010.

Nair, P.J., S. Godin-Beekmann, A. Pazmiño, A. Hauchecorne, G. Ancellet, I. Petropavlovskikh, L.E. Flynn, and L. Froidevaux, Coherence of long-term stratospheric ozone vertical distribution time series used for the study of ozone recovery at a northern mid-latitude station, *Atmos. Chem. Phys.*, *11* (10), 4957-4975, doi: 10.5194/acp-11-4957-2011, 2011.

Nair, P.J., S. Godin-Beekmann, L. Froidevaux, L.E. Flynn, J.M. Zawodny, J.M. Russell III, A. Pazmiño, G. Ancellet, W. Steinbrecht, H. Claude, T. Leblanc, S. McDermid, J.A.E van Gijsel, B. Johnson, A. Thomas, D. Hubert, J.-C. Lambert, H. Nakane, and D.P.J. Swart, Relative drifts and stability of satellite and ground-based stratospheric ozone profiles at NDACC lidar stations, *Atmos. Meas. Tech.*, *5* (6), 1301-1318, doi: 10.5194/ amt-5-1301-2012, 2012.

Nair, P.J., S. Godin-Beekmann, J. Kuttippurath, G. Ancellet, F. Goutail, A. Pazmiño, L. Froidevaux, J.M. Zawodny, R.D. Evans, H.J. Wang, J. Anderson, and M. Pastel, Ozone trends derived from the total column and vertical profiles at a northern mid-latitude station, *Atmos. Chem. Phys.*, *13* (20), 10373-10384, doi: 10.5194/acp-13-10373-2013, 2013.

Neely, R.R. III, O.B. Toon, S. Solomon, J.-P. Vernier, C. Alvarez, J.M. English, K.H. Rosenlof, M.J. Mills, C.G. Bardeen, J.S. Daniel, and J.P. Thayer, Recent anthropogenic increases in SO_2 from Asia have minimal impact on stratospheric aerosol, *Geophys. Res. Lett.*, *40* (5), 999-1004, doi: 10.1002/grl.50263, 2013.

Nevison, C.D, S. Solomon, and R.S. Gao, Buffering interactions in the modelled response of stratospheric O_3 to increased NO_x and HO_x, *J. Geophys. Res.*, *104*, 3741-3754, doi: 10.1029/1998JD100018, 1999.

Newchurch, M.J., E.-S. Yang, D.M. Cunnold, G.C. Reinsel, J.M. Zawodny, and J.M. Russell III, Evidence for slowdown in stratospheric ozone loss: First stage of ozone recovery, *J. Geophys. Res.*, *108* (D16), 4507, doi: 10.1029/2003JD003471, 2003.

Newman, P.A., J.S. Daniel, D.W. Waugh, and E.R. Nash, A new formulation of equivalent effective stratospheric chlorine (EESC), *Atmos. Chem. Phys.*, *7* (17), 4537-4522, doi: 10.5194/acp-7-4537-2007, 2007.

Oberländer, S., U. Langematz, K. Matthes, M. Kunze, A. Kubin, J. Harder, N.A. Krivova, S.K. Solanki, J. Pagaran, and M. Weber, The Influence of spectral solar irradiance data on stratospheric heating rates during the 11 year solar cycle, *Geophys. Res. Lett.*, *39* (1), L01801, doi: 10.1029/2011GL049539, 2012.

Oberländer S., U. Langematz, and S. Meul, Unravelling impact factors for future changes of the Brewer-Dobson circulation, *J. Geophys. Res.*, *118* (18), 10296-10312, doi: 10.1002/jgrd. 50775, 2013.

Oman, L.D., and A.R. Douglass, Improvements in total column ozone in GEOSCCM and comparisons with a new ozone-depleting substances scenario, *J. Geophys. Res.*, *119* (9), doi: 10.1002/2014JD021590, 2014.

Oman, L.D., D.W. Waugh, S.R. Kawa, R.S. Stolarski, A.R. Douglass, and P.A. Newman, Mechanisms and feedbacks causing changes in upper stratospheric ozone in the 21st century, *J. Geophys. Res.*, *115*, D05303, doi: 10.1029/2009JD012397, 2010a.

Oman, L.D., D.A. Plummer, D.W. Waugh, J. Austin, J.F. Scinocca, A.R. Douglass, R.J. Salawitch, T. Canty, H. Akiyoshi, S. Bekki, P. Braesicke, N. Butchart, M.P. Chipperfield, D. Cugnet, S. Dhomse, V. Eyring, S. Frith, S.C. Hardiman, D.E. Kinnison, J.-F. Lamarque, E. Mancini, M. Marchand, M. Michou, O. Morgenstern, T. Nakamura, J.E. Nielsen, D. Olivié, G. Pitari, J. Pyle, E. Rozanov, T.G. Shepherd, K. Shibata, R.S. Stolarski, H. Teyssèdre, W. Tian, Y. Yamashita, and J.R. Ziemke, Multimodel assessment of the factors driving stratospheric ozone evolution over the 21st century, *J. Geophys. Res.*, *115* (D24), D24306, doi: 10.1029/2010 JD014362, 2010b.

Oman, L.D., J.R. Ziemke, A.R. Douglass, D.W. Waugh, C. Lang, J.M. Rodriguez, and J.E. Nielsen, The response of tropical tropospheric ozone to ENSO, *Geophysical Res. Lett.*, *38* (13), L13706, doi: 10.1029/2011 GL047865, 2011.

Oman, L., A. Douglass, J. Ziemke, J. Rodriguez, D. Waugh, and J. Nielsen, The ozone response to ENSO in Aura satellite measurements and a chemistry-climate simulation, *J. Geophys. Res.*, *118* (2), 965-976, doi: 10.1029/2012JD018546, 2013.

Ossó, A., Y. Sola, J. Bech, and J. Lorente, Evidence for the influence of the North Atlantic Oscillation on the total ozone column at northern low latitudes and midlatitudes during winter and summer seasons, *J. Geophys. Res.*, *116* (D24), D24122, doi: 10.1029/2011JD016539, 2011.

Ott, L., B. Duncan, S. Pawson, P. Colarco, M. Chin, C. Randles, T. Diehl, and E. Nielsen, Influence of the 2006 Indonesian biomass burning aerosols on tropical dynamics studied with the GEOS-5 AGCM, *J. Geophys. Res.*, *115* (D14), D14121, doi: 10.1029/2009JD013181, 2010.

Petropavlovskikh, I., P.K. Bhartia, and J.J. DeLuisi, New Umkehr ozone profile retrieval algorithm optimized for climatological studies, *Geophys. Res. Lett.*, *32*, L16808, doi: 10.1029/2005GL023323, 2005.

Pitari, G., V. Aquila, B. Kravitz, A. Robock, S. Watanabe, I. Cionni, N. De Luca, G. Di Genova, E. Mancini, and S. Tilmes, Stratospheric ozone response to sulfate geoengineering: Results from the Geoengineering Model Intercomparison Project (GeoMIP), *J. Geophys. Res.*, *119* (5), 2629-2653, doi: 10.1002/2013JD020566, 2014.

Plummer, D.A., J.F. Scinocca, T.G. Shepherd, M.C. Reader, and A.I. Jonsson, Quantifying the contributions of stratospheric ozone changes from ozone depleting substances and greenhouse gases, *Atmos. Chem. Phys.*, *10* (18), 8803-8820, doi: 10.5194/acp-10-8803-2010, 2010.

Poberaj, C.S., J. Staehelin, and D. Brunner, Missing stratospheric ozone decrease at southern hemisphere middle latitudes after Mt. Pinatubo: A dynamical perspective, *J. Atmos. Sci.*, *68* (9), 1922-1945, doi: 10.1175/JAS-D-10-05004.1, 2011.

Portmann, R.W., and S. Solomon, Indirect radiative forcing of the ozone layer during the 21st century, *Geophys. Res. Lett*., *34*, L02813, doi: 10.1029/2006GL028252, 2007.

Portmann, R.W., J.S. Daniel, and A.R. Ravishankara, Stratospheric ozone depletion due to nitrous oxide: Influences of other gases, *Phil. Trans. R. Soc. Lond. B Biol. Sci.*, *367* (1593), 1256-1264, doi: 10.1098/rstb.2011.0377, 2012.

Randel, W.J., and E.J. Jensen, Physical processes in the tropical tropopause layer and their roles in a changing climate, *Nature Geosci*., *6* (3), 169-176, doi: 10.1038/ngeo1733, 2013.

Randel, W.J., and A.M. Thompson, Interannual variability and trends in tropical ozone derived from SAGE II satellite data and SHADOZ ozonesondes, *J. Geophys. Res.*, *116* (D7), D07303, doi: 10.1029/2010JD015195, 2011.

Randel, W.J., and F. Wu, A stratospheric ozone profile data set for 1979–2005: Variability, trends, and comparisons with column ozone data, *J. Geophys. Res.*, *112*, D06313, doi: 10.1029/2006JD007339, 2007.

Randel, W.J., R.R. Garcia, N. Calvo, and D. Marsh, ENSO influence on zonal mean temperature and ozone in the tropical lower stratosphere, *Geophys. Res. Lett.*, *36* (15), L15822, doi: 10.1029/2009GL039343, 2009.

Randeniya, L.K., P.F. Vohralik, and I.C. Plumb, Stratospheric ozone depletion at northern mid latitudes in the 21st century: The importance of future concentrations of greenhouse gases nitrous oxide and methane, *Geophys. Res. Lett.*, *29* (4), 1051, doi: 10.1029/2001GL014295, 2002.

Ravishankara, A.R., J.S. Daniel, and R.W. Portmann, Nitrous oxide (N_2O): The dominant ozone-depleting substance emitted in the 21st century, *Science*, *326* (5949), 123-125, doi: 10.1126/science.1176985, 2009.

Reinsel, G.C., E.C. Weatherhead, G.C. Tiao, A.J. Miller, R.M. Nagatani, D.J. Wuebbles, and L.E. Flynn, On detection of turnaround and recovery in trend for ozone, *J. Geophys. Res.*, *107* (D10), 4078, doi: 10.1029/2001JD000500, 2002.

Reinsel, G.C., A.J. Miller, E.C. Weatherhead, L.E. Flynn, R. Nagatani, G.C. Tiao, and D.J. Wuebbles, Trend analysis of total ozone data for turnaround and dynamical contributions, *J. Geophys. Res.*, *110*, D16306, doi: 10.1029/2004JD004662, 2005.

Remsberg, E.E., Decadal-scale responses in middle and upper stratospheric ozone from SAGE II version 7 data, *Atmos. Chem. Phys.*, *14*, 1039-1053, doi: 10.5194/acp-14-1039-2014, 2014.

Remsberg, E., and G. Lingenfelser, Analysis of SAGE II ozone of the middle and upper stratosphere for its response to a decadal-scale forcing, *Atmos. Chem. Phys.*, *10* (23), 11779-11790, doi: 10.5194/acp-10-11779-2010, 2010.

Revell L.E., G.E. Bodeker, P.E. Huck, B.E. Williamson, and E. Rozanov, The sensitivity of stratospheric ozone changes through the 21st century to N_2O and CH_4, *Atmos. Chem. Phys.*, 12, 11309-11317, doi: 10.5194/acp-12-11309-2012, 2012a.

Revell L.E., G.E. Bodeker, D. Smale, R. Lehmann, P.E. Huck, B.E. Williamson, E. Rozanov, and H. Struthers, The effectiveness of N_2O in depleting stratospheric ozone, *Geophys. Res. Lett.*, *39* (15), L15806, doi: 10.1029/2012GL052143, 2012b.

Rieder, H.E., J. Staehelin, J.A. Maeder, T. Peter, M. Ribatet, A.C. Davison, R. Stübi, P. Weihs, and F. Holawe, Extreme events in total ozone over Arosa – Part 1: Application of extreme value theory, *Atmos. Chem. Phys.*, *10*, 10021-10031, doi: 10.5194/acp-10-10021-2010, 2010a.

Rieder, H.E., J. Staehelin, J.A. Maeder, T. Peter, M. Ribatet, A.C. Davison, R. Stübi, P. Weihs, and F. Holawe, Extreme events in total ozone over Arosa – Part 2: Fingerprints of atmospheric dynamics and chemistry and effects on mean values and long-term changes, *Atmos. Chem. Phys.*, *10* (20), 10033-10045, doi: 10.5194/acp-10-10033-2010, 2010b.

Rieder, H.E., L. Frossard, M. Ribatet, J. Staehelin, J.A. Maeder, S. Di Rocco, A.C. Davison, T. Peter, P. Weihs, and F. Holawe, On the relationship between total ozone and atmospheric dynamics and chemistry at mid-latitudes – Part 2: The effects of the El Niño/Southern Oscillation, volcanic eruptions and contributions of atmospheric dynamics and chemistry to long-term total ozone changes, *Atmos. Chem. Phys.*, *13* (1), 165-179, doi: 10.5194/acp-13-165-2013, 2013.

Rosenfield, J.E., and A.R. Douglass, Doubled CO_2 effects on NO_y in a coupled 2D model, *Geophys. Res. Lett.*, *25* (23), 4381-4384, 1998.

Sakazaki, T., M. Fujiwara, C. Mitsuda, K. Imai, N. Manago, Y. Naito, T. Nakamura, H. Akiyoshi, D. Kinnison, T. Sano, M. Suzuki, and M. Shiotani, Diurnal ozone variations in the stratosphere revealed in observations from the Superconducting Submillimeter-Wave Limb-Emission Sounder (SMILES) on board the International Space Station (ISS), *J. Geophys. Res.*, *118* (7), 2991-3006, doi: 10.1002/jgrd.50220, 2013.

Salawitch, R.J., D.K. Weisenstein, L.J. Kovalenko, C.E. Sioris, P.O. Wennberg, K. Chance, M.K.W. Ko, and C.A. McLinden, Sensitivity of ozone to bromine in the lower stratosphere, *Geophys. Res. Lett.*, *32*, L05811, doi: 10.1029/2004GL021504, 2005.

Scarnato, B., J. Staehelin, R. Stübi, and H. Schill, Long term total ozone observations at Arosa (Switzerland) with Dobson and Brewer instruments (1988–2007), *J. Geophys. Res.*, *115*, D13306, doi: 10.1029/2009JD011908, 2010.

Schneider, N., F. Selsis, J. Urban, O. Lezeaux, J. De La Noë, and P. Ricaud, Seasonal and diurnal ozone variations: Observations and modeling, *J. Atmos. Chem.*, *50* (1), 25-47, doi: 10.1007/s10874-005-1172-z, 2005.

Scinocca, J.F., D.B. Stephenson, T.C. Bailey, and J. Austin, Estimates of past and future ozone trends from multimodel simulations using a flexible smoothing spline methodology, *J. Geophys. Res.*, *115* (D3), D00M12, doi: 10.1029/2009JD013622, 2010.

Shapiro, A.V., E.V. Rozanov, A.I. Shapiro, T.A. Egorova, J. Harder, M. Weber, A.K. Smith, W. Schmutz, and T. Peter, The role of the solar irradiance variability in the evolution of the middle atmosphere during 2004-2009, *J. Geophys. Res.*, *118* (9), 3781-3793, doi: 10.1002/jgrd.50208, 2013.

Shepherd, T.G., Dynamics, stratospheric ozone, and climate change, *Atmos.-Ocean*, *46* (1), 117-138, doi: 10.3137/ao.460106, 2008.

Shepherd, T.G., and A.I. Jonsson, On the attribution of stratospheric ozone and temperature changes to changes in ozone-depleting substances and well-mixed greenhouse gases, *Atmos. Chem. Phys*., *8* (5), 1435-1444, doi: 10.5194/acp-8-1435-2008, 2008.

Shepherd, T.G., and C. McLandress, A robust mechanism for strengthening of the Brewer-Dobson circulation in response to climate change: Critical-layer control of subtropical wave breaking, *J. Atmos. Sci.*, *68* (4), 784-797, doi: 10.1175/2010JAS3608.1, 2011.

Shepherd, T.G., D.A. Plummer, J.F. Scinocca, M.I. Hegglin, V.E. Fioletov, M.C. Reader, E. Remsberg, T. von Clarmann, and H.J. Wang, Reconciliation of halogen-induced ozone loss with the total-column ozone record, *Nature Geosci*., *7*, 443-449, doi: 10.1038/ngeo2155, 2014.

Sinnhuber, B.-M., N. Sheode, M. Sinnhuber, M.P. Chipperfield, and W. Feng, The contribution of anthropogenic bromine emissions to past stratospheric ozone trends: A modelling study, *Atmos. Chem. Phys.*, *9* (8), 2863-2871, doi: 10.5194/acp-9-2863-2009, 2009.

Sioris, C.E., C.A. McLinden, V.E. Fioletov, C. Adams, J.M. Zawodny, A.E. Bourassa, C.Z. Roth, and D.A. Degenstein, Trend and variability in ozone in the tropical lower stratosphere over 2.5 solar cycles observed by SAGE II and OSIRIS, *Atmos. Chem. Phys.*, *14* (7), 3479-3496, doi: 10.5194/acp-14-3479-2014, 2014.

Sitnov, S., Influence of the 11-year solar cycle on the effects of the equatorial quasi-biennial oscillation, manifesting in the extratropical northern atmosphere, *Clim. Dyn.*, *32*, 1-17, doi: 10.1007/s00382-007-0362-6, 2009.

Smit, H.G.J., W. Straeter, B.J. Johnson, S.J. Oltmans, J. Davies, D.W. Tarasick, B. Goegger, R. Stubi, F.J. Schmidlin, T. Northam, A.M. Thompson, J.C. Witte, I. Boyd, and F. Posny, Assessment of the performance of ECC ozonesondes under quasi-flight conditions in the environmental simulation chamber: Insights from the Juelich Ozone Sonde Intercomparison Experiment (JOSIE), *J. Geophys. Res.*, *112*, D19306, doi: 10.1029/2006 JD007308, 2007.

Sofieva, V.F., N. Rahpoe, J. Tamminen, E. Kyrölä, N. Kalakoski, M. Weber, A. Rozanov, C. von Savigny, A. Laeng, T. von Clarmann, G. Stiller, S. Lossow, D. Degenstein, A. Bourassa, C. Adams, C. Roth, N. Lloyd, P. Bernath, R.J. Hargreaves, J. Urban, D. Murtagh, A. Hauchecorne, F. Dalaudier, M. van Roozendael, N. Kalb, and C. Zehner, Harmonized dataset of ozone profiles from satellite limb and occultation measurements, *Earth Syst. Sci. Data*, *5* (2), 349-363, doi: 10.5194/essd-5-349-2013, 2013.

Solomon, S., P.J. Young, and B. Hassler, Uncertainties in the evolution of stratospheric ozone and implications for recent temperature changes in the tropical lower stratosphere, *Geophys. Res. Lett.*, *39* (17), L17706, doi: 10.1029/2012GL052723, 2012.

Soukharev, B.E., and L.L. Hood, Solar cycle variation of stratospheric ozone: Multiple regression analysis of long-term satellite data sets and comparisons with models, *J. Geophys. Res*., *111*, D20314, doi: 10.1029/2006 JD007107, 2006.

SPARC (Stratosphere-troposphere Processes And their Role in Climate), SPARC Report on the Lifetimes of Stratospheric Ozone-Depleting Substances, Their Replacements, and Related Species, edited by M. Ko, P. Newman, S. Reimann, and S. Strahan, SPARC Report No. 6, WCRP-15/2013, 2013.

SPARC CCMVal (Stratosphere-troposphere Processes And their Role in Climate), *SPARC Report on the Evaluation of Chemistry-Climate Models*, edited by V. Eyring, T.G. Shepherd, and D.W. Waugh, SPARC Report No. 5, WCRP-132, WMO/TD-No. 1526, 478 pp., available: http://www.atmosp.physics.utoronto.ca/ SPARC/ccmval_final/ index.php, 2010.

Steinbrecht, W., H. Claude, F. Schönenborn, I.S. McDermid, T. Leblanc, S. Godin, T. Song, D.P.J. Swart, Y.J. Meijer, G.E. Bodeker, B.J. Connor, N. Kämpfer, K. Hocke, Y. Calisesi, N. Schneider, J. de la Noë, A.D. Parrish, I.S. Boyd, C. Brühl, B. Steil, M.A. Giorgetta, E. Manzini, L.W. Thomason, J.M. Zawodny, M.P. McCormick, J.M. Russell III, P.K. Bhartia, R.S. Stolarski, and S.M. Hollandsworth-Frith, Long-term evolution of upper stratospheric ozone at selected stations of the Network for the Detection of Stratospheric Change (NDSC), *J. Geophys. Res.*, *111* (D10), D10308, doi: 10.1029/2005JD006454, 2006.

Steinbrecht, W., H. Claude, F. Schönenborn, I.S. McDermid, T. Leblanc, S. Godin-Beekmann, P. Keckhut, A. Hauchecorne, J.A.E. Van Gijsel, D.P.J. Swart, G.E. Bodeker, A. Parrish, I.S. Boyd, N. Kämpfer, K. Hocke, R.S. Stolarski, S.M. Frith, L.W. Thomason, E.E. Remsberg, C. Von Savigny, A. Rozanov, and J.P. Burrows, Ozone and temperature trends in the upper stratosphere at five stations of the Network for the Detection of Atmospheric Composition Change, *Int. J. Remote Sens.*, *30*, 3875-3886, doi: 10.1080/01431160902821841, 2009.

Steinbrecht, W., U. Köhler, H. Claude, M. Weber, J.P. Burrows, and R.J. van der A, Very high ozone columns at northern mid-latitudes in 2010, *Geophys. Res. Lett.*, *38* (6), L06803, doi: 10.1029/2010GL046634, 2011.

Stolarski, R.S., and S.M. Frith, Search for evidence of trend slow-down in the long-term TOMS/SBUV total ozone data record: The importance of instrument drift uncertainty, *Atmos. Chem. Phys.*, *6*, 4057-4065, 2006.

Stolarski, R.S., A.R. Douglass, E.E. Remsberg, N.J. Livesey, and J.C. Gille, Ozone temperature correlations in the upper stratosphere as a measure of chlorine content, *J. Geophys. Res.*, *117* (D10), D10305, doi: 10.1029/2012 JD017456, 2012.

Strahan, S.E., A.R. Douglass, R.S. Stolarski, H. Akiyoshi, S. Bekki, P. Braesicke, N. Butchart, M.P. Chipperfield, D. Cugnet, S. Dhomse, S.M. Frith, A. Gettelman, S.C. Hardiman, D.E. Kinnison, J.-F. Lamarque, E. Mancini, M. Marchand, M. Michou, O. Morgenstern, T. Nakamura, D. Olivié, S. Pawson, G. Pitari, D.A. Plummer, J.A. Pyle, J.F. Scinocca, T.G. Shepherd, K. Shibata, D. Smale, H. Teyssèdre, W. Tian, and Y. Yamashita, Using transport diagnostics to understand chemistry climate model ozone simulations, *J. Geophys. Res.*, *116* (D17), D17302, doi: 10.1029/2010JD015360, 2011.

Studer, S., K. Hocke, A. Shanz, H. Schmidt, and N. Kämpfer, A climatology of the diurnal variations of stratospheric and mesospheric ozone over Bern, Switzerland, *Atmos. Chem. Phys.*, *14* (12), 5905-5919, doi: 10.5194/acp-14-5905-2014, 2014.

Swartz, W.H., R.S. Stolarski, L.D. Oman, E.L. Fleming, and C.H. Jackman, Middle atmosphere response to different descriptions of the 11-yr solar cycle in spectral irradiance in a chemistry-climate model, *Atmos. Chem. Phys.*, *12* (13), 5937-5948, doi: 10.5194/acp-12-5937-2012, 2012.

Taylor, K.E., R.J. Stouffer, and G.A. Meehl, An overview of CMIP5 and the experiment design, *Bull. Amer. Meteorol. Soc.*, *93* (4), 485-498, doi: 10.1175/BAMS-D-11-00094.1, 2012.

Tegtmeier, S., V.E. Fioletov, and T.G. Shepherd, A global picture of the seasonal persistence of stratospheric ozone anomalies, *J. Geophys. Res.*, *115* (D18), D18119, doi: 10.1029/2009JD013011, 2010.

Tegtmeier, S., M.I. Hegglin, J. Anderson, A. Bourassa, S. Brohede, D. Degenstein, L. Froidevaux, R. Fuller, B. Funke, J. Gille, A. Jones, Y. Kasai, K. Krüger, E. Kyrölä, G. Lingenfelser, J. Lumpe, B. Nardi, J. Neu, D. Pendlebury, E. Remsberg, A. Rozanov, L. Smith, M. Toohey, J. Urban, T. von Clarmann, K.A. Walker, and R.H.J. Wang, SPARC Data Initiative: A comparison of ozone climatologies from international satellite limb sounders, *J. Geophys. Res.*, *118* (21), 12229-12247, doi: 10.1002/2013JD019877, 2013.

Telford, P., P. Braesicke, O. Morgenstern, and J. Pyle, Reassessment of causes of ozone column variability following the eruption of Mount Pinatubo using a nudged CCM, *Atmos. Chem. Phys.*, *9* (13), 4251-4260, doi: 10.5194/acp-9-4251-2009, 2009.

Thompson, A.M., S.K. Miller, S. Tilmes, D.W. Kollonige, J.C. Witte, S.J. Oltmans, B.J. Johnson, M. Fujiwara, F.J. Schmidlin, G.J.R. Coetzee, N. Komala, M. Maata, M. Mohamad, J. Nguyo, C. Mutai, S.-Y. Ogino, F. Raimundo Da Silva, N.M. Paes Leme, F. Posny, R. Scheele, H.B. Selkirk, M. Shiotani, R. Stübi, G. Levrat, B. Calpini, V. Thouret, H. Tsuruta, J. Valverde Canossa, H. Vömel, S. Yonemura, J. Andrés Diaz, N.T. Tan Thanh, and H.T. Thuy Ha, Southern Hemisphere Additional Ozonesondes (SHADOZ) ozone climatology (2005-2009): Tropospheric and tropical tropopause layer (TTL) profiles with comparisons to OMI-based ozone products, *J. Geophys. Res.*, *117* (D23), D23301, doi: 10.1029/2011JD016911, 2012.

Tourpali, K., C.S. Zerefos, D.S. Balis, and A.F. Bais, The 11-year solar cycle in stratospheric ozone: Comparison between Umkehr and SBUVv8 and effects on surface erythemal irradiance, *J. Geophys. Res.*, *112* (D12), D12306, doi: 10.1029/2006JD007760, 2007.

Trickl, T., H. Giehl, H. Jäger, and H. Vogelmann, 35 yr of stratospheric aerosol measurements at Garmisch-Partenkirchen: From Fuego to Eyjafjallajökull, and beyond, *Atmos. Chem. Phys.*, *13* (10), 5205-5225, doi: 10.5194/acp-13-5205-2013, 2013.

Tully, M.B., A.R. Klekociuk, and S.K. Rhodes, Trends and variability in total ozone from a mid-latitude Southern Hemisphere site: The Melbourne Dobson record 1978-2012, *Atmos. Ocean*, *0*, 1-8, doi: 10.1080/07055900. 2013.869192, 2013.

Urban, J., N. Lautié, C. Jimenez, E. Le Flochmoën, C. Jiménez, P. Eriksson, J. de la Nöe, E. Dupuy, M. Ekström, L. El Amraoui, U. Frisk, D. Murtagh, M. Olberg, and P. Ricaud, Odin/SMR limb observations of stratospheric trace gases: Level 2 processing of ClO, N_2O, HNO_3, and O_3, *J. Geophys. Res.*, *110*, D14307, doi: 10.1029/ 2004JD005741, 2005.

van der A, R.J., M.A.F. Allaart, and H.J. Eskes, Multi sensor reanalysis of total ozone, *Atmos. Chem. Phys.*, *10* (22), 11277-11294, doi: 10.5194/acp-10-11277-2010, 2010.

Van Roozendael, M., R. Spurr, D. Loyola, C. Lerot, D. Balis, J.-C. Lambert, W. Zimmer, J. van Gent, J. van Geffen, M. Koukouli, J. Granville, A. Doicu, C. Fayt, and C. Zehner, Sixteen years of GOME/ERS-2 total

ozone data: The new direct-fitting GOME Data Processor (GDP) version 5 – Algorithm description, *J. Geophys. Res.*, *117* (D3), D03305, doi: 10.1029/2011JD016471, 2012.

van Vuuren D.P., J. Edmonds, M. Kainuma, K. Riahi, A. Thomson, K. Hibbard, G.C. Hurtt, T. Kram, V. Krey, J.-F. Lamarque, T. Masui, M. Meinshausen, N. Nakicenovic, S.J. Smith, and S.K. Rose, The representative concentration pathways: An overview, *Clim. Change*, *109*, 5-31. doi: 10.1007/s10584-011-0148-z, 2011.

Vernier, J.-P., L.W. Thomason, J.-P. Pommereau, A. Bourassa, J. Pelon, A. Garnier, A. Hauchecorne, L. Blanot, C. Trepte, D. Degenstein, and F. Vargas, Major influence of tropical volcanic eruptions on the stratospheric aerosol layer during the last decade, *Geophys. Res. Lett.*, *38* (12), L12807. doi: 10.1029/2011GL047563, 2011.

Vernier, J-P., L.W. Thomason, T.D. Fairlie, P. Minnis, R. Palikonka, and K.M. Bedka, Comment on "Large volcanic aerosol load in the stratosphere linked to asian monsoon transport," *Science*, *339* (6120), 647, doi: 10.1126/science.1227817, 2013.

Vigouroux C., M. De Mazière, P. Demoulin, C. Servais, F. Hase, T. Blumenstock, I. Kramer, M. Schneider, J. Mellqvist, A. Strandberg, V. Velazco, J. Notholt, R. Sussmann, W. Stremme, A. Rockmann, T. Gardiner, M. Coleman, and P. Woods, Evaluation of tropospheric and stratospheric ozone trends over Western Europe from ground-based FTIR network observations, *Atmos. Chem. Phys.*, *8* (23), 6865-6886, doi: 10.5194/acp-8-6865-2008, 2008.

Vitt, F.M., and C.H. Jackman, A comparison of sources of odd nitrogen production from 1974 through 1993 in the Earth's middle atmosphere as calculated using a two-dimensional model, *J. Geophys. Res.*, *101* (D3), 6729-6739, doi: 10.1029/95JD03386, 1996.

von Clarmann, T., M. Höpfner, S. Kellmann, A. Linden, S. Chauhan, B. Funke, U. Grabowski, N. Glatthor, M. Kiefer, T. Schieferdecker, G.P. Stiller, and S. Versick, Retrieval of temperature, H_2O, O_3, HNO_3, CH_4, N_2O, $ClONO_2$ and ClO from MIPAS reduced resolution nominal mode limb emission measurements, *Atmos. Meas. Tech.*, *2* (1), 159-175, doi: 10.5194/amt-2-159-2009, 2009.

Vyushin, D., V.E. Fioletov, and T.G. Shepherd, Impact of long-range correlations on trend detection in total ozone, *J. Geophys. Res.*, *112*, D14307, doi: 10.1029/2006JD008168, 2007.

Vyushin, D., T.G. Shepherd, and V.E. Fioletov, On the statistical modeling of persistence in total ozone anomalies, *J. Geophys. Res.*, *115*, D16306, doi: 10.1029/2009JD013105, 2010.

Wang, R., L. Froidevaux, J. Anderson, R.A. Fuller, P.F. Bernath, M.P. McCormick, N.J. Livesey, J.M. Russell III, K.A. Walker, and J.M. Zawodny, GOZCARDS merged data for ozone monthly zonal means on a geodetic latitude and pressure grid, version 1.01, Greenbelt, MD, USA, NASA Goddard Earth Science Data and Information Services Center, doi: 10.5067/MEASURES/GOZCARDS/DATA3006, 2013.

Wang, S., K.-F. Li, T.J. Pongetti, S.P. Sander, Y.L. Yung, M.-C. Liang, N.J. Livesey, M.L. Santee, J.W. Harder, M. Snow, and F.P. Mills, Midlatitude atmospheric OH response to the most recent 11-y solar cycle., *Proc. Natl. Acad. Sci.*, *110* (6), 2023-2028, doi: 10.1073/pnas.1117790110, 2013.

Waters, J.W., L. Froidevaux, R.S. Harwood, R.F. Jarnot, H.M. Pickett, W.G. Read, P.H. Siegel, R.E. Cofield, M.J. Filipiak, D.A. Flower, J.R. Holden, G.K. Lau, N.J. Livesey, G.L. Manney, H.C. Pumphrey, M.L. Santee, D.L. Wu, D.T. Cuddy, R.R. Lay, M.S. Loo, V.S. Perun, M.J. Schwartz, P.C. Stek, R.P. Thurstans, M.A. Boyles, K.M. Chandra, M.C. Chavez, G.-S. Chen, B.V. Chudasama, R. Dodge, R.A. Fuller, M.A. Girard, J.H. Jiang, Y. Jiang, B.W. Knosp, R.C. LaBelle, J.C. Lam, K.A. Lee, D. Miller, J.E. Oswald, N.C. Patel, D.M. Pukala, O. Quintero, D.M. Scaff, W. Van Snyder, M.C. Tope, P.A. Wagner, and M.J. Walch, The Earth Observing System Microwave Limb Sounder (EOS MLS) on the Aura satellite, *IEEE Trans. Geosci. Rem. Sens.*, *44* (5), 1075-1092, doi: 10.1109/TGRS.2006.873771, 2006.

Waugh, D.W., and V. Eyring, Quantitative performance metrics for stratospheric-resolving chemistry-climate models, *Atmos. Chem. Phys.*, *8* (18), 5699-5713, doi: 10.5194/acp-8-5699-2008, 2008.

Waugh, D.W., L. Oman, S.R. Kawa, R.S. Stolarski, S. Pawson, A.R. Douglass, P.A. Newman, and J.E. Nielsen, Impacts of climate change on stratospheric ozone recovery, *Geophys. Res. Lett.*, *36*, L03805, doi: 10.1029/2008GL036223, 2009.

Weatherhead, E.C., G.C. Reinsel, G.C. Tiao, C.H. Jackman, L. Bishop, S.M.H. Frith, J. DeLuisi, T. Keller, S.J. Oltmans, E.L. Fleming, D.J. Wuebbles, J.B. Kerr, A.J. Miller, J. Herman, R. McPeters, R.M. Nagatani, and J.E. Frederick, Detecting the recovery of total column ozone, *J. Geophys. Res.*, *105* (D17), 22201-22210, 2000.

Weber, M., L.N. Lamsal, M. Coldewey-Egbers, K. Bramstedt, and J.P. Burrows, Pole-to-pole validation of GOME WFDOAS total ozone with groundbased data, *Atmos. Chem. Phys.*, *5* (5), 1341-1355, doi: 10.5194/acp-5-1341-2005, 2005.

Weber, M., S. Dikty, J.P. Burrows, H. Garny, M. Dameris, A. Kubin, J. Abalichin, and U. Langematz, The Brewer-Dobson circulation and total ozone from seasonal to decadal time scales, *Atmos. Chem. Phys.*, *11* (21), 11221-11235, doi: 10.5194/acp-11-11221-2011, 2011.

Weber, M., W. Chehade, V.E. Fioletov, S.M. Frith, C.S. Long, W. Steinbrecht, and J.D. Wild, Stratospheric ozone [in "State of the Climate in 2012"], *Bull. Amer. Meteorol. Soc.*, *94* (8), S36-S37, doi: 10.1175/2013BAMS StateoftheClimate.1, 2013.

Wehrli, C., W. Schmutz, and A.I. Shapiro, Correlation of spectral solar irradiance with solar activity as measured by VIRGO, *Astron. Astrophys.*, *556* (L3), doi: 10.1051/0004-6361/201220864, 2013.

WMO (World Meteorological Organization), *Scientific Assessment of Ozone Depletion: 1994*, Global Ozone Research and Monitoring Project–Report No. 37, Geneva, Switzerland, 1995.

WMO (World Meteorological Organization), *Scientific Assessment of Ozone Depletion: 1998*, Global Ozone Research and Monitoring Project–Report No. 44, Geneva, Switzerland, 1999.

WMO (World Meteorological Organization), *Scientific Assessment of Ozone Depletion: 2002*, Global Ozone Research and Monitoring Project–Report No. 47, Geneva, Switzerland, 2003.

WMO (World Meteorological Organization), *Scientific Assessment of Ozone Depletion: 2006*, Global Ozone Research and Monitoring Project–Report No. 50, 572 pp., Geneva, Switzerland, 2007

WMO (World Meteorological Organization), *Scientific Assessment of Ozone Depletion: 2010*, *Global Ozone Research and Monitoring Project–Report No. 52*, Geneva, Switzerland, 2011.

Woods, T.N., and G.J. Rottman, Solar ultraviolet variability over time periods of aeronomic interest, in *Atmospheres in the Solar System: Comparative Aeronomy*, edited by M. Mendillo, A. Nagy, and J.H. Waite, vol. 130 of AGU Monographs, p. 221, American Geophysical Union, Washington DC, doi: 10.1029/130GM14, 2002.

Yang, E.-S., D.M. Cunnold, R.J. Salawitch, M.P. McCormick, J. Russell III, J.M. Zawodny, S. Oltmans, and M.J. Newchurch, Attribution of recovery in lower-stratospheric ozone, *J. Geophys. Res.*, *111*, D17309, doi: 10.1029/2005JD006371, 2006.

Ziemke, J.R., S. Chandra, L.D. Oman, and P.K. Bhartia, A new ENSO index derived from satellite measurements of column ozone, *Atmos. Chem. Phys.*, *10* (8), 3711-3721, doi: 10.5194/acp-10-3711-2010, 2010.

Ziemke, J.R., and S. Chandra, Development of a climate record of tropospheric and stratospheric column ozone from satellite remote sensing: Evidence of an early recovery of global stratospheric ozone, *Atmos. Chem. Phys.*, *12*, 5737-5753, doi: 10.5194/acp-12-5737-2012, 2012.

Zubov, V., E. Rozanov, T. Egorova, I. Karol and W. Schmutz, The role of external factors in the evolution of the ozone layer and stratospheric circulation in 21st century, *Atmos. Chem. Phys.*, *13* (9), 4697-4706, doi: 10.5194/acp-13-4697-2013, 2013.

APPENDIX 2A
Ozone Data Sets

1) Ground-Based Measurement Systems

The World Ozone and Ultraviolet Data Centre (WOUDC) archives a record of ground-based total column ozone observations (http://www.woudc.org). This includes Dobson spectrophotometers (since the 1920s), automated Brewer spectrometers (since the 1980s), and filter instruments (Bojkov et al., 1994; Fioletov et al., 2008). At many ground stations, the Brewer instruments have supplemented or replaced the Dobsons (Scarnato et al., 2010). Dobson Umkehr ozone profiles provide a long historical record, with regular measurements beginning in 1957 at several stations around the world (Figure 2A-1). In addition to Dobson spectrometers, Brewer instruments in principle also provide Umkehr measurements since the 1990s (Petropavlovskikh et al., 2005).

Zenith-sky visible spectral measurements from SAOZ (Système d'Analyse par Observation Zénithale) instruments (Hendrick et al., 2011) are another source of total column ozone data, as are Fourier-Transform Infrared spectrometers (FTIRs). Both SAOZ and FTIR instruments are part of the NDACC network (Network for Detection of Atmospheric Composition Change, http://www.ndsc.ncep.noaa.gov/) and the GAW (Global Atmosphere Watch) network (Table 2-3). Selected time series extend back to the early 1990s (SAOZ) and 1995 (FTIR). In addition to the total ozone column, the FTIR instruments also provide low vertical resolution ozone profiles.

Ozonesondes have been used since the middle 1960s for routine monitoring of ozone profiles at a number of stations around the world. Figure 2A-1 shows the network of ozonesonde stations, and other ground-based ozone profiling stations used in this Assessment. Most networks are biased toward populated Northern Hemisphere areas (Figure 2A-1), with additional capabilities over Antarctica (Liu et al., 2013). The Southern Hemisphere Additional Ozonesondes project (SHADOZ: Thompson et al., 2012) has added substantially to the global coverage since 1998. Ozonesonde observations are also the backbone of the MATCH network of measurements (see Chapter 3), which are made in unpopulated regions of the NH and are crucial for monitoring ozone depletion in Arctic winter and spring.

Ozone measurements by lidar systems have been in operation since the late 1980s (Steinbrecht et al., 2009; Nair et al., 2012; Kirgis et al., 2013). Currently they are available at 12 stations, mostly in the NH, but fewer stations have long records that are used in this Assessment (Table 2-3; Figure 2A-1).

Ground-based microwave radiometers have been used for stratospheric ozone monitoring since the 1990s (Boyd et al., 2007; Studer et al., 2014). Stations are mostly in the Northern Hemisphere, with one station operating in the Southern Hemisphere (Lauder, New Zealand, see Figure 2A-1).

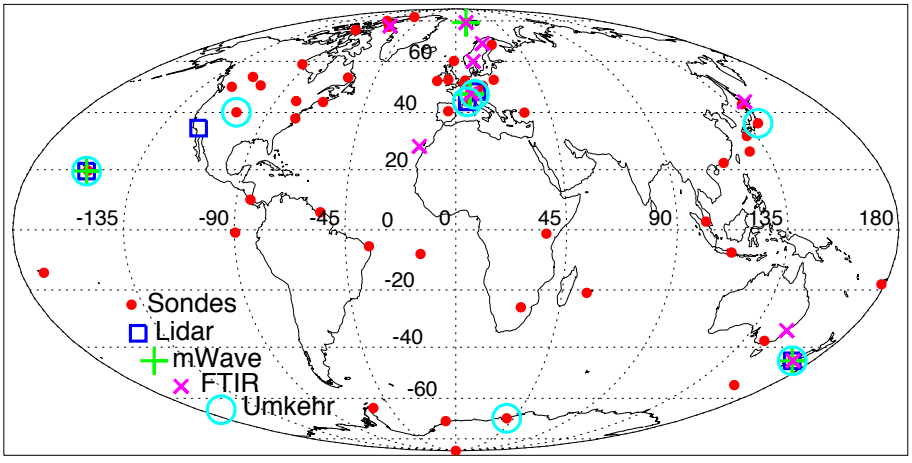

Figure 2A-1. Ground-based ozone profiling stations used in this Assessment. See Table 2-3 for details on the few stations running lidars, microwave radiometers, Fourier-Transform Infrared spectrometers (FTIRs), or Umkehr measurements.

2) Nadir-Viewing Satellite Instruments

The longest available satellite ozone record comes from Solar Backscatter Ultraviolet (SBUV) measurements. The Nimbus-4 BUV instrument collected ozone profiles between 1970 and 1976 from a sun-synchronous polar orbit. Routine measurements of profiles and total ozone from polar-orbiting satellites began in the late 1970s with the Nimbus-7 SBUV, followed by SBUV/2 instruments on several NOAA satellites. At least one SBUV instrument has been operational at all times since 1978. SBUV retrievals provide coarse-resolution vertical profiles. Partial column data are integrated to produce a total column ozone record. A series of similar instruments (i.e., Ozone Monitoring Instrument (OMI) and Ozone Mapping and Profiler Suite (OMPS)) have also flown on more recent research satellites (e.g., Kroon et al., 2011; Kramarova et al., 2014), with sensors designed to detect total ozone with smaller spatial footprints than the SBUV instruments. WMO (2011) used total ozone obtained using the V8 retrieval algorithm, which included a homogenization of the time series (Stolarski and Frith, 2006). SBUV data based on the more recent retrieval algorithm (V8.6: Bhartia et al., 2013; McPeters et al., 2013) are used in this Assessment.

Several European instruments have collected global data from the satellite polar orbiting platforms since 1995. These are: the Global Ozone Monitoring Experiment (GOME: 1995–2011); the Scanning Imaging Spectrometer for Atmospheric Chartography (SCIAMACHY: 2002–2012), Ozone Monitoring Instrument (OMI: since 2004) and GOME-2 aboard Metop-A (since 2007) and Metop-B (since 2012). Various UV total ozone algorithms are applied to these sensors: WFDOAS (Coldewey-Egbers et al., 2005), TOSOMI/TOGOMI (Antón et al., 2011), and GDP5/GODFIT (van Roozendael et al., 2012; Lerot et al., 2014). Generally, all algorithms show very good agreement (within 1%) with ground-based data and with other satellite data (e.g., Weber et al., 2005, 2013; Koukouli et al., 2012; Lerot et al., 2014). A variant of the TOSOMI/TOGOMI algorithm called OMI-DOAS (Kroon et al., 2008) has routinely been used to retrieve total column ozone from OMI (since 2004).

3) Solar and Stellar Occultation Instruments

Solar and stellar occulation instruments provide the highest vertical resolution in ozone profile measurements from space, typically 2 km, and generally provide very accurate ozone profiles. However, their global sampling is rather sparse compared to limb-scattering and limb-emission instruments. These instruments are:

- The Stratospheric Aerosol and Gas Experiment II (SAGE II) provides one of the longest single instrument data sets (1984 to 2005) of ozone profile information. The ozone values in the new version (v7.0, see Table 2-2) are 1–2% lower than in the previous version (6.2) due to the change of the ozone absortion cross section used in the retrieval (Damadeo et al., 2013; Remsberg, 2014).
- The Halogen Occultation Experiment (HALOE) aboard the Upper Atmosphere Research Satellite (UARS) has collected ozone profiles (cloud to mesosphere) from 1991 to 2005 with ~2 km resolution. Further information about profiles can be found at NASA Goddard Earth Sciences Data & Information Services Center (GES DISC): http://daac.gsfc.nasa.gov/. Although the HALOE record is not used directly in this Assessment, it is part of the Global OZone Chemistry And Related trace gas Data records for the Stratosphere (GOZCARDS) data set (R. Wang et al., 2013).
- The Global Ozone Monitoring by Occultation of Stars (GOMOS) on Envisat is a star-occultation instrument measuring in the UV, visible and near infrared spectrum. It provided global, nighttime ozone profiles in the altitude range 15–100 km with 2–3 km vertical resolution (e.g., Bertaux et al., 2010; Kyrölä et al., 2010, 2013).
- The Atmospheric Chemistry Experiment-Fourier Transform Spectrometer (ACE-FTS) was launched in 2004 aboard the SCISAT satellite. Although its record is short for trend analysis, it is used in the The HARMonized data set of OZone profiles (HARMOZ) database (Sofieva et al., 2013).

4) Limb-Scattering Instruments

Limb-scattering instruments have a typical vertical resolution of 3–4 km and provide very dense sampling of the daytime portion of the globe using backscattered solar radiation. These instruments are:

- The Optical Spectrograph and Infrared Imager System (OSIRIS) instrument was launched in 2001 on the Odin satellite (McLinden et al., 2012).
- The Scanning Imaging Absorption spectroMeter for Atmospheric CHartographY (SCIAMACHY) was launched on Envisat in 2002 and operated until 2012 (Gottwald and Bovensmann, 2011).
- The OMPS (Ozone Mapping and Profiler Suite) is a mission providing limb scatter ozone profiles since 2012 (Kramarova et al., 2014). While its record is too short for ozone assessment, it is the only recently launched new limb sounder. OMPS may play an important role in extending the observational record beyond the lifetime of other existing satellite ozone profilers.

5) Limb-Emission Instruments

Limb emission instruments operate in the thermal infrared and microwave part of the spectrum, meaning they can provide measurements in both day and night, and they provide a much denser sampling than the occultation instruments. They have similar vertical resolution and sampling characteristics as the limb-scattering instruments.

- Since 2001, the Sub-Millimetre Radiometer (SMR) aboard the Odin platform has provided twice-weekly measurements of global stratospheric ozone between 12 and 60 km altitude with random uncertainty estimated at 20%. Retrieved ozone profiles have a vertical resolution of about 3 km in the stratosphere (Urban et al., 2005).
- Sounding of the Atmosphere using Broadband Emission Radiometry (SABER) is another emission instrument providing ozone profiles. SABER data are not used for trend analysis in this Ozone Assessment, but the orbital characteristics make the data useful for estimating the diurnal cycle (Studer et al., 2014; Section 2.3.2). Further information can be found at http://saber.gats-inc.com/overview.php.
- The Michelson Interferometer for Passive Atmospheric Sounding (MIPAS) on board Envisat provided daily infrared sensing of global ozone profiles, and many other trace gases, from late 2002, and in a different mode, from late 2004 until April 2012, covering the ~10–70 km altitude range with resolution decreasing from 2 km at the bottom to 5 km at the top of the profile (von Clarmann et al., 2009). Several processers for MIPAS exist. MIPAS data are included in the HARMOZ data set (Sofieva et al., 2013).
- Since 2004, the EOS-Aura Microwave Limb Sounder (Aura MLS) has provided near-global information on ozone profiles (and many other trace gases) between the upper troposphere and the mesosphere. Ozone profiles are retrieved from microwave emissions (Waters et al., 2006; Livesey et al., 2006). The Upper Atmosphere Research Satellite (UARS) Microwave Limb Sounder (UARS MLS) is a predecessor to Aura MLS (Barath et al., 1993). Both MLS records are used in the GOZCARDS combined data set (Froidevaux et al., 2008; R. Wang et al., 2013).

6) Additional Combined Ozone Data Sets Not Used in the Assessment

- SBUV V8.6 NOAA merged data set, where bias corrections in overlapping periods have been applied (see http://larss.science.yorku.ca/QOS2012pdf/6071.pdf; data available at ftp://ftp.cpc.ncep.noaa.gov/SBUV_CDR/).
- SWOOSH (Stratospheric Water and Ozone Satellite Homogenized, http://www.esrl.noaa.gov/csd/groups/csd8/swoosh/)
- BDBP (Binary Data Base of Profiles; Hassler et al., 2009, 2014; Bodeker et al., 2013).
- The trajectory-mapped ozonesonde data set (Liu et al., 2013).